SCREENING FOR POTENT MICROBIAL ANTAGONISTS AS AN ALTERNATIVE FOR THE CONTROL OF CANDIDA

Nilofar Motorwala[1], Ushma Mistry[2], Nafisa Patel[3], Naresh Butani[4]

[1,2,3,4] *Naran Lala College of Professional and Applied Sciences, Navsari, Gujarat, (India)*

ABSTRACT

Candida albicans is a potent opportunistic human pathogen causing systemic as well superficial infection in mucous membranes of gastrointestinal and urinary tracts. It is the most common cause of vulvovaginitis in females as well as oral thrush. The search for novel strain of Bacillus subtilis from complex habitat having anticandidal activity would be an effective alternative to combat against the drug resistance. The isolate UK-3, later identified as Bacillus subtilis, showed antimicrobial activity during the screening process. Extract from the fermented broth by ethyl acetate showed anticandidal activity by agar diffusion method.

Keywords: ***Anticandida activity, Antifungal compound, Bacillus subtilis, Candidiasis, Vulvovaginitis.***

I. INTRODUCTION

Candida usually occurs as a normal flora of the human body but it can occur as an opportunistic pathogen causing superficial as well as systemic infection[1]. The pathogenesis of candidial infections is responsible for different types of disease manifestations. These pathogenic yeasts invade the mucous membrane and causes candidiasis in immunocompromised persons and the people who are at a greater risk are those suffering from HIV, cancer and those undergoin organ transplantation[2,3]. Among the 163 species of candida occurring on different habitat, Candida *albicans* is the common cause of oral thrush, candidiasis, candiduria as well as vulvovaginitis in females[2,4]. The prevalence of *C. albicans* is accounted to 70-90% while the other species is rarely isolated from clinical samples. In one study out of the total yeast isolated 47.6 % werepredominantly C. *albicans.*The percent occurrence of *Candida albicans* in India accounts up to 43% in the last ten years [4].

The Bacillus group of organisms as a potent producers of polypeptide antibiotics. Out of the 29 species of Bacillus isolated from soil most of them showed inhibition against gram positive and gram negative bacteria[5]. These organisms produces various classes of bacteriocins[6], surface-active biosurfactants[7] which includes lipopeptides and glycopeptides like inturins[8], surfactins[9], fengycins[10], kurstakins[11], bacillomycins[12] and mycosubtilin[13]. The antibiotics producing species mainly belong to *B. subtilis, B. polymyxa, B. brevis, B. licheniformis, B. circulans and B. cereus.* These group of organisms have been extensively exploited to produce antibiotics which are effective mostly for the gram positive bacteria, However, the production of large spectrum antibiotics as well as anti-fungal antibiotics producing organisms are relatively very less[14]. Moreover the available antifungal drugs are either ineffective against some fungi or may develop drug resistance resulting into no cure for variety of fungal infections. Candida species are important human pathogen and these organisms differ in their susceptibility against the common available antifungal agents[15]. Out of the total 213 isolates

from the clinical samples the most common are *Candida tropicalis* (56%) followed by *Candida albicans* (33%)[16]. A huge potential is been observed in the Bacillus strains due to their antimicrobial activity against pathogens[17] due to its activities of low toxicity and biodegradability. The search of novel microorganism as well as its products specifically Bacillus from microbiologically unexplored ecosystems is still an area of interest.

II. MATERIAL AND METHODS

2.1 Sample Collection

Soil samples were collected from the agricultural fields surrounding Navsaricity, Gujarat, India. Soil samples were collected from the rhizospheric soil area in sterile polyethylene bag, tightlypacked and immediately transferred to Microbiology Laboratory of NLCPAS, Navsari and stored in refrigerator till use.

2.2 Isolation of Microorganism

2.2.1 Isolation of Microorganisms from Soil Samples.

All these soil samples were serially diluted and spread on Nutrient agar plates containing 0.5% peptone; 0.3% beef extract; 1.5 % agar; 0.5% NaCl; and the pH was adjusted to 7.2 soil samples for isolation and enumeration. Plates were incubated at 37°C for 24 hr. After incubation the isolated bacterial colonies were studied and subjected for the screening of anticandidal activity.

2.2.2 Isolation of Candida Albicans from Clinical Samples

Urine samples from the patients suffering from urinary tract infection were collected from Advance Diagnostic laboratory, Surat and organisms were isolated and identified by growing them on CHROMagar media and further identified by BD Pheonix™.

2.3 Screening of Antagonistic Strains by in Vitro Antagonism Experiments

Screening of antagonistic activity of the soil isolate was carried out by spreading (except the center) the *Candida albicans* obtained from the clinical samples on the Nutrient Agar plates. Each isolated microorganism was streaked in circular form in the center of plate. Inoculated plates were incubated at 37°C for 24- 48 hr. Screening was done on the basis of the zone of inhibition produced by the soil isolate.

2.4 Identification of Isolate

The identification of the soil isolate, giving zone of inhibition against *Candida albicans*, was carried out from morphological, cultural and biochemical study. Further identification of the isolate was done on the BD Pheonix™.

2.5 Production and Extraction of Antifungal Compound

A loopful of purified culture of the isolate was inoculated aseptically in 100 ml of nutrient broth (pH 7.2) and incubated at 28°C in shaker incubator at 150 rpm for 72 hr. After incubation, the fermented broth was centrifuged to remove the bacterial cells and further filtered. The filtrate was mixed with ethyl acetate in the ratio of 1:1 (v/v) and shaken vigorously for 1 hr in a solvent extraction funnel. The solvent phase was separated

from the aqueous phase and evaporated to dryness in water bath at 80° - 90°C and the residue was used to assess the anticandidal activity.

2.6 Study of Anticandidal Activity

Determination of antifungal activities of pure bacterial culture was performed by using agar well diffusion method. Wells were made in the agar medium and filled with 200 µl of extract. To determine the effect of the extract, *Candida albicans* was spread on the surface of sabouraud dextrose agar and incubated at 28°C for 48-72hr. Control plates were prepared in the same way without addition of the extract. After the incubation diameter of zone of inhibition was measured.

III RESULTS & DISCUSSION

3.1 Isolation & Identification of Soil Isolate

Bacillus group of organisms isolated from complex habitat are most abundant producers of antimicrobial peptides. Multiple strains are found to produce antimicrobial peptides which exhibit selective inhibition. Many of these strains are reported to produce wide variety of biosurfactants like inturins or surfactins[18]. Out of the 25 isolates obtained from the soil sample, 5 isolates showed antimicrobial activity during the screening process. Out of these five isolates, Isolate UK3 was observed to be most potent in having antimicrobial activity having maximum zone of inhibition. Hence the UK3 isolate (Fig.-1) was further identified to be *Bacillus subtilis* from the morphological characteristics showing gram positive rods, the colonies were large, flat and become creamy after 48 hours. The further identification by Pheonix^{TM} confirmed the isolate UK3 to be *Bacillus subtilis.*

Fig.-1: Cultural Characterization of The Soil Isolate Showing Antagonistic Activity.

3.2 Isolation of Candida Albicans from Clinical Samples

Fifty urine samples were analyzed microbiologically obtained from patients suspected from suffering from UTIs. The suspected organisms were isolated and identified as per the morphological, cultural, biochemical characteristics. Twenty urine samples showed the presence of pathogens out of which the presence of *Candida albicans* was confirmed in two samples showing 10% occurrence rate (Fig.-2).

Fig.-2: Candida Albicans Isolated from Urinary Samples.

3.3 Study of Anti-Candidal Activity

It has been reported in many cases co-production of varieties of lipoproteins like surfactin/ intruin as well as surfactin/mycosubtilin[13,18].Researches are done to screen and characterize these novel antimicrobial peptides and develop them as a potential alternative in therapeutic and food industries. The antifungal activities of Bacillus strain can be enhanced by manipulating the nutritional requirements. Optimal antifungal activity was obtained when sucrose was used as carbon source followed by glucose. In one such experiment marked increase in surfactin production was observed in *Bacillus subtilis* MZ-7 when sucrose was supplemented[19,20].Addition of fructose, ribose, starch, maltose, glycerol and arabinose increased the microbial activity while mannitol, starch and inorganic carbon sources like $CaCO_3$ did not enhance antifungal activity[21].

In the present study the anticandidal activity of *Bacillus subtilis* was assessed by using different amounts of the antimicrobial extract of *Bacillus subtilis*. Seven different volumes of the cell free extract were poured in the wells made in agar plates seeded with *Candida albicans*. Well 1 having 20 µl and well 2 having 40 µl failed to give any inhibition against the test organism. While well 3 with 70 µl showed the inhibition zone of 2 mm, well 4 having 100 µl showed the zone of 4 mm, well 5 having 200 µl gave a zone of 6mm, well 6 having 400 µl gave a zone of 11mm while well 7 gave the maximum zone of inhibition of 22 mm. The minimum inhibitory concentration sufficient to inhibit the pathogen *Candida albicans* was obtained in 70µl of the extract and the maximum inhibition was given by 700 µl of the extract (Fig.-3).

Fig.-3: Anti Candidal Activity Shown By Bacillus Subtilis.

IV. CONCLUSION

Microbial source has always been an effective alternative for producing anti-fungal agents against the pathogenic fungi and the need for novel sources and their products is an area of research especially in cases of development of drug resistance. *Bacillus subtilis* are potent organisms producing a wide range of antimicrobial substances accounting for antibacterial, antifungal and antiviral activities. Exploring the unexplored complex habitats of ecosystem may end up in obtaining such novel strains and their metabolites. Characterizing these antimicrobial substances would become an effective alternative against multiple organisms. Manipulating their growth conditions would enhance their antifungal activities as well as optimizing their concentrations and further purifications is still an area of research as well as interest.

REFERENCES

[1] A. Nerurkar, P. Solanky, N. Chavda, H. Baria, and B. Desai, Isolation of *Candida* Species in clinical specimens and its virulence factor: The biofilm, 2012.

[2] B. Jha, S. Dey, M. Tamang, M. Joshy, P. Shivananda, and K. Brahmadatan, Characterization of *Candida* species isolated from cases of lower respiratory tract infection, *Kathmandu University medical journal 4(3)*, 2005, 290-294.

[3] Y.M. Clayton, and W. Noble, Observations on the epidemiology of *Candida albicans*, *Journal of clinical pathology*, *19(1)*, 1966, 76.

[4] I. Das, P. Nightingale, M. Patel, and P. Jumaa, Epidemiology, clinical characteristics, and outcome of candidemia: experience in a tertiary referral center in the UK, *International Journal of Infectious Diseases*, *15(11)*, 2011, 759-763.

[5] M. Yilmaz, H. Soran, and Y. Beyatli, Antimicrobial activities of some *Bacillus spp.* strains isolated from the soil, *Microbiological Research*, *161(2)*, 2006, 127-131.

[6] T.R. Klaenhammer, Genetics of bacteriocins produced by lactic acid bacteria, *FEMS microbiology reviews*, *12(1-3)*, 1993, 39-85.

[7] S. Mukherjee, P. Das, and R. Sen, Towards commercial production of microbial surfactants, *Trends in biotechnology*, *24(11)*, 2006, 509-515.

[8] Y.F. Ye, Q. Q. Li, F. Gang, G. Q. Yuan, J.-H. Miao, and L. Wei, Identification of antifungal substance (Iturin A 2) produced by *Bacillus subtilis* B47 and its effect on southern corn leaf blight, *Journal of Integrative Agriculture*, *11(1)*, 2012, 90-99.

[9] K. Arima, A. Kakinuma, and G. Tamura, Surfactin, a crystalline peptidelipid surfactant produced by *Bacillussubtilis*: Isolation, characterization and its inhibition of fibrin clot formation, *Biochemical and biophysical research communications*, *31(3)*, 1968, 488-494.

[10] N. Vanittanakom, W. Loeffler, U. Koch, and G. Jung, Fengycin-A novel antifungal lipopeptide antibiotic produced by *Bacillus subtilis* F-29-3, *The Journal of antibiotics*, *39(7)*, 1986, 888-901.

[11] Y. Hathout, Y. P. Ho, V. Ryzhov, P. Demirev, and C. Fenselau, Kurstakins: A New Class of Lipopeptides Isolated from *Bacillus thuringiensis*, *Journal of natural products*, *63(11)*, 2000, 1492-1496.

[12] N. Roongsawang, J. Thaniyavarn, S. Thaniyavarn, T. Kameyama, M. Haruki, T. Imanaka, M. Morikawa, and S. Kanaya, Isolation and characterization of a halotolerant *Bacillus subtilis* BBK-1 which produces three kinds of lipopeptides: bacillomycin L, plipastatin, and surfactin, *Extremophiles*, *6(6)*, 2002, 499-506.

[13] E.H. Duitman, L.W. Hamoen, M. Rembold, G. Venema, H. Seitz, W. Saenger, F. Bernhard, R. Reinhardt, M. Schmidt, and C. Ullrich, The mycosubtilin synthetase of *Bacillus subtilis* ATCC6633: a multifunctional hybrid between a peptide synthetase, an amino transferase, and a fatty acid synthase, *Proceedings of the National Academy of Sciences*, *96(23)*, 1999, 13294-13299.

[14] H.P. Bais, R. Fall, and J.M. Vivanco, Biocontrol of *Bacillus subtilis* against infection of Arabidopsis roots by Pseudomonas syringae is facilitated by biofilm formation and surfactin production, *Plant physiology*, *134(1)*, 2004, 307-319.

[15] Y. L. Yang, Y.A. Ho, H. H. Cheng, M. Ho, and H. J. Lo, Susceptibilites of *Candida* Species to Amphotericin B and Fluconazole The Emergence of Fluconazole Resistance in *Candida tropicalis*, *Infection Control*, *25(01)*, 2004, 60-66.

[16] S. Jaya, and V. Harita, *Candida* Species Isolated from Various Clinical Samples and Their Sus-ceptibility Patterns to Antifungals, *J Med Microbiol*, *1(1)*, 2013, 23.

[17] P. Kim, H. Bai, D. Bai, H. Chae, S. Chung, Y. Kim, R. Park, and Y.T. Chi, Purification and characterization of a lipopeptide produced by *Bacillus thuringiensis* CMB26, *Journal of applied microbiology*, *97(5)*, 2004, 942-949.

[18] C.C. Huang, T. Ano, and M. Shoda, Nucleotide sequence and characteristics of the gene, lpa-14, responsible for biosynthesis of the lipopeptide antibiotics iturin A and surfactin from *Bacillus subtilis* RB14, *Journal of fermentation and bioengineering*, *76(6)*, 1993, 445-450.

[19] M.M. Al-Ajlani, M.A. Sheikh, Z. Ahmad, and S. Hasnain, Production of surfactin from *Bacillus subtilis* MZ-7 grown on pharmamedia commercial medium, *Microbial cell factories*, *6(1)*, 2007, 17.

[20] S. Joshi, S. Yadav, and A.J. Desai, Application of response-surface methodology to evaluate the optimum medium components for the enhanced production of lichenysin by *Bacillus licheniformis* R2, *Biochemical Engineering Journal*, *41(2)*, 2008, 122-127.

[21] N.M. El-Banna, Effect of carbon source on the antimicrobial activity of *Corynebacterium kutscheri* and *Corynebacterium xerosis*, *African Journal of Biotechnology*, *5(10)*, 2006.

STUDY ON ANTI-HELMINTHOSPORIUM COMPOUND PRODUCING BACTERIA BACILLUS SUBTILIS

[1]Maitry Shah,[2] Krishna Bhavsar, [3]Naresh Butani,
[4]Nafisa Patel, [5]Ravin Rawal

[1,2,3,4,5] Naran Lala College of Professional and Applied Sciences, Navsari, Gujarat, (India)

ABSTRACT

Phyto pathogenic fungi are a serious problem for crop and vegetable due to its damaging effects. In indirect way it also causes serious problem in human and animals by producing mycotoxins. Helminthosporium spp. is one of phyto pathogenic fungi responsible for causing blight in very important food crop like, wheat and oats. It also causes leaf spots in many plants and responsible for root rots in cereals. Spot blotch caused by Bipolaris sorokiniana is one of the most important foliar diseases limiting wheat production in warmer, nontraditional growing areas. Due to infection of such fungi up to 15% crop loss has been reported. So, it is very important to manage this pathogen. Infection caused by such fungi can be controlled by application of antifungal compounds or by applying biocontrol agents. Major limiting factor for antifungal compound application is its low solubility and toxicity. In order to find new safer antifungal compound or biocontrol agent, present research work has been undertaken. From the agricultural soil samples, various microorganisms had been isolated and screened for its antifungal compound production. Anti-Helminthosporium activity was studied by agar cup method. Screened bacterium was identified as Bacillus subtilis, having capacity of production of antifungal compound. Bacillus subtilis can be applied as biocontrol agent.

Keywords: Antifungal activity, Antifungal compound, Helminthosporium spp., Bacillus subtilis, Phyopathogen

I. INTRODUCTION

Fungal pathogens pose serious problems worldwide and cause a number of plants and animal diseases such as ringworm, athlete's foot, and several more serious diseases. Plant diseases caused by fungi include rusts, smuts, rots, and may cause severe damage to crop[1]. Fungal pathogens cause devastating losses of crops and postharvest fruits throughout the world [2], and are a major threat to crop. Post-harvest food spoilage also represents a potential health hazard for humans due to the production by phytopathogens of toxic metabolites [3]. *Helminthosporium* is a generic name, for a group of fungal species, well known for its phytopahogenicity. These species are commonly associated with leaf spots or blights, foot rots, and other disease syndromes on cultivated and wild *Poaceae*. Their ability to cause devastating disease has occasionally resulted in famine and loss of human life [4] or in great economic loss [5]. Other plant groups are also affected: palms [6], cacti [7], *Leucospermum spp*., beans, forage legumes[8], rubber, Musa, and coffee [9] are reported as hosts. In addition,

mycoses in domestic animals and man increasingly are being attributed to these fungi. They have been implicated in mycotoxicoses in grazing animals, and mycoparasitic activity by them has been reported [10]. Spot blotch caused by *Bipolaris sorokiniana* is one of the most important foliar diseases limiting wheat production in warmer, nontraditional growing areas. Due to infection of such fungi up to 15% crop loss has been reported [11].

Antifungal antibiotics, effective against fungal disorders, are relatively few mainly because of their solubility and toxicity problems [12,13]. Many artificial chemical fungicides have been used to prevent and kill fungi in various environments. However, because of their huge populations and high frequency of mutation, a large amount of pathogenic fungi may easily acquire resistance to frequently used fungicides. Several important chemical fungicides such as anilinopyrimidine, benzimidazoles, demethylation inhibitors (DMI), dicarboximide, phenylpyrrole, Qo respiration inhibitors, and strobilurin, have lost their efficacy against pathogenic fungi in the field [2]. Excessive use of chemical fungicides in agriculture has led to deteriorating human health, environmental pollution, and development of pathogen resistance to fungicide [1]. To reduce the risk of crop disease and enhance the safety of food and the environment, new, safer fungicides should be discovered and developed [14].

In order to screen new antifungal compound, we had isolated many microorganism and screened for its antifungal activity. Morphological and metabolic characteristic of isolated strain was studied in detail. Antifungal activity against *Helminthosporium spp*. was studied using agar cup method.

II. MATERIAL AND METHODS

2.1 Sample Collection

Several soil samples were collected from the vicinity of Navsari City, Gujarat, India. Soil samples were collected in sterile polyethylene bag, close tightly and immediately transferred to Microbiology Laboratory of NLCPAS, Navsari. Samples were stored in refrigerator till next use.

2.2 Isolation of Microorganism

Serial dilution spread plating method is used for the isolation and enumeration of microorganisms. Isolation was carried out on sterile nutrient agar plate (composition : 0.5% peptone; 0.3% beef extract; 1.5 % agar; 0.5% NaCl; pH was adjusted to 7.2). Aliquots were spread on the plates. Plates were incubated at 37 C for 24 h. Next day, various bacterial colonies were observed and subjected for screening of anti-Helminthosporium activity.

2.3 Screening of Microorganism

Screening was carried out by spreading *Helminthosporium spp*. on the sabouraud dextrose agar plate (Composition: Table 1) . Each isolated microorganism was streaked in circular form in the center of plate. Inoculated plates were incubated at 30 C for 24- 48 hr. Screening was done on the basis of its size of zone of inhibition produced by microorganism.

2.4 Identification of isolate

Morphological study of isolate was carried out by studying Gram staining characteristics. Various biochemical characteristic analyses were done on the BD Pheonix^{TM} [15].

2.5 Production and Extraction of Antifungal compound

Stage 1: Fermentation

Nutrient broth (pH 7.2,100 ml) was prepared and then under aseptic conditions a loop full of purified growth added. This broth was incubated at 28°C in shaking incubator at 150 rpm for 5 days. After 5 days the inoculums for fermentation process was ready for use.

Stage 2: Extraction

After fermentation, the medium was harvested and centrifuged to remove cells and debris. Supernatant is collected in a sterilized screw cap bottle. Filter the fermented broth. The filtrate was mixed with ethyl acetate in the ratio of 1:1 (v/v) and shaken vigorously for 1 h in a solvent extraction funnel.

The solvent phase that contains antibacterial compound was separated from the aqueous phase. Solvent phase was evaporated to dryness in water bath at 80 - 90°C and the residue is used to check antibacterial activity [16].

2.6 Study of Antifungal activity

Determination of antifungal activities of pure bacterial culture was performed by using modified agar cup method. To determine the effect of bacteria on *Helminthosporium spp*., bacteria was spread on the surface of sabouraud dextrose agar.

One mycelial disk (6 mm in diameter), from the edge of 3 to 5- day-old-colony of *Helminthosporium* spp. grown on SDA, was put onto the center of each plate. Inoculated sabouraud dextrose agar plates were incubated at 28°C for 4 days. Control plates were prepared in the same way without spreading bacteria. After 4 days, diameter of fungal colony was measured.

III.RESULT AND DISCUSSION

3.1 Sample Collection

Soil is considered as a rich source of the microorganisms. Soil samples were collected from the agricultural land from the vicinity of the Navsari District, Gujarat. Soil-borne bacteria that are antagonistic to plant pathogens could make a substantial contribution to prevention of plant diseases[17].

3.2 Isolation of Microorganism

Isolation was done on Nutrient Agar plate. Total 30 different types of bacteria were isolated from the soil samples on the basis of its colony characteristics (Fig. 1).

3.3 Screening of Microorganism

Screening of the organism was done its ability to form zone of inhibition. As a result of screening one bacterial strain, designated as UKB2, was selected for further study (Fig. 2). UKB2 was Gram positive, motile, rods in chain. Colony was irregular shaped, flat and become creamy after 48 hours.

Table 1 Composition of Sabouraud Dextrose Agar

Sr. No.	Component	Amount
1	Peptone	10 gm
2	Glucose	40 gm
3	NaCl	05 gm
4	Agar	20 gm
5	Distilled Water	1000 ml
	pH	5.2

Figure 1 Colony Characteristics of UKB2 **Figure 2 Screening of anti-*Helminthosporium* microorganism**

3.3 Identification of Isolate

On the basis of its Biochemical characteristics, studied with the help of Pheonix^{TM} , UKB2 was identified as *Bacillus subtilis*. Pheonix^{TM} is one of the reliable automated identification systems [18].

3.4 Study of Antifungal activity

Antifungal activity was studied by the agar cup method. Results showed that the diameter of the fungal colony on the test plate was 3 mm while on control the diameter of fungal colony was 70 mm (Fig. 3).

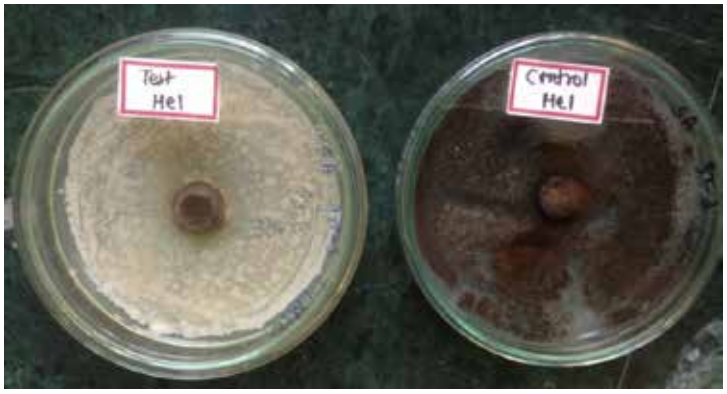

Figure 1 Anti-Helminthosporium Activity of *Bacillus Subtilis*

There are various reports available that variety of antifungal compound is produced by *Bacillus subtilis*. It had been already reported that an antifungal compound, known as Bacillomycin, is produced by *Bacillus subtilis*. It also produced some volatile compounds, having antifungal activity[19].

3.5 Study of Antifungal activity of extracted compound

Ethyl acetate extracted metabolites also showed antifungal activity.

IV. CONCLUSION

As *Helminthosporium spp*. is causing very serious problems in our food crops like wheat, new infection management strategies must be devised. As *Bacillus subtilis* is showing promising anti-Helminthosporium activity, it can be applied as biocontrol agent. Extracted compound is also showing this activity, so, purified compound can be also applied after toxicity study of the compound. In future, purified compound isolation and its toxicity should be studied.

REFERENCES

[1] H. Sharma, and L. Parihar, Antifungal activity of extracts obtained from actinomycetes, *Journal of Yeast and Fungal Research*, *1(10)*, 2010, 197-200.

[2] H. Chen, L. Wang, C. Su, G. Gong, P. Wang, and Z. Yu, Isolation and characterization of lipopeptide antibiotics produced by Bacillus subtilis, *Letters in applied microbiology*, *47(3)*, 2008, 180-186.

[3] Z. Zhang, S. Zhang, and M. Wua, Isolation, Purification and Structure Determination of a Novel Antifungal Compound.

[4] S. Padmanabhan, The great Bengal famine, *Annual Review of Phytopathology*, *11*, 1973, 11-24.

[5] A. Ullstrup, The impacts of the southern corn leaf blight epidemics of 1970-1971, *Annual Review of Phytopathology*, *10(1)*, 1972, 37-50.

[6] L. Forsberg, Foliar diseases of nursery-grown ornamental palms in Queensland, *Australasian Plant Pathology*, *14(4)*, 1985, 67-71.

[7] A. Chase, Stem rot and shattering of Easter cactus caused by Drechslera cactivora [Rhipsalidopsis gaertneri, Ornamental], *Plant Diseases (USA)*, 1982.

[8] M.B. Ellis, Dematiaceous hyphomycetes, *Dematiaceous hyphomycetes.*, 1971.

[9] V. Smedegård-Petersen, Pathogenesis and genetics of net-spot blotch and leaf stripe of barley caused by Pyrenophora teres and Pyrenophora graminea, 1976.

[10] J. Alcorn, The taxonomy of" Helminthosporium" species, *Annual Review of Phytopathology*, *26(1)*, 1988, 37-56.

[11] E. Duveiller, and I. Garcia Altamirano, Pathogenicity of Bipolaris sorokiniana isolates from wheat roots, leaves and grains in Mexico, *Plant pathology*, *49(2)*, 2000, 235-242.

[12] S. Raytapadar, and A. Paul, Isolation of actinomycetes from different soils of West Bengal and variations in their antimicrobial spectrum, *Environment and ecology. Kalyani*, *13(4)*, 1995, 884-888.

[13] J. Berdy, The discovery of new bioactive microbial metabolites: screening and identification, *Progress in industrial microbiology*, *27*, 1989, 3-27.

[14] F. Coloretti, S. Carri, E. Armaforte, C. Chiavari, L. Grazia, and C. Zambonelli, Antifungal activity of lactobacilli isolated from salami, *FEMS microbiology letters*, *271(2)*, 2007, 245-250.

[15] E. Stefaniuk, A. Baraniak, M. Gniadkowski, and W. Hryniewicz, Evaluation of the BD Phoenix automated identification and susceptibility testing system in clinical microbiology laboratory practice, *European Journal of Clinical Microbiology and Infectious Diseases*, *22(8)*, 2003, 479-485.

[16] H.M. Atta, An antifungal agent produced by Streptomyces olivaceiscleroticus AZ-SH514, *World Applied Sci. J*, *6(11)*, 2009, 1495-1505.

[17] M. Islam, Y. Jeong, Y. Lee, and C. Song, Isolation and Identification of Antifungal Compounds from *Bacillus subtilis* C9 Inhibiting the Growth of Plant Pathogenic Fungi, *Mycobiology*, *40(1)*, 2012, 59-66.

[18] J. Snyder, G. Munier, and C. Johnson, Direct Comparison of the BD Phoenix System with the MicroScan WalkAway System for Identification and Antimicrobial Susceptibility Testing of *Enterobacteriaceae* and Nonfermentative Gram-Negative Organisms, *Journal of Clinical Microbiology*, *46(7)*, 2008, 2327–2333.

[19] L. Yongfeng, C. Zhiyi, T. Ng, Z. Jie, M. Zhou, S. Fuping, L. Fan, and L. Youzhou, Bacisubin, an antifungal protein with ribonuclease and hemagglutinating activities from *Bacillus subtilis* strain B-916, *Peptides*, *28*, 2008.

COMPARATIVE STUDY OF DYE DECOLORIZING FFICIENCY OF MALACHITE GREEN BY BACILLUS MEGATERIUM, PSEUDOMONAS AERUGINOSA, AND ASPERGILLUS NIGER

Brijal Patel[1], Rashmita patel[2], Kalia Tajuddin[2], Patel Amir[2]

[1,2] Department Of Microbiology Naran Lala College of Professional and Applied Science, Navsari (India)

ABSTRACT

The triphenylmethane dye, malachite green used widely in various industrial processes possesses severe environmental concern, causing major health problems to human beings. In the present study Comparative study of, decolourization of malachite green using Bacillus megaterium, Pseudomonas aeruginosa and Aspergillus niger were investigated by optimizing various Parameter like pH,temperature,BOD,COD,static and shaking condition.It was found that maximum Decolorization given by Bacillus megaterium 98% at pH-7,and 96 % by P.aeruginesa. During study it was observed that Static and anaerobic condition prove most effective for dye decolorization.The dye decolorization was further confirmed by COD & BOD Analysis.

Key words: Biodegradation, Bushnell & Hass medium (BHM), Malachite green

I. INTRODUCTION

In industries like textile, paper and leather, about 20 variants of dyes *viz* azo dyes, reactive dyes, triphenyl methane dyes, etc. are used for dyeing [1] . These chemical dyes may be organic, polymeric or inorganic in nature and can be visible and viable even at very low concentrations. Mostly, synthetic dyes are recalcitrant in nature and furthermore found to be carcinogenic and mutagenic[2]. Malachite green, one of the basic and widely used dye was chosen as model dye compound for the present investigation.

Various physical and chemical methods like coagulation or adsorption of dyes, ultra-filtration, ion-exchange, chemical oxidation, electrolysis etc have been developed for the elimination of dyes from the wastewater since many years [4] . However these methods are not very much applied because of their high cost, high energy requirements and hazardous by-products[5]. Also these techniques generate a huge volume of sludge and cause secondary pollution due to the formation of sludge and hazardous by-products [6].

Biological methods are generally considered environment friendly as they can lead to complete mineralization of organic pollutants at low cost [7]. Bioremediation may be the most effective method for treating industrial dyes wastewater [8].

Literature review indicates numerous bacteria, fungi were able to decolorize as well as degrade the dye compounds. According to this, biological method must be an alternative method of choice because of its eco-friendly products [9][10][11].so present study conducted to find decolorization efficiency of *Bacillus megaterium*, *Pseudomonas aeruginosa* and *Aspergillus niger*.

II.MATERIALS AND METHODS

2.1 Dyes and Chemicals

All media component and chemicals are analytical grade and purchased from Hi-media laboratories(Mumbai, India). Malachite green was purchased from Loba chemie Pvt. Ltd. All other reagents used were of analytical grade.

2.2 Medium

The *Bacillus Megaterium, Pseudomonas aeruginosa* cultures were routinely grown at 37°C and *Aspergillus Niger* grown at 27°C in the basal culture medium, Bushnell and Hass medium (BHM) containing the following in g/l, $MgSo_4$ 0.2,$CaCl_2$ 0.02, KH_2 PO 1.0, K $_2HPO_4$ 1.0, NH $_4$No 1.0, FeCl 0.05, Glucose 0.9, Yeast extract 0.9, Malachite Green 10-200 ppm.

2.3 Plate Assay

Plate assay was performed for the detection of decolourizing activity of bacteria. The nutrient agar and Malachite Green dye was autoclaved at 121oC for 15 minutes. Cultures were plated on nutrient agar plates containing Malachite Green (100ppm). The plates were wrapped with parafilm and were incubated at 37oC for 7days. The plates were observed for clearance of the surrounding the colonies.

2.4 Measurement of Dye Concentration

The dye concentrations were measured with a UV/VIS spectrophotometer at regular intervals during the decolorisation process.The concentration of azo dye was detected spectrophotometrically by reading the culture supernatant at its specific max after centrifugation at 10,000 rpm for 10 min. The dye concentrations were determined from the attenuance (O.D) of the culture 610 nm.

2.5 Decolorization Activity was Calculated as Follows:

$$\text{Decolorization}(\%) = \frac{\text{Initial absorbance} - \text{Observed absorbance}}{\text{Initial absorbance}} \times 100$$

2.6 Study of Physico-Chemical Parameters

Decolorization was studied using Static and shaking condition as well as different temperature ,27 ◦c37°C, and 55 °C and Different pH [12].

2.7 Estimation of Chemical Oxygen Demand (COD)

Chemical oxygen demand was measured by the standard Potassium dichromate method. 1ml of initial medium containing dye solution, decolorized medium, distilled water was added to COD Tube sample 1, sample 2, Blank respectively. Then 1.5ml of distilled water & reducing agent potassium dichromate and 3.5ml COD acid were added to each tube. Duplicates were put up for all the tubes. All the tubes were kept in the COD incubator at 148oC for 2 hrs. After incubation the entire content were transferred to a conical flask. A drop of ferroin indicator was added to it and was titrated against FAS in the burette.(

The readings were noted

$$\text{COD mg/l} = \frac{A-B \times N \times \text{Equi weight of } O2 \times 1000}{\text{Volu of sample}}$$

A-volume of Ferrous Ammonium Sulphate used for blank

B-volume of ferrous Ammonium Sulphate used for sample

Equivalent weight of oxygen - 8

N-Normality of FAS - 0.1

COD values were compared between the initial medium containing dye solution and decolorized medium.

2.8 Estimation of Biological Oxygen Demand (BOD)

1ml of initial medium containing dye solution, decolorized medium, distilled water was added to airtight BOD bottles sample 1, sample 2, Blank respectively. Place desired volume of water in a suitable bottle and add 1ml of each of Phosphate buffer, MgSO , 4FeCl and seeding/L of water. Before use 3 bring dilution water temperature to 200C. Dilution water was aerated with organic free filtered air. All the bottles are kept in BOD incubator at 200C for 5 days. After incubation 1ml of MnSO , Alkali iodide solution and sulphuric acid was added to form brown color solution. After color formationthey were titrated against their Na SO for their BOD values.

The readings were noted.

$$BOD \quad Mg/l \quad = \frac{B - T(v) \times 250}{S(v)}$$

B-volume of Na SO used for blank ,

T (v)-volume of Na So used for sample 2

S (v)-volume of sample

III. RESULT

3.1 Effect of Culture Conditions on Dye Decolorization

(Table-1 &2) The static and shaking conditions showed a profound effect on the dye decolourization efficiency [13] Both the bacterial species and fugie were exhibit dye decolorizing activity only when incubated under the stationary condition (36 hr) .out of them *B.megaterium* was give 100% decolorization at static and 91 % at static condition at 36 hr. Anaerobic or static conditions were necessary for bacterial decolorization through the cell growth was poorer than that under aerobic conditions [14].Under aerobic conditions azo dyes are generally resistant to attack by bacteria[15]. Azo dye decolorization by bacterial species if often initiated by enzymatic reduction of azo bonds, the presence of oxygen normally inhibits the azo bond reduction activity since aerobic respiration may dominate utilization of NADH; thus impeding the electron transfer from NADH to azo bonds..

Table-1 Effect of static condition on Decolorization

Sr No.	Static condition	% of Decolorization		
		Bacillus Megaterium	*Pseudomonas Aeruginosa*	*Aspergillus Niger*
1	12	80	65	18
2	24	97	82	31
3	36	100	98	60

Table-2-Effect of shaking condition on Decolorization

Sr No.	Shaking condition	% of Decolorization		
		Bacillus Megaterium	*Pseudomonas Aeruginosa*	*Aspergillus Niger*
1	12	69.5	60	13
2	24	80	72	25
3	36	91	88	50
		–		

3.2 Effect of Temperature on Dye Decolorization

The dye decolorization activity of our culture was found to increase with increase in incubation temperature from 27c◦ to 37^{o}C with maximum activity attained at 37^{o}C(Table-3)and (graph-1). Further increase in temperature resulted in maginal reduction in decolorization activity of isolates may due to sensitivity at higher temperature.

3.2 Table-3 Effect of Temprature on Decolorization

Sr No.	Temprature	% of Decolorization		
		Bacillus Megaterium	*Pseudomonas Aeruginosa*	*Aspergillus Niger*
1	27◦c	89	65	43
2	37◦c	98	96	21
3	55◦c	70	20	12

3.3 Effect of Ph on Dye Decolorization

Bacterial culture generally exhibited maximum decolorization rate at pH values near 7 and fungi near pH 5.Table-4 and Grah -2 shows that decolorization rate increase as pH shift from 5-7 .Further decreased decolorization rate obtain at pH 8.Fungi Give maximum decolorization near pH 5 indicate acidic environment needed for growth.

Table-4 Effect of pH on Decolorization

Sr No.	pH	% of Decolorization		
		Bacillus Megaterium	*Pseudomonas Aeruginosa*	*Aspergillus Niger*
1	5	60	55	60
2	6	75	65	23
3	7	95	89	20
4	8	83	80	12

Graph-1 Effect of pH on Decolorization

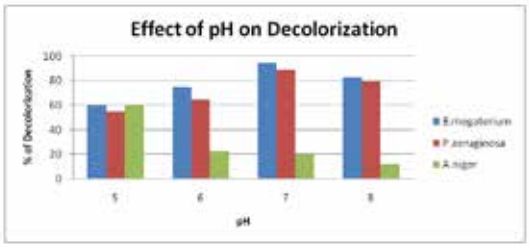

3.4 Cod Determination

The Chemical oxygen demand was measured by calculating the amount of oxidizing agent i.e., K_2 Cr_2 O_4 consumed during oxidation of organic matter (biodegradable and nonbiodegradable) under acidic conditions. Chemical oxygen demand of degraded dye solution gets considerably reduced after degradation. COD of the solutions after degradation shows significant decrease from 20- 2 mg/l (Table-5 and Graph-2).

Table-5 Effect of chemical Oxygen demand on Decolorization

Sr No.	COD(Mg/L)	% of Decolorization		
		Bacillus Megaterium	*Pseudomonas Aeruginosa*	*Aspergillus Niger*
1	Initial	12	20	16
2	12	10	11	10
3	24	6.3	8	6
4	36	4.0	5	2

Graph-2 Effect of Chemical oxygen Demand on decolorization

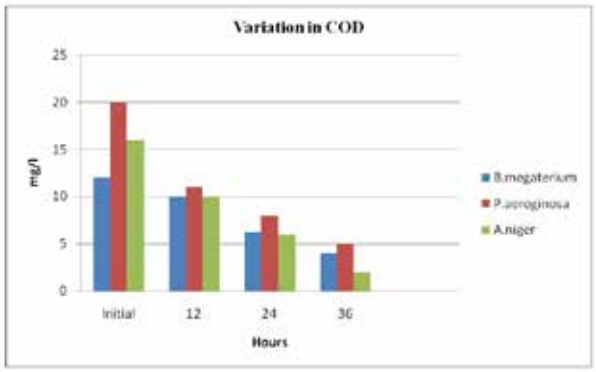

3.5 Bod Determination

The rate of removal (that is Consumption) of Oxygen by microorganism in aerobic degradation of the dissolved or even particulate organic matter in water that is called Biological Oxygen Demand (BOD).The BOD determination was used todetermine the relative oxygen requirements of dye solution.BOD Of all samples dcrease from 7.2-1 mg/l(Table-6 &Graph-3). The test measures the Oxygen utilized during a specified incubation period for the biochemical degradation of organic matter (Carbonaceous demand) and the oxygen used to utilize in organic material such as sulfides and ferrous iron. It also may measure the oxygen used to oxidize reduce forms of Nitrogen (Nitrogenous demand).

Table-6 Effect of Biological oxygen Demand on Decolorization

Sr No.	BOD(Mg/L)	% of Decolorization		
		BacillusMegaterium	Pseudomonas Aeruginosa	Aspergillus Niger
1	Initial	6	7.2	6.4
2	12	2.4	5.2	4.0
3	24	1.8	4	3.2
4	36	1.0	2.7	3

Graph-3 variation in Biological oxygen Demand during Decolorization

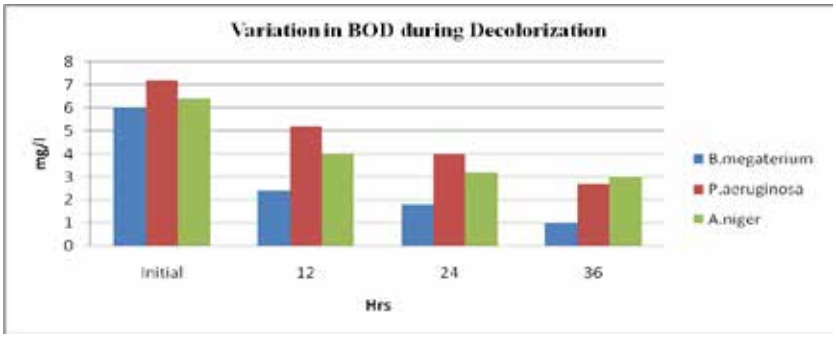

IV. CONCLUSION

Bioremediation has proved to be a very effective method in encountering the textile dye pollution in an eco-friendly manner. This approach creates a promising hope for remediation of the environment which is polluted by hazardous dyes.The present study confirms the ability of bacterial culture *Bacillus megaterium* to decolorize the malachite green with decolorization efficiency of 98% and *Peudomonas.aeruginose* with 96% efficiency.

The ability of the strain to tolerate, decolorize and degrade malachite green at high concentration gives it an advantage for the treatment of textile industry wastewater. However the potential of the bacteria needs to be demonstrated for its application in the treatment of dye containing industrial effluents using appropriate bioreactors. This study further recommends the identification and purification of enzymes from isolates and their kinetics involved in the degradation of malachite green. Further research on this bacterial strain could explore new tools and techniques to evolve viable and eco friendly solutions for the treatment of dyes in the industrial effluents.

V. ACKNOWLEDGMENTS

Our special thanks to Principle sir, Dr sunil naik and Head of department microbiology Dr. Nafisa patel of Naran lala college of professional and applied science for their Guidence, support and encouragement as well as for research facilities.

REFERENCES

[1] Jain R, Mathur M, Sikarwar S, Mital A. Removal of hazardous dye, rhodamine B through photocatalytic and adsorption treatments. Journal of Environmental Management **2007**; 85(4):956-964.

[2] Dae-Hee A, Won-Seok C, Tai-Il Y. Dyestuff wastewater treatment using chemical oxidation, physical adsorption and fixed bed bio - film process. Process Biochemistry **1999**; 34:429-439.

[3] Pearce, C. I., Lioyd, J. R. and Guthrie, J. T., 2003. The removal of colour from textile wastewater using whole bacterial cells: a review. *Dyes and pigments* **58**: 179-186.

[4] Andreas Kandelbauer; Angelika Erlacher; Artur Cavaco-Paulo; M George Guebitz, *Biocatalysis and Biotransformation*, **2004,** 22 (5/6), 331-339.

[5] M Meenakshi Sundaram; K Shahul Hameed, *Journal of Chem. and Pharm. Res.*, **2012**, 4(4), 2070-2080.

[6] J Maier; A Kandelbauer; A Erlacher; A Cavaco-Paulo; GM Gübitz, *Applied and Environmental Microbiology*, **2004,** 70 (2), 837-844.

[7] A Pandey; P Singh; L Iyengar, *International Biodeterioration & Biodegradation*, **2007,** 59, 73-84.

[8] K Nozaki; CH Beh; M Mizuno; T Isobe; M Shiroishi; T Kanda, *Journal of Bioscience and Bioengineering*, **2008,** 105, 69–72.

[9] Acuner E. and Dilek F.B. Treatment of tectilon yello 2G by Chlorella vulgaris. Process Biochem**. 2004** ,39, 623-631.

[10] Aksh Z. and Donmez G. A comparative study on the biosorption characteristics of some yeasts for remozal blue reactive dye. Chemosphere,**2003**,50, 1075-1083.

[11] Anjali P., Poonam S. and Leela I. Bacterial decolorization and degradation of azo dyes. Int. Biodet. Biodeg. **2004**,59,73-84.

[12] Guang-fei Liu, Ji-ti Zhou, Jing Wang, Zhi- Yong song and Yuan-yuan QV, **2006** Bacterial decolorization of azo dyes by Rhodopseudomonas palustrips, World *Journal of Microbiology and Biotchnology* **22** 1069-1074.

[13] Hu, T. L., 1994. Decolorization of reactive azo dyes by transformation with Pseudomonas luteola. *Bioresources technology* **49**: 47-51.

[14] Chang, J. S., and Lin Y. C., **2001.** Decolorization of Recombinant E.coli strain harboring azo dye decolorizing determinants from Rhodococcus sp. *Biotechnology Letters* **23**: 631-636.

[15] Chang, J.S. & Kuo, T.S. **2000** Kinetics of bacterial decolorization of azo dye with E.coli No3. *Bioresource Technology* **75**, 107 - 111.

A STANDARDIZED QUANTIFICATION TECHNIQUE FOR EVALUATION, INTERPRETATION OF DE-MRI SCANS

Nasreen Sulthana.D[1], Asif Hussain.S[2]

[1]M.Tech Scholar, [2]Associate Professor, E.C.E, AITS, Rajampet, Andhra Pradesh, (India)

ABSTRACT

Delayed-enhancement magnetic resonance imaging (DE-MRI) is an effective technique for detecting left atrial (LA) fibrosis both pre and postradiofrequency ablation for the treatment of atrialfibrillation. Fixed thresholding models are frequently utilized clinically to segment and quantify scar in DE-MRI due to their simplicity. These methods fail to provide a standardized quantification due to inter- observer variability. Quantification of scar can be used as an endpoint in clinical studies and therefore standardization is important. In this paper, we propose a segmentation algorithm for LA fibrosis quantification and investigate its performance. The algorithm was validated using numerical phantoms and 15 clinical data sets from patients undergoing LA ablation. We demonstrate that the approach produces good concordance with expert manual delineations. The method offers a standardized quantification technique for evaluation and interpretation of DE-MRI scans.

Keywords: Delayed-Enhancement MRI, Left Atrium, Image Segmentation, Fibrosis.

I. INTRODUCTION

Atrial fibrillation (AF) affects approximately 2.3 million people in the USA with significant co morbidity and mortality[1], [2]. It is a condition that increases the risk of stroke by a factor of six-fold and doubles the mortality rate of patients when compared to age-matched controls. Since it was shown that ectopic beats from the pulmonary veins (PV) give rise to AF [3] the treatment of AF using radiofrequency catheter ablation (RFCA) has become an important and common procedure. In this procedure, ablation lesions are created in a circular fashion around the PV Ostia to electrically isolate the PVs, and thus the ectopic focal points, from the rest of the left atrium (LA). This treatment can provide a cure for the majority of patients and prevent the requirement for long-term pharmacotherapy. However, for a high proportion of patients (15%_46%) [4]_[6], there is recurrence of AF. This normally requires a second or third re-do ablation procedure and thus has a high burden on health care. It is important to select patients who will respond better to RFCA to reduce recurrence rates. Several studies have shown that it is possible to predict the outcome of RFCA procedures from the fibrosis extent in LA [7]_[10]. A scoring system based on the degree of fibrosis has been developed, leading to treatment stratification [8]. Other recent studies have also highlighted the significance of the extent of fibrosis or scar in LA post-ablation for predicting outcome [11], evaluate effectiveness of ablation technologies [12] and helping to gain a better understanding of the left atrial substrate [13].In this context, magnetic resonance imaging (MRI) has been shown to be effective for non-invasive imaging of the LA .In particular, Gadolinium delayed-enhancement (DE) MRI has the ability to detect changes that take place in the LA both pre- and post-ablation and recent studies have shown that it could potentially be useful for selecting suitable candidates for RFCA [8]. DE-MRI is acquired with an inversion recovery gradient echo sequence performed after

administration of Gadolinium yielding an image at an inversion time which is chosen to null the signal from healthy myocardium. Due to the differential washout kinetics of Gadolinium, scar or fibrotic areas are differentiated from healthy tissue. Fibrotic or scar tissues in the myocardium appear with a signal intensity (SI) above normal myocardium. Fig. 1 shows some examples of DE-MRI with intensities significantly higher than myocardium.

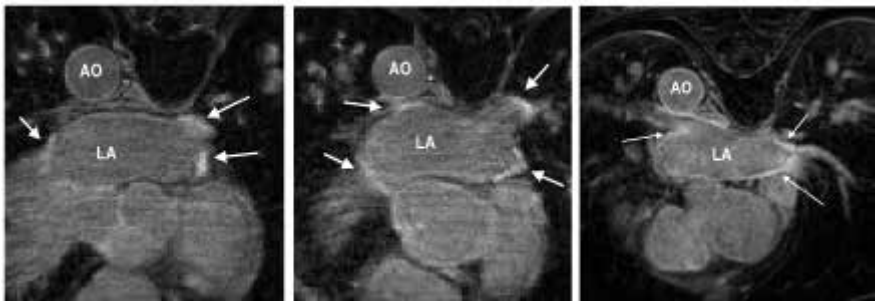

Fig 1. DE-MRI images from three separate patients taken 3 months post-ablation. Arrows indicate areas of enhancement. Abbreviations: AO - aorta, LA - left atrium.

Quantification of scar or fibrosis from DE-MRI is challenging due to various reasons [14]. The thin myocardium of the LA wall leads to low signal-to-noise ratio. Contrast variation in these images can be an issue due to choice of inversion time. Also the complex geometry of the LA results in some transverse slices where a very small section of the anatomy is visible, making manual quantification in these areas highly observer dependent. Finally, patients suffering from AF often have an irregular heart rate and breathing making it hard to acquire good quality respiratory- and cardiac-gated images. Quantification from such images become difficult to auto-mate and manual quantification tends to be highly observer- dependent. In this work, a scar quantification approach is proposed and investigated. The method exploits a well-known image segmentation approach known as graph-cuts [15]. Segmentation is achieved using a combination of scar intensity model priors and Gaussian-tting to tissues in the unseen image to be segmented. The final labelling is achieved by optimizing a cost function using graph-cuts.

1.1 Previous Works

Quantification and segmentation of ventricular scar from DE-MRI images have been studied in several investigations. Refer to Table 1 for a brief summary. A common method for detecting scar or fibrosis is to use a fixed model of thresholding between two and six standard deviations (SD) above the mean intensity of healthy myocardium [16]_[19]. This requires the user to manually outline remote or healthy myocardium. Another common method is the Full-Width- At-Half-Maximum (FWHM) which sets scar to be intensities greater than 50% of manually outlined hyper-enhanced myocardium [19]. Other approaches exist to compute the threshold automatically [17] or by applying clustering[20], [21], or with graph-cuts [22].The aforementioned works were primarily developed for the left ventricle. For the LA, methods have been proposed for endocardial surface-based segmentation [23] and threshold- based volumetric segmentation [7], [14], [24]. In [23], the maximum intensity projection (MIP) of the DE-MRI SI on the segmented LA shell is used to visualize enhancing intensities on the surface. This technique has an important drawback: it is only a visualization of intensities and

thus not a segmentation technique with no volumetric segmentation as output. In [7], a volumetric segmentation of pre-ablation LA fibrosisis proposed by obtaining suitable measurements from the intensity histogram within atrial wall. This has a disadvantage that the LA wall is thin and thus its manual segmentation can have significant inter-observer variation. Other methods have employed fixed models for pre-ablation fibrosis [24] and post-ablation scar [25] with variable thresholding. In summary, a fixed thresholding model cannot handle all the different variabilities encountered in LA DE-MRI and these are both from the varied internal factors (size, distribution and heterogeneity of scar) and varied external factors (resolution, image noise, inversion time, surface coil intensity variation). The inversion time choice can generate the appearance of more or less scar, and change the appropriate scar threshold. Motion blurring also reduces the appearance of scar.

1.2 Contributions

In this work, we present a method for segmenting and thus quantifying LA fibrosis in DE-MRI. It is based on a probabilistic tissue intensity model of DE-MRI data, which is derived from both training and the unseen data. It offers two advantages: 1) It does not require manual outlining of base-line healthy myocardium, and 2) It provides greater accuracy than fixed models with no inter-observer variation. The algorithm was evaluated and compared with existing clinically-used methods using local pixel overlap measures. Performance was analyzed by exploring various scar contrast levels. An abbreviated version of this work was published in
[31] and [32]. In this current version, we present the approach with more details including additional experiments and validation. We also include an automated adaptive step that allows for variation in the scar signal level and avoids sub optimal scar intensity models. Furthermore, we present a much more comprehensive validation of the algorithm on a larger clinical cohort. The algorithm was also used recently in a segmentation challenge [33], segmenting sixty DE-MRI datasets from three imaging centres.

II. CLINICAL AND IMAGING PROTOCOLS

2.1 Patients

15 patients were followed up at 6 months following their first ablation for the treatment of paroxysmal AF. The procedures were carried out in the cardiac catheterization laboratory at St. Thomas Hospital, London, U.K. All patients gave writ- ten permission to take part in this local ethics committee
Approved study.

2.2 Ablation Procedure

A catheter was placed in the coronary sinus to provide a reference for electro anatomic mapping and to enable LA pacing. Two transept punctures were made to access the LA using standard long sheaths (St. Jude Medical, MN, USA). A three-dimensional (3D) LA geometry was created using either Ensite NavX (St. Jude Medical, MN, USA) or CARTO (Biosense Webster, Diamond Bar, CA, USA). A circular mapping catheter was then placed in each PV in turn while the corresponding LA-PV ostium was targeted with wide area circumferential ablation. Energy was delivered through a 3.5 mm irrigated tip catheter with _ow limited to 17 ml/min, power limited to 30 W on the anterior wall and 20 W on the posterior wall and temperature limited to 50_C. Ablation lesions were marked on the LA geometry when there had been an 80% reduction in the local electrogram voltage or after 30 seconds of energy delivery. The clinical endpoint was electrical isolation of all PVs.

2.3 MRI Scanning Procedure

MRI scanning was performed before and after the ablation procedure. Pre-ablation scanning was performed 24 hours prior to the procedure and post-ablation scanning was per- formed 6 months after the procedure. The proposed algorithm in this work was developed and evaluated primarily for post ablation images. All scanning was performed on a 1.5T Achieva scanner (Philips Healthcare, The Netherlands). The examination began with a survey and reference scans, and an interactive scan to determine the four-chamber orientation of the heart. For anatomical information, a 3D magnetic resonance angiography (MRA) scan with whole-heart coverage (1_1_2mm3 acquired, 1_1_1mm3 reconstructed, 20 secs duration) was acquired following the injection of 0.4 ml/kg double dose of a gadolinium-diethylenetriaminepentaacetate (Gd-DTPA) contrast agent. This scan was not cardiac-gated. This scan was followed by a 3D respiratory navigated and cardiac-gated, 3D balanced steady-state free precession (b-SSFP) acquisition in a sagittal orientation with whole- heart coverage (1:3 _ 1:3 _ 2:6mm3 acquired, 1:3 _ 1:3 _ 1:3mm3 reconstructed, 6 mins duration). The scan for the visualization of delayed-enhancement was a 3D ECG-triggered, free breathing inversion recovery (IR) turbo eldecho (TFE) with respiratory-navigated and cardiac-gated with whole heart coverage (0:6 _ 0:6 _ 4mm3 acquired, 0:6_0:6_ 2mm3 reconstructed, 3 mins duration). Data were acquired within a window of 150 ms every one RR interval, with a low-high k-space ordering and spatial pre-saturation
with inversion recovery (SPIR) fat suppression. The IR time delay was determined from the Look Locker sequence, and was set at an inversion time (TI) intermediate between the optimal TIs to null myocardium and blood. This scan was performed approximately 20 mins after contrast administration. The slices were set for complete coverage of both left and right atria. Slice orientation was in the four-chamber view for AF ablation to optimize visualization of the pulmonary veins.Note that the scan times quoted above are actual scan times. Typical respiratory gating efficiency is 50% but this varies considerably in this particular patient population.

2.4 Segmentation Algorithm

Fig. 2 shows an overview of the algorithm. The inputs were a DE-MRI image and a segmentation of the LA from an anatomical scan. The LA segmentation was obtained from the b-SSFP whole-heart scan by an automatic approach based on a statistical shape model [34], and was followed where necessary by manual correction by a human rater (throughout this paper, the terms human rater or observer refer to someone who has experience viewing tomographic images and can correctly identify the LA endocardium and fibrosis in the LA myocardium). The b-SSFP image was chosen over MRA as it was acquired at the same phase in the cardiac cycle as the DE-MRI. The MRA, though it provides better anatomical visualization, was not cardiac gated and it can be dif_cult to resolve the differences between this and the DE-MRI with registration. The anatomical images were registered to the DE images using the DICOM header data, and then refined by rigid and affine registration steps [35]. Affine registration was necessary to account for the differing PV angles in the scans. This defined the endocardial LA boundary in the DE images.

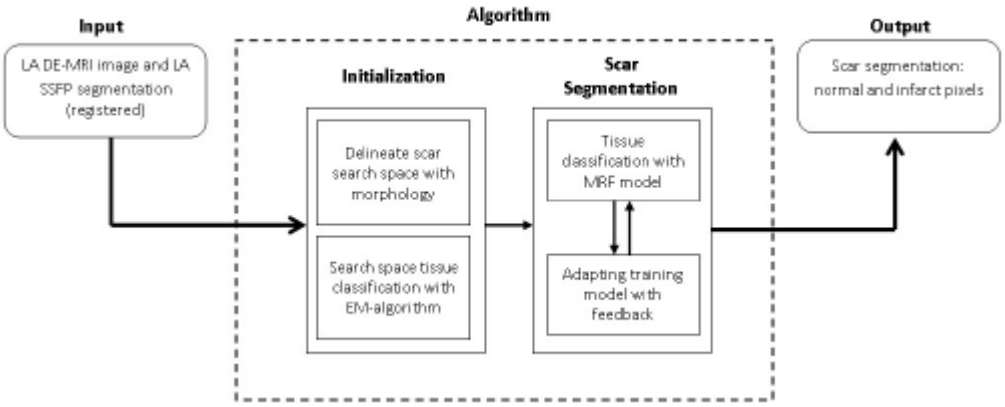

FIGURE 2. An overview of the steps involved in the segmentation process. The pipeline takes as input MRI images and outputs binary segmentations (rounded boxes). The processing pipeline is illustrated here with each separate stage in the algorithm. Smaller boxes represent sub-stages. The scar segmentation stage is iterative as indicated by the bi-directional arrows.

2.5 Scar Segmentation

Segmentation of scars from DE-MRI images can be defined as assigning a label *fp* €{non-scar; scar} for every voxel *p* in the search space of the image. The search space is defined as a region _3 mm from the endocardial border obtained from the atrial geometry extraction. This is within the limits of atrial wall [23]. Given the observed intensities in the atrial wall and prior knowledge of scars, the segmentation problem is solved using a probabilistic framework where the maximum *a posteriori* (MAP) estimate is computed using Bayes' theorem:

Arg max p(f/I)=(p(I/f) p(f))/p(I)

F

where **f** is the total label configuration and **I** are all observed intensities in the image. The image likelihood *p*(**I**/**f**) describes how likely is the observed image given a label configuration **f**. The prior *p*(**f**) encodes any prior knowledge of the healthy and scar tissue classes.

2.6 Intensity Models

The likelihood *p*(**I**j**f**) of the observed intensities in the image can be estimated. Assuming that the voxel intensities are independent, the total likelihood for the image is given as:

$$p(\mathbf{I}|\mathbf{f}) = \prod_{p \in I} p(I_p|f_p)$$

The negative logarithm or the log-likelihood gives the total intensity energy contributed by each voxel:

$$E_{\text{data}} = -\sum_{p \in I} \ln p(I_p|f_p)$$

We first consider the intensity energy contribution from the scar tissue class, i.e. for the function *p*(**I**/*fp* = 1) and then for the non-scar class.

2.7 Smoothness Constraint

To ensure smoothness and avoid discontinuities in the final segmentation, the *E*prior term of the MRF energy function in Eq. 3 penalised for assigning different labels to neighbouring voxels sharing similar intensity levels. The Lorentzian error norm was employed, which is a robust metric for measuring intensity differences within a neighbourhood

$$\varphi(p,q) = 1 + \frac{1}{2}\left(\frac{|I_p - I_q|}{\sigma}\right)^2$$

The scale _ can be estimated from the DE-MRI image and depends on the variance of the actual scar and non-scar tissue class intensity distributions. With decreasing scale, the algorithm becomes less forgiving to small differences in intensities. Given that it is technically challenging to acquire high quality DE-MRI scans that show a clear distinction between scar and non-scar tissue, a larger value for the scale is almost always preferred

2.8 Optimization

The optimization of the MRF energy function in Eq. 2 yields the desired image segmentation for scar. In [15], it was shown that it is possible to _nd the global optimum of functions of this type using the graph-cut method. In the graph-cut method, the MRF energy function is converted to a directional graph and the minimum *s-t* cut gives the desired segmenta- tion. A graph *G* D h*V*; *E*i with two terminal nodes *s* and *t* representing the scar and healthy segmentation labels. The graph has a set of nodes *V* for every voxel in the image and *E* is the set of edges connecting these nodes (see Fig. 3). There are edges connecting every voxel to the two terminal nodes also known as the *t*-links. There are also edges connecting neighbouring nodes called the *n*-links. Each of these edges has a non-negative weight assigned to it. The *t*-link edge weights are obtained from the non-scar and scar tissue intensity priors in Eqs. 8 and 6 respectively. The *n*-link edge weights are obtained from Eq. 9. An *s-t* cut on *G* partitions the nodes into two disjoint sets belonging to either the foreground or the background classes. Every *s-t* cut incurs a cost and corresponds to a segmentation labelling **f**.

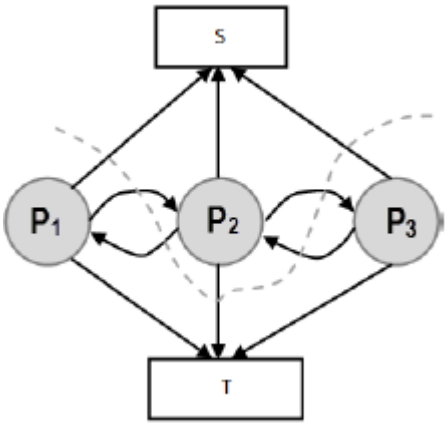

Fig 3. An illustration of an s-t cut through a simple graph that represents the energy functional of an image containing only 3 voxels.

The total cost of an *s-t* cut is equivalent to the sum of the edge weights the cut passes through. Fig. 3 graph of an image with only 3 voxels computes a possible segmentation. Note how the *t*-links are assigned a value based on

the affinity of the node to the particular class label. In a similar way, the *n*-links represent affinity for neighbouring voxels, holding nodes with similar intensities together and resisting to a cut passing through them resulting in a labeling of neighbouring voxels into two separate tissue classes.

III. EXPERIMENTS

The algorithm was evaluated on both numerical phantom andreal patient MRI datasets as described below.

3.1 Numerical Phantom Data

In the rest of the paper, the true location of scar is referred to as the ground-truth for scar. The extent of scarring during ablation is non-deterministic and there is also confounding pre-ablation fibrosis. Therefore, identifying locations where ablations were made is not sufficient to be a surrogate for the ground truth for scar. Moreover, there is a high degree of inter- and intra-observer variability in manual segmentations of scar. These make evaluating algorithms more difficult and challenging. To overcome these issues, numerical phantoms were employed to extensively validate the algorithm.

3.1.1 Phantom Construction

The phantom was constructed in a four step process. The result of some steps is shown in Fig. 4. In the _rst step the LA geometry was extracted from a typical patient dataset. In the second step, a 2.5 mm wall was constructed around the LA. This represented LA wall. In a third step, regions were manually drawn within the constructed LA wall; these regions represented scar. In the final fourth step, intensities were sampled randomly from pre-determined distributions. These distributions belong to LA wall and blood-pool, and are measured and obtained from real MRI data. This ensured likeness of the phantoms to real MRI. Scar was filled with intensities from blood-pool *but* multiplied by a factor of 1.0 or above, and thus an SC-BP ratio of at-least 1.0 was maintained. This ratio emulated the selection of different inversion times for nulling the blood pool and was varied in experiments that follow. It is important to simulate partial voluming, anisotropic voxel sizes and noise in the phantoms. An anisotropic blur was applied with a kernel size of 2 mm in the through-plane direction and 1 mm in the in-plane direction. Gaussian white noise (_ D 0; _ D 1) was added to the image.

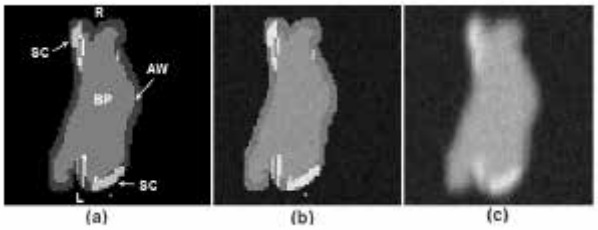

Fig 4. Images of a single-slice through a phantom taken at each stage of its construction process: (a) the phantom template with blood pool (BP) and atrial wall (AW) outlined semi-automatically using morphological dilation; scar (SC) drawn manually. (b) Assignment of intensity levels drawn randomly from pre-defined Gaussian distributions, with separate distributions for each tissue class. (c) In-plane and through-plane blurring followed by the addition of Gaussian white noise. Abbreviations: L - left side, R - right side.

3.1.2 Phantom Experiments

Numerical phantoms were generated by varying the SC-BP contrast ratio between 1.0 to 3.0. Some instances of these phantoms can be seen in Fig. 5. This evaluated the algorithm's performance on scar with varying contrast in relation to blood pool. The noise in the phantoms was maintained at signal-to-noise (SNR) of 9.0. This was the average SNR observed on a cohort of clinical datasets. Training (*n* D 50) and testing (*n* D 50) data sets were generated accordingly. To make training as realistic as possible, it was separately trained on SC-BP ratios: 1.5_1.8 and 1.8_2.1. The algorithm was compared to ground-truth using the Dice overlap co-efficient [37].

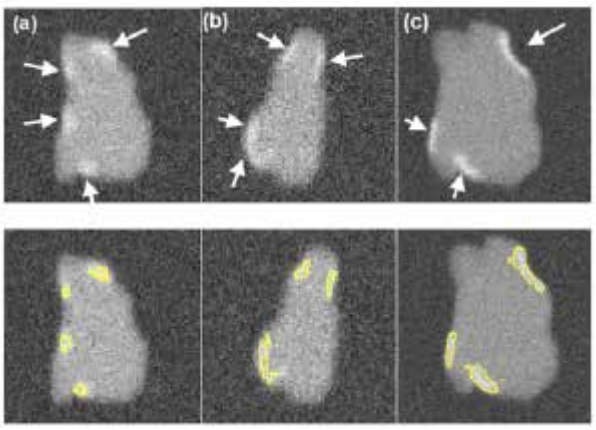

FIGURE 5. Single slices through three different phantoms with numerically generated scars indicated by the arrows (Top row). SC-BP contrast is varied keeping SNR constant at 9.0. SC-BP: (a) 1.4, (b) 1.6 and (c) 1.8. The segmentations from the algorithm are also shown (Bottom row). In a separate experiment, the SNR was varied from 4 to 16 along with the SC-BP contrast ratios. A single instance of the algorithm was tested and this was trained on the SC-BP range 1.8_2.1. The Dice overlap of the segmentation with ground truth was compared. In addition to the above experiments on scar enhancement and noise variation, the performance of the algorithm and fixed models (FWHM and *n*-SD) were compared on the same dataset. Five separate phantoms were used from which 200 different scarred regions were identified and their SC-BP contrast ratio noted. The accuracy with each method segmented each of the 200 regions was measured with Dice and reported.

3.1.3 Clinical Data

A total of 15 clinical human datasets were available. In these set of experiments, segmentations from the algorithm were compared to the combined manual segmentations of three observers. In addition to this, the algorithm was also compared to fixed models: FWHM and *n*-SD methods. Training for the algorithm was accomplished using the leave-one-out principle, where 14/15 datasets were used for training and 1/15 used for testing. In the test scan, segmentation performance was measured both locally and globally for the image. For local comparison, performance on individual sections of scar was measured (a total of 155 regions were considered) and for a global comparison, total scar volume was measured. The pre-processing (left atrium geometry extraction and registration) was the same for each approach. Three experienced observers manually segmented scars in each DE-MRI scan. They were combined to generate a consensus segmentation or *pseudo*-ground truth for each scan. This is necessary in order to consolidate inter-observer variability's. Segmentations were combined using the STAPLE algorithm described in [38]. For each voxel, a probability estimate for the scar label could be computed. The STAPLE ground-truth was then be obtained by considering voxels to be scar if their probability is greater than 0.7, or 70%. This is a reasonable threshold capable of generating a strong

consensus segmentation (In [38] the authors chose a lower consensus at 50%). To explore this threshold further, an experiment was performed by varying the threshold. Segmentations were available from five experienced observers on a random subset of the clinical datasets. The segmentations were combined using STAPLE and three thresholds were considered:1) < 20%, 2) _ 20% and 3) _ 70%. This generated different consensus segmentations with varying degrees of consensus against which the algorithm's performance was measured. Finally, to further explore whether better training of the algorithm leads to better segmentations and thus better

performance, different instances of the algorithm are evaluated by incrementing the number of training set.
It is important to note that segmentations from the proposed algorithm were obtained without any user interact-tion necessary at any step of the algorithm. The most com putationally demanding step was that of graph-cuts. On images of the resolution described above, there are typically 50 000_100 000 nodes that require processing. However, each step of the iterative process took less than a minute. The total running time of the proposed approach is less than a minute on a 2.5 GHz PC.

3.2 Evaluation Metrics

To our experience, there is no single metric which works best for comparing segmentation overlaps. We chose two different metrics to quantify segmentation overlap.

3.2.1 Regional Overlap

The Dice co-efficient of similarity is a well-known metric [37]. It is given by:

$$D = \frac{2|X \cap Y|}{|X| + |Y|} \times 100$$

where X is the region in ground-truth and Y is the region in the algorithm. j$X \setminus Y$ j is total overlapping pixels and jXj; jY j are total number of pixels in each region. A Dice of 100 denotes perfect overlap.

3.2.1 Sensitivity And Specificity

The proportion of true positives and true negatives in the detection process was analyzed by means of Receiver Operating Characteristic (ROC) curves where possible.

3.2.3 Total Scar Volume

Segmentations were also compared by measuring the total scar volume. This is mostly how scar is quantified and inter preted in clinical studies [39] and also serves as an important indicator for the total scar burden on the atrium.

IV. RESULTS

4.1 Numerical Phantoms

4.1.1 Scar Contrast

Fig. 6 show results from testing the algorithm on phantoms generated by varying the SC-BP contrast. Segmentation overlap with known true location of scarwas measured using Dice.The algorithm performs well

within its training range with median Dice _ 80 in both ranges: 1:5 _ SC-BP _ 1:8 [Fig. 6(a)] and 1:8 _ SC-BP _ 2:2 [Fig. 6(b)]. Outside its training area, the algorithm showed that it is able to adapt to excellent SC-BP contrast (_ 2:2) and good segmentations were achieved. Values of SC-BP explored in this experiment included realistic DE-MRI values but SC-BP _ 3:0 is very difficult to achieve in practice. To summarise, this experiment evaluated the algorithm across a wide dynamic SC-BP con- trast range and the algorithm's approximation of ground truth was found to be good.

4.1.2 Noise Variation

Fig. 7 show results from testing the algorithm on phantoms generated by varying SNR. The SNR is varied between 4 and 16. The algorithm is trained on datasets generated with SC-BP ranging between 1:8 _ SC-BP _ 2:1. Results show that SC-BP dictates over SNR for achieving good segmentations. Note segmentations are poor with SC-BP D 1:2 when SNR D 4 and with SNR D 16. But this is improved when SC-BP _ 1:8 demonstrating that the algorithm is robust to noise. SNR in actual DE-MRI is typically around 9.0 and the algorithm is seen to perform well in this range.

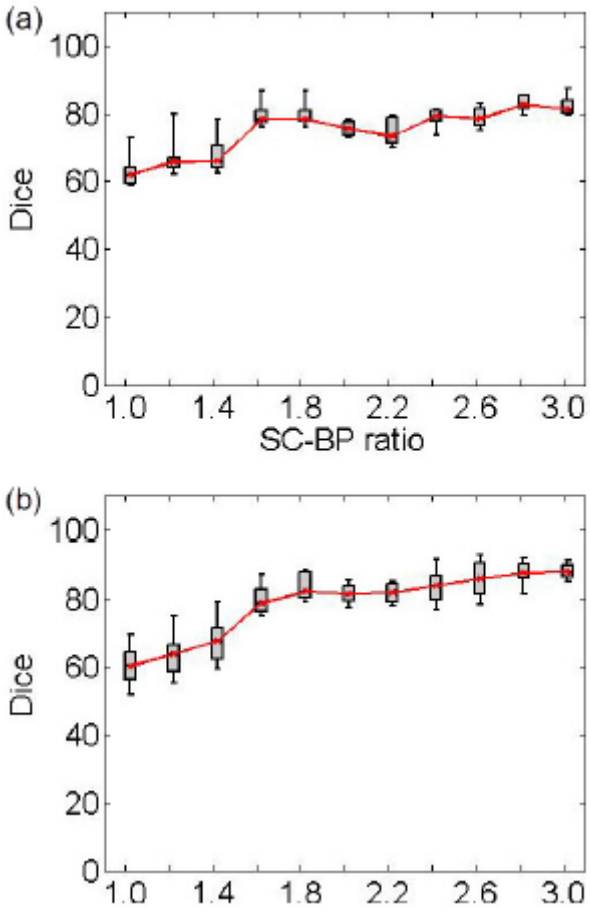

Fig 6. Performance of algorithm on numerical phantoms with increasing SC-BP contrast and SNR fixed at 9.0. Each graph is an instance of the algorithm: (a) trained on 1.5 to 1.8, and (b) trained on 1.8 to 2.1. The trend-lines show the median. Boxes in the plot indicate the 9th, 25th, 50th, 75th and 91st percentiles

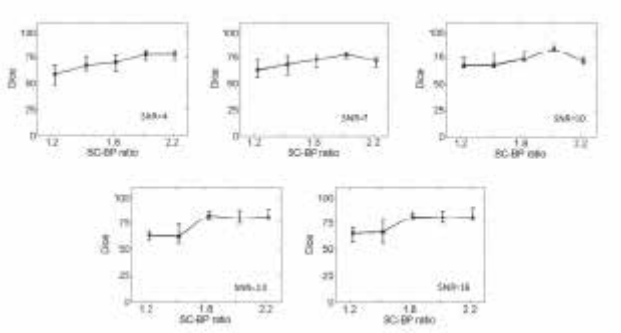

Fig 7. Performance of algorithm on numerical phantoms with varying SNR. The SNR is varied between 4 to 16. The median Dice segmentation overlap is plotted for the trend line shown.

4.1.3 Comparison With Fixed Models

Fig. 8 show how the algorithm and fixed models per- formed on the same datasets. A total of 200 scarred regions were identified in live anatomically-unique phantoms. Their SC-BP contrast were computed and the overlap accuracy noted for each method. This allowed each method to be evaluated on specific SC-BP ratios and the plots in Fig. 8 show the segmentation accuracy trend. Fixed models 3,4,6-SD generated better segmentations than FWHM when scar contrast is between 1.2 to 2.2. However, FWHM improved substantially with higher scar contrast (SC-BP > 2:2 in Fig. 8), which is when the 50 percent cut-off was more reasonable. Overall, as illustrated in Fig. 8, the algorithm maintained good accuracy when compared to fixed models in numerical phantoms.

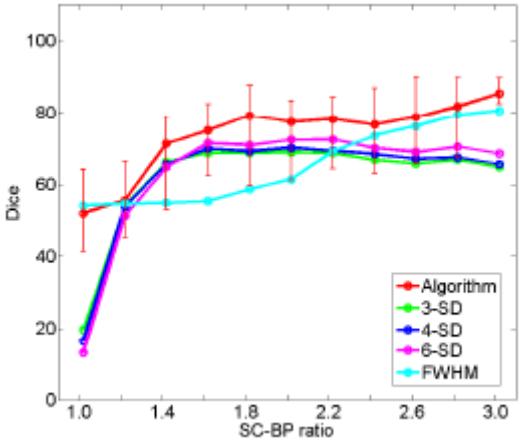

Fig 8. Comparing performance of algorithm with fixed models on numerical phantoms. Fixed models namely 3-SD, 4-SD, 6-SD and FWHM were evaluated. The trend-lines show the median Dice computed from 200 different scarred regions obtained from 5 separate phantoms

The failure of FWHM revealed in this experiment is further illustrated in Fig. 9 (see columns 1 and 2). When the contrast in scar is not high, 50 percent of maximal signal as considered in FWHM, is not optimal and leaks in segmentation are inevitable [Fig. 9 (row 3)].

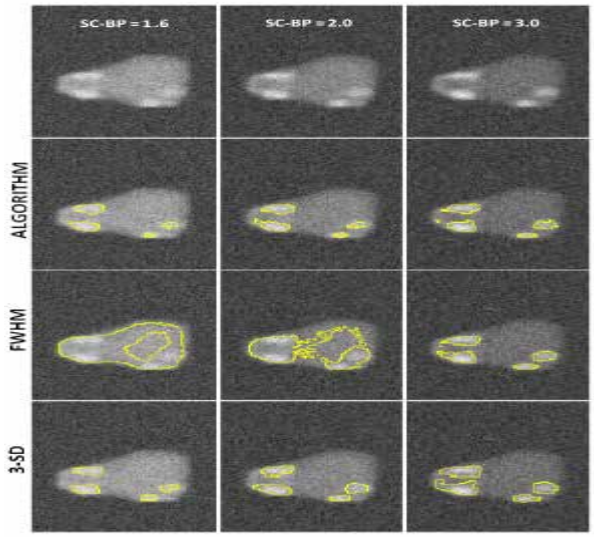

Fig 9. Instances where 50% cut-off in FWHM is not optimal. First row: Original images of phantom with variable scar contrast. Second row: Algorithm's segmentation. Third row: Segmentation from FWHM with leaks. Fourth row: Segmentation from 3-SD.

4.2 Clinical Data

4.2.1 Comparison With Fixed Models Using Overlap Metric

In the clinical datasets, performance of algorithm and fixed models were tested by measuring overlap with pseudo ground-truth (STAPLE) and comparing segmentation outputs in terms of scar volumes. For assessing performance based on overlap, each method was tested on individual SC-BP contrast levels: 1.0, 1.4, 1.8, 2.2, 2.6 and 3.0. This was possible by sampling 155 individual scarred regions from the clinical scans, measuring their SC-BP contrast ratio and testing how well each method segmented it. Results are given in Fig. 10.

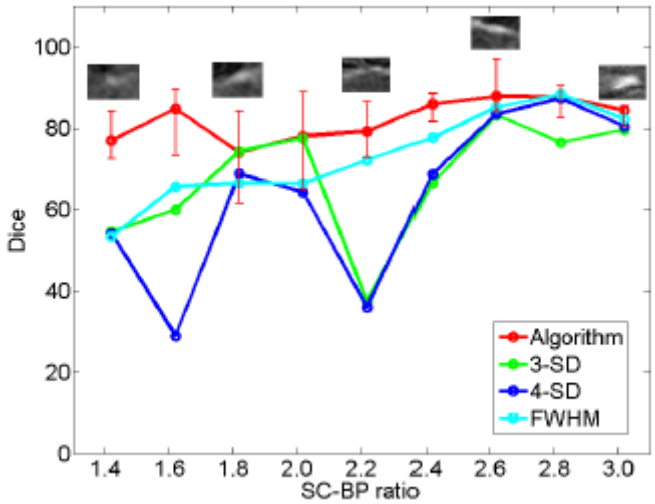

FIGURE 10. Comparing performance of fixed models with algorithm on patient scans. The performance over a total of 155 scarred regions are shown here. The trend-lines show the median. Five example snapshots of scar are also given to illustrate SC-BP contrast levels. Note SC-BP ratios analysed range from 1.4 to 3.0. Fixed models perform less accurately than the algorithm when SC-BP is less than 2.5. At excellent and rarely attainable SC-BP levels (>> 2:5),

this trend changes and all models perform equally well. FWHM and the algorithm perform consistently across the entire SC-BP range used in this experiment, with 3- and 4-SD models outputting less accurate segmentations on scar at certain SC-BP contrast levels (1.6,2.2). This is because scar is not adequately segmented by 3- or4-SD due to non-overlapping intensities between model and actual. These results highlight that the algorithm performs consistently on actual DE-MRI and across realistic SC-BP levels. Performance of fixed models is found to be variable.

4.2.2 Comparison with Fixed Models Using Quantified Volume

Assessment of performance using total scar volume reported by each method is important as this is mostly how scar is quantified and interpreted for clinical studies. Results obtained from scar volume quantified by each *run* of method are given in Fig. 11 for six clinical datasets. Each method was run three separate times with inputs (i.e. normal and hyper-enhanced myocardium) fed from three independent observers. Volume reported by each method was compared to the volume reported by three independent experienced observers (see *Manual method* in Fig. 11).

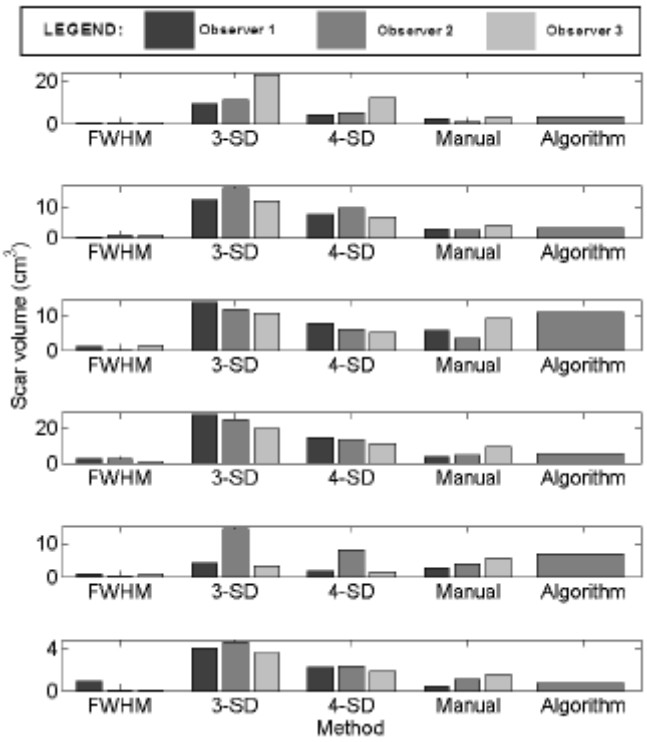

Fig 11. Assessment of inter-observer variation in fixed models, manual segmentation and algorithm. Six clinical cases are illustrated here

The algorithm correlated well with manual scar volumes. All three runs of the algorithm produced the same result as depicted by the single bar in Fig. 11. All other methods showed vari- ations in the quantified volume. This variation was primarily due to observer variability in selecting normal or hyper-enhanced tissue required for _xed models. This high- lights that a standardized quantification for scar using a fixed model approach (FWHM and SD) can be difficult to achieve.

4.2.3 Qualitative Comparison On De-Mri Scans

Segmentation quality was assessed by overlaying region contours over the original DE-MRI slices. It was generally observed that in images with excellent SC-BP contrast, contours followed scar boundaries accurately in both algorithm and fixed models. Fixed models 3 and 6-SD were less accurate. An example is shown in Fig. 15 where segmentations similar to the consensus segmentation [Fig. 15(b)] could be obtained. Fixed models showed poor correlation when the SC-BP contrast is not sufficiently high. An example is shown in Fig. 16 where FWHM and the algorithm fared well with the algorithm providing a better approximation to the consensus segmentation. Fixed models 3 and 6-SD have gross errors in their segmentations due to a large overlap of intensities between their scar model and actual healthy tissue. Such segmentations are not usable for clinical studies and the operator would require to resort to threshold re-adjustment.

4.2.4 Analyzing Algorithm Performance By Varying Consensus Levels Of Pseudo Ground Truth

The algorithm's performance on a subset of clinical datasets was evaluated by varying the STAPLE threshold and thus the level or strength of the consensus segmentation. Results are plotted in Fig. 12 showing segmentation overlap on three consensus levels. There was a small difference in the algorithm's performance noted when SC-BP contrast levels were low. With higher SC-BP the performance was nearly similar. When SC-BP contrast is poor, the consensus or agreement between observers can be low. By lowering the acceptable consensus threshold (to 20%), dubious pixels are included in the ground truth where 2/10 observers would agree that it is scar. As the algorithm generally selects pixels which have close affinity to its models and priors, dubious pixels are omitted by the algorithm. There is a decrease in performance when segmentations with low consensus are presented.

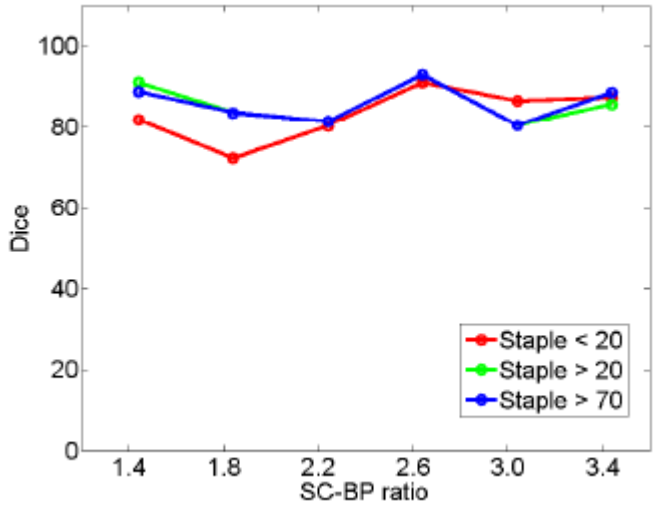

Fig 12. Performance trends of the algorithm on STAPLE consensus ground truths. Each curve represents performance on consensus segmentations, with consensus varied from 20% (weak) to 70% (strong).

4.2.5 Analyzing Algorithm Performance By Varying Strength Of The Training Set

The algorithm's training set was incrementally increased and its segmentation overlap performance was noted. There was little notable difference in the performance. Results are plotted in Fig. 13. Training had an impact on

performance only when the training set and test set had similar SC-BP contrast levels. If these vastly differ, initial iterations of the algorithm generate poor segmentations and these progressively become better in later iterations when the scar intensity model is continuously adapted with feedback from previous iterations (refer to 'adapting training step' in Fig. 2).

4.2.6 Roc Analysis

The true positive and true negatives rates were analyzed by looking at sensitivity and specifity of the algorithm and the fixed-models. A ROC curve between sensitivity and specificity was only plotted, where each point on the curve represented a decision threshold. The plots are given in Fig. 14 for the *n*-SD fixed model's ROC curve, where the decision threshold was varied between *n* D 1 to *n* D 6. Since both the algorithm and FWHM do not require a decision threshold for obtaining segmentations, their overall sensitivity and specificity on all datasets was plotted

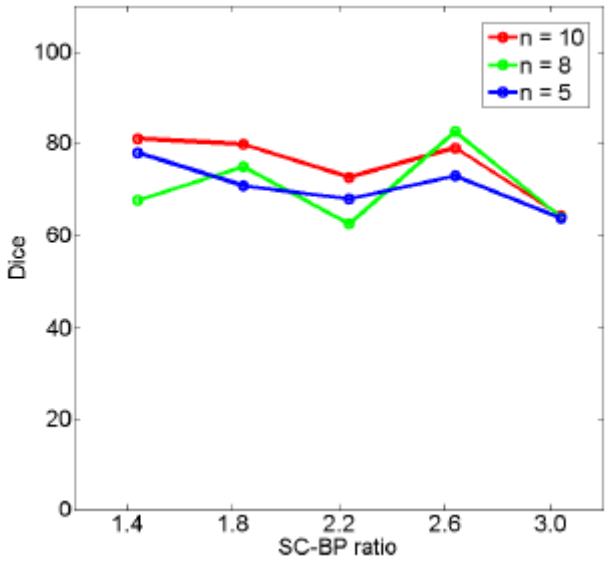

Fig 13. Performance trends of the algorithm by increasing the training set. Each curve represents an instance of the algorithm trained on n D 9; 7; 5 datasets.

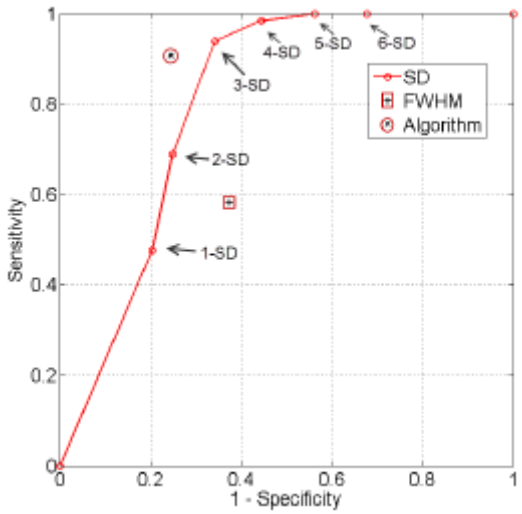

Fig 14. ROC analysis of the algorithm, FWHM and n-SD method. The ROC curve is only plotted for the n-SD method and the overall sensitivity and specificity is plotted for the parameter-less proposed algorithm and FWHM.

The *n*-SD fixed model approach has low specificity for *n* D 1; 2; 3 and increasingly mislabelled healthy tissues as scar. However, its higher sensitivity indicated that scar tissues are mostly labelled correctly. This reversed with *n* D 4; 5; 6 and the trade-offs between sensitivity and specificity was seen to be optimal when *n* D 4; 5. Overall, the algorithm maintained both higher sensitivity and specificity than the fixed models as indicated in the ROC plot. The FWHM fell behind in this global ROC analysis and this is in-line with earlier tests on individual regions where it was shown that its 50% cut-off is too low for scar with low SC-BP, but more suitable for high SC-BP ratios.

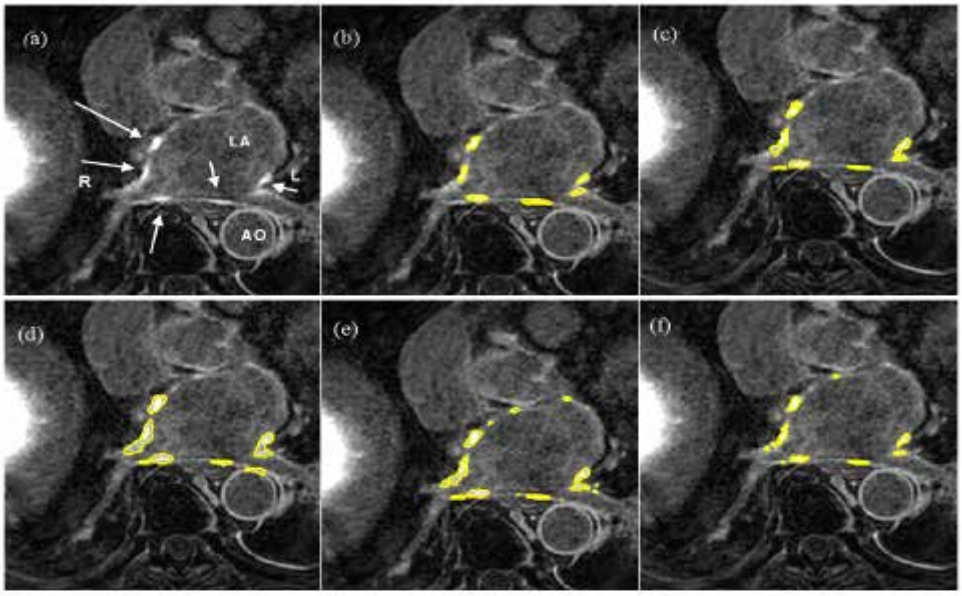

FIGURE 15. Segmentations on clinical scans I: (a) original scan, (b) consensus STAPLE segmentation, (c) Algorithm, (d) FWHM, (e) 3-SD, (f) 6-SD. Arrows show enhancement. This scan has excellent SC-BP contrast and all methods except 3-SD and 6-SD demonstrate good accuracy. Abbreviations: AO - Aorta, LA - Left atrium, R - Right side, L - left side.

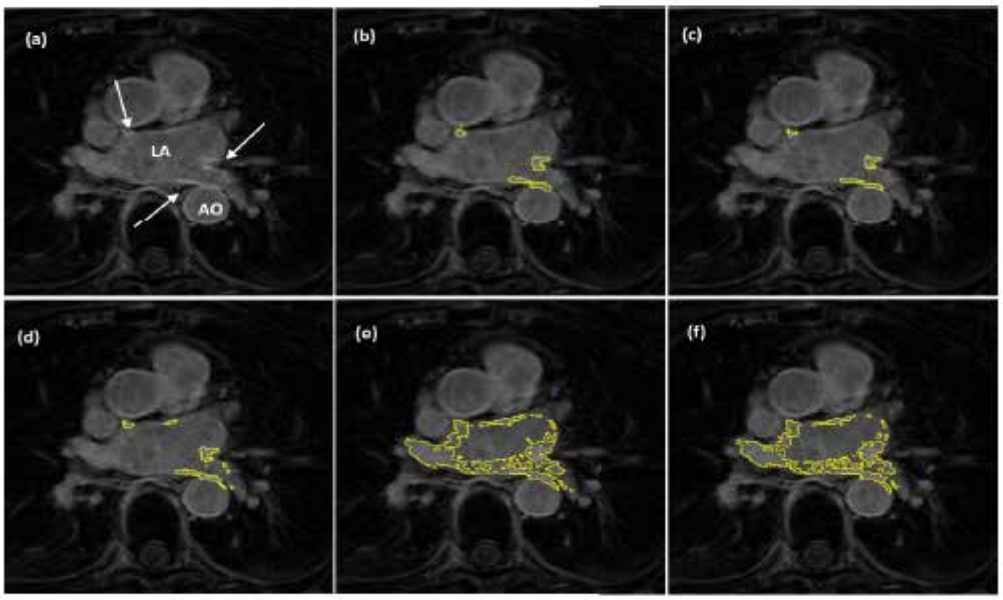

Fig 16. Segmentations on clinical scans II: (a) original scan, (b) consensus STAPLE segmentation, (c) Algorithm, (d) FWHM, (e) 3-SD, (f) 6-SD. Arrows show enhancement. This scan has excellent SC-BP contrast and all methods except 3-SD and 6-SD demonstrate good accuracy.Abbreviations: AO - Aorta, LA - Left atrium, R - Right side, L - left side.

V. DISCUSSION

In this work a segmentation algorithm was investigated for fast quantification of fibrosis in DE-MRI scans. The proposed algorithm offers the following advantages: 1) Segments fibrosis without requiring a manual outline of remote or healthy myocardium. This is beneficial since remote myocardium tends to have low SNR and manual selection suffers from\ high observer variability. 2) The algorithm does not routinely generate false positives as was observed in existing fixed model methods: FWHM and *n*-SD. 3) The algorithm is developed particularly for left atrial fibrosis segmentation and all present approaches were developed for ventricle scans. 4) Analysis of DE-MRI scans was shortened to an average of 30 seconds when compared to existing semi-automatic approaches requiring 2 minutes per scan on average. The algorithm along with existing approaches was tested on both numerical phantoms and clinical datasets. Numerical phantoms provided with a wide dynamic range of variation.

VI. CONCLUSION

DE-MRI is becoming a preferred method for non-invasive imaging of myocardial scar. The amount of scar predicts whether a patient will respond to RFCA procedures. Thus accurately quantifying scar is important and has implications in patient selection for RFCA. Currently, SD and FWHM fixed thresholding models are frequently utilized clinically to quantify scar due to their simplicity. Present literature has only evaluated these methods using global image measures and thus their deficiencies could not be noted. In this work, there are two important contributions: 1) SD and FWHM fixed models are evaluated on individual regions of scar and thus various scar contrast ratios are examined to show they fail when some contrast levels do not suit the selected threshold in SD or 50% cut-off in FWHM. This is further confirmed and validated in numerical phantoms. 2) the proposed algorithm has the potential to standardize quantification of scar from routine clinical scans; it

requires no threshold selection and is shown to be more sensitive and specific than SD and FWHM in scar detection. Accurate and standardized quantification will allow appropriate selection of patient candidates for RFCA. This could considerably reduce the recurrence rates, procedure risk and high financial burden associated with unsuccessful RFCA treatment. Patients not deemed appropriate for RFCA based on their scar assessment could be treated far less invasively using drug therapy. A standardized quantification of scar in DE-MRI is thus necessary.

ACKNOWLEDGMENT

Dandu Nasreen Sulthana born in kalakada, chittoor dist, A.P, India in 1992. He received B.Tech Degree in Electronics & Communication Engg. From JNT University, Anantapur, India. Presently he is pursuing M.Tech (DECS) from Annamacharya Institute of Technology & Sciences, Rajampet, A.P., India.

S. Asif Hussain did his B. Tech and M.Tech,P.hd in Electronics&Communication Engineering (ECE) from JNT University,Anantapur, India. He is an associative professor in the Department of ECE at the Annamacharya Institute of Technology & Sciences (an Autonomous Institute), in Rajampet, Andhra Pradesh. He is also the Academic Council Member of the Institute. His research interests include signal processing, time series analysis, and biomedical image processing. He is a life member of professional bodies like ISTE, BMESI,IACSIT, IAENG etc. He has presented many research papers at national and international conferences.

REFERENCES

[1] A. Go *et al.*, ``Prevalence of diagnosed atrial fibrillation in adults," *J. Amer. Med. Assoc.*, vol. 285, no. 18, pp. 2370_2375, 2001.

[2] J. P. Piccini *et al.*, ``Incidence and prevalence of atrial fibrillation and associated mortality among medicare beneficiaries: 1993_2007," *Circulat., Cardiovascular Qual. Outcomes*, vol. 5, no. 1, pp. 85_93, 2012.

[3] M. Haissaguerre *et al.*, ``Spontaneous initiation of atrial fibrillation by ectopic beats originating in the pulmonary veins," *New England J. Med.*, vol. 339, no. 10, pp. 659_666, 1998.

[4] C. Pappone *et al.*, ``Circumferential radiofrequency ablation of pulmonary vein ostia: A new anatomic approach for curing atrial fibrillation," *Circulation*, vol. 102, no. 21, pp. 2619_2628, 2000.

[5] H. Oral *et al.*, ``Circumferential pulmonary-vein ablation for chronic atrial fibrillation," *New England J. Med.*, vol. 354, no. 9, pp. 934_41, 2006.

[6] C. Sohns *et al.*, ``Quantitative magnetic resonance imaging analysis of the relationship between contact force and left atrial scar formation after catheter ablation of atrial fibrillation," *J. Cardiovascular Electrophysiol.*, vol. 25, no. 2, pp. 138_145, 2014.VOLUME 2, 2014 1

MAES BASED IMAGE TRANSMISSION TECHNIQUE FOR IMPROVING THE LEVEL OF SECURITY

Sasikala.Y[1], Riyazuddin.K[2]

[1]*M.Tech Scholar, E.C.E, AITS, Rajampet, Andhra Pradesh,(India)*

[2]*Assistant Professor, E.C.E, AITS, Rajampet, Andhra Pradesh,(India)*

ABSTRACT

The security and performance analysis of encryption has been performed using the histograms, correlation coefficients, information entropy, key sensitivity analysis, differential analysis, key space analysis, encryption/decryption rate analysis etc. A new secure image transmission technique is proposed, which transforms automatically a given large-volume secret image into a secret-fragment-visible mosaic image of same size. A scheme of handling the overflows/underflow in the converted pixel color values by recording the color differences in the untransformed color space is also proposed. The information required for recovering the secret image is embedded into the created mosaic image by a lossless data hiding scheme using a key. In this proposed method the key standards depends on the modification to the Advanced Encryption Standards(MAES) to reflect a high level security and better image encryption

Keywords: Color Transformation, Data Hiding, Image Encryption, Mosaic Image, Secuer Image Transmission

I.INTRODUCTION

Currently it is an important ascept to protect confidential data from unauthorized access. Multimedia content may be text audio, still images, animation and video. The image from various sources are frequently utilized and transmitted through the internet for various applications ,such as medical imaging system, and military image databases. These images usually contain confidential information so that they should be protected from leakages during transmission. There are two types of techniques used for secure image transmission .They are image encryption and data hiding . Image encryption uses natural property of an image, such as high redundancy and strong spatial correlation. Shannon's confusion and diffusion properties are used get an encrypted image, The encrypted image contains noise, the attacker's know the correct key they didn't get secret image. The encrypted image is a noise image so that no one can obtain. The secret image from it unless he/she has the correct key. However, the encrypt image is a meaningless file, which cannot provide additional information before decryption and may arouse an attacker's attention during transmission due to its randomness in form .An alternative to avoid this problem is data hiding that hides a secret message into a cover images so that no one can realize the existence of the secret data, in which the data type of the secret message investigated in this paper is an image .Existing data hiding methods mainly utilize the techniques of LSB substitution, histogram shifting, difference expansion, prediction-error expansion, recursive histogram modification and discrete cosine/wavelet transformations. However, in order to reduce the distortion of the resulting image, an upper bound for the distortion value is usually set on the payload of the cover image. In this paper, a new technique

for secure image transmission is proposed, which transforms a secret image into a meaningful mosaic image with the same size and looking like a preselected target image. The transformation process in controlled by a secret key, and only with the key can a person recover the secret image nearly lossless form the mosaic image. The proposed method is inspired by Lai and Tsai, in which a new type of computer at image, called secret-fragment-visible mosaic image, was proposed. The mosaic image is the result of rearrangement of the fragments of a secret image in disguise of another image called to target image preselected from a database.

fig 1.Result yield by the proposed method. (a) Secret image. (b) Target image. (c) Secret-fragment-visible mosaic image created from (d) By the proposed method.

But an obvious weakness of Lai and Tsai is the requirement of a large image database so that the selected target image. Using their method, the user is not allowed to select freely his/her favourite image for use as the target image. It is therefore desired in this study to remove this weakness of the method, while keeping in merit, that is, it is aimed to design a new method that can transform a secret image into a secret fragment-visible mosaic image of the same size that has the visual appearance of any freely selected target image without the need of a database. The proposed method is new in that a meaningful mosaic image is created in contrast with the image encryption method that only creates meaningless noise images. Also, the proposed method can transform a secret image into a distinguishing mosaic image without compression,

II.IDEAS OF THE PROPOSED METHOD

The proposed method includes two main phases as shown by the flow diagram of fig.

1) Mosaic image creation and
2) Secret image recovery.

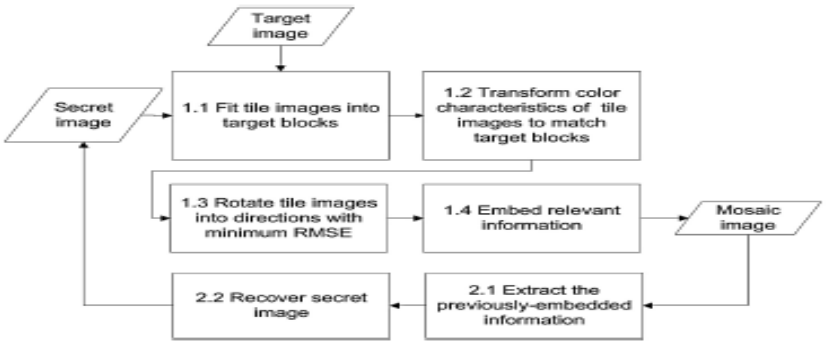

Fig 2: Flow diagram of the proposed method

In the first phase, a mosaic image is yielded, which consists of the fragments of an input secret image with colour corrections according to a similarity criterion based on colour variations. The phases includes four stages

1.Fitting the tile images of the secret image into the target blocks of a preselected target images.

2.Transforming the colour characteristic of each tile image in the secret image to become that of the corresponding target block in the target images.

3.Rotating each tile image into a direction with the minimum RMSE value with respect to its corresponding target block;

4.Embedding relevant information into to created mosaic image for future recovery of the secret image. In the second phase, the embedded information is extracted to recovery nearly losslessly the secret image from the generated mosaic image. The phase includes two stages.1) Extracting the embedded information for secret image recovery from the mosaic image and 2) Recovering the secret image using the extracted information.

III.IDEAS OF MOSAIC IMAGE GENERATION

Problems encounterd in generating mosaic images are discussed in this section with solution to them proposed.

3.1 Color Transformation between blocks

In the first phase of the proposed method, each tile image *T* in the given secret image is fit into a target block *B* in a preselected target image. Since the color characteristics of *T* and *B* are different from each-other , how to change their color distributions to make them look alike is the main issue here. Reinhard *et al.* proposed a color transfer scheme in this aspect, which converts the color characteristic of an image to be that of another in the l$\alpha\beta$ color space. This idea is an answer to the issue and is adopted in this paper, except that the RGB color space instead of the l$\alpha\beta$ one is used to reduce the volume of the required information for recovery of the original secret image. More specifically, let *T* and *B* be described as two pixel sets $\{p_1,p_2,p_3,\}$,and $\{p'_1,p'_2,p'_3,\}$, respectively. Let the color of each *pi* be denoted by (*ri*, *gi*, *bi*) and that of each*p'i* by (*r'i*, *g'i*, *b'i*). At first, we compute the means and standard. deviations of *T* and *B*, respectively, in each of the three color channels R, G, and B by the following formulas:

$$\mu_C = 1/n\sum_{i=1}^{n} ci \qquad \mu_C = 1/n\sum_{i=1}^{n} ci' \qquad (1)$$

$$\sigma_C = \sqrt{1/n\sum_{i=1}^{n}(ci-\mu i)^2} \qquad \sigma'_C = \sqrt{1/n\sum_{i=1}^{n}(ci''-\mu i'')^2} \qquad (2)$$

in which *ci* and c_i' denote the C-channel values of pixels *pi* and *pi'*, respectively, with *c* = *r*, *g*, or *b* and C=R, G,or B.Next, we compute new color values (*r̋i*, *g̋i*, *b̋i*). for each *pi* in *T* by 2

$$c_{i''} = q_c(c_i - \mu_c) + \mu_c' \qquad (3)$$

we use the following formula which is the inverse of (3):

$$ci = (1/qc)(ci - \mu_c'') + \mu_c' \qquad (4)$$

Further more, we have to embed into the created mosaic image sufficient information about the new tile image *T'* for use in the later stage of recovering the original secret image. For this, theoretically we can use (4) to compute the original pixel value of p_i. However, the involved mean and standard deviation values in the formula are all real numbers, and it is impractical to embed real numbers, each with many digits, in the generated mosaic image. Therefore, we limit the numbers of bits used to represent relevant parameter values in (3) and (4). Specifically, for each color channel we allow each of the means of *T* and *B* to have 8 bits with its value in the range of 0 to 255, and the standard deviation quotient q_c in (3) to have 7 bits with its value in the range of 0.1 to 12.8. That is, each mean is changed to be the closest value in the range of 0 to 255, and each q_c is changed to

be the closest value in the range of 0.1 to 12.8. We do not allow *qc* to be 0 because otherwise the original pixel value cannot be recovered back by (4) for the reason that 1/*qc* in (4) is not defined when *qc* =0.

3.2 Choosing Appropriate Target Blocks And Rotating Bloc To Fit Better With Smaller Rmse Value

In transforming the color characteristic of a tile image *T* to be that of a corresponding target block *B* as described above, how to choose an appropriate *B* for each *T* is an issue. For this, we use the standard deviation of the colors in the block as a measure to select the most similar *B* for each *T*. Specially, we sort all the tile images to form a sequence, S_{tile}, and all the target blocks to form another, S_{target} , according to the average values of the standard deviations of the three color channels. Then, we fit the first in S_{tile} into the first in S_{target}, fit the second in S_{tile} into the second in S_{target} , and so on. Additionally, after a target block *B* is chosen to fit a tile image *T* and after the color characteristic of *T* is transformed, we conduct a further improvement on the color similarity between the resulting tile image *T'* and the target block *B* by rotating *T* ' into one of the four directions, 0^o, 90^o, 180^o, and 270^o, which yields a rotated version of *T*" with the minimum root mean square error (RMSE) value with respect to *B* among the four directions for final use to fit *T* into *B*.

3.3 Hndling Overflows/Underflows in Color Transformation

After the color transformation process is conducted as described previously, some pixel values in the new tile image *T* ' might have overflows or underflows. To deal with this problem, we convert such values to be non-overflow or non underflow ones and record the value differences as residuals for use in later recovery. Specifically, we convert all the transformed pixel values in *T'* not smaller than 255 to be 255, and all those not larger than 0 to be 0. Next, we compute the differences between the original pixel values and the converted ones as the residuals and record them as part of the information associated with *T*" Accordingly, the pixel values, which are just on the bound of 255 or 0, however, cannot be distinguished from those with overflow/underflow values during later recovery since all the pixel values with overflows/underflows are converted to be 255 or 0 n. To solve this problem, we record the residual values in the untransformed color space rather than in the transformed one. That is, by using the following two formulas, we compute first the smallest possible color value *cS* (with *c* = *r*, *g*, or *b*) in *T* that becomes larger than 255, as well as the largest possible value *cL* in *T* that becomes smaller than 0, respectively, after the color transformation process has been conducted

$$C_S=[(1/q_c)(225-\mu_c')+\mu_c] \quad (5)$$

$$C_S=[(1/q_c)(225-\mu_c')+\mu_c]$$

Next, for an untransformed value c_i which yields an overflow after the color transformation, we compute its residual as$|c_i - c_S|$; and for c_i which yields an underflow, we compute its residual as $|c_L - c_i|$. Then, the possible values of the residuals of c_i will all lie in the range of 0 to 255 as can be verified. Consequently, we can simply record each of them with 8 bits. And finally, because the residual values are centralized around zero, we use further in this study the Huffman encoding scheme to encode the residuals in order to reduce the number of required bits to represent them.

3.4 Embedding Information For Secret Image Recovery

In order to recover the secret image from the mosaic image, we have to embed relevant recovery information into the mosaic image. For this, we adopt a technique proposed by Coltuc and Chassery and apply it to the least significant bits of the pixels in the created mosaic image to conduct data embedding. Unlike the classical LSB replacement methods , which substitute LSBs with message bits directly, the reversible contrast mapping method applies simple integer transformations to pairs of pixel values. Specifically, the method conducts forward and backward integer transformations as follows, respectively, in which (x,y) are a pair of pixel values and (x', y') are the transformed ones.The method yields high data embedding capacities close to the highest bit rates and has the lowest complexity reported so far. The information required to recover a tile image T which is mapped to a target block B includes: 1) the index of B; 2) the optimal rotation angle of T; 3) the truncated means of T and B and the standard deviation quotients, of all color channels; and 4) the overflow/underflow residuals. These data items for recovering a tile image T are integrated as a five-component bit stream of the form

$$\boldsymbol{M = t_1t_2. . .t_mr_1r_2m_1m_2. . .m_{48}q_1q_2. . .q_{21}d_1d_2. . .d_k}$$

in which the bit segments $t_1t_2 \ldots t_m$, r_1r_2, $m_1m_2 \ldots m_{48}$, $q_1q_2 \ldots q_{21}$, and $d_1d_2 \ldots d_k$ represent the values of the index of B, the rotation angle of T, the means of T and B, the standard deviation quotients, and the residuals, respectively. In more detail, the numbers of required bits for the five data items in M are discussed below: 1) the index of B needs m bits to represent, with m computed by

$$\boldsymbol{m = [\log[(WS \times HS)/NT]\ ]}$$

in which WS and HS are respectively the width and height of the secret image S, and NT is the size of the target image T; 2) it needs two bits to represent the rotation angle of T because there are four possible rotation directions; 3) 48 bits are required to represent the means of T and B because we use eight bits to represent a mean value in each color channel; 4) it needs 21 bits to represent the quotients of T over B in the three color channels with each channel requiring 7 bits; and 5) the total number k of required bits for representing all the residuals depends on the number of overflows or underflows in T".

IV. ALGORITHMS OF THE PROPOSED METHOD

Based on the above discussions, the detailed algorithms for mosaic image creation and secret image recovery may now be described respectively as Algorithms 1 and 2.

Algorithm 1 Mosaic image creation

Input: a secret image S, a target image T, and a secret key K.

Output: a secret-fragment-visible mosaic image F.

Steps:

Stage 1. ***Fitting The Tile Images Into The Target Blocks.***

Step 1. If the size of the target image T is different from that of the secret image S, change the size of T to be identical to that of S; and divide the secret image S into n tile images $\{T1, T2, \ldots, Tn\}$ as well as the target image T into n target blocks $\{B1, B2, \ldots, Bn\}$ with each Ti or Bi being of size NT .

Step 2. Compute the means and the standard deviations of each tile image *Ti* and each target block *Bj* for thethree color channels according to (1) and (2); and compute accordingly the average standard deviations for *Ti* and *Bj* , respectively, for $i = 1$ through n and $j = 1$ through n.

Step 3. Sort the tile images in the set $S_{tile} = \{T1, T2, \ldots, Tn\}$ and the target blocks in the set $S_{target} = \{B1, B2, \ldots, Bn\}$ according to the computed average standard deviation values of the blocks; map in order the blocks in the sorted S_{tile} to those in the sorted S_{target} in a 1-to-1 manner; and reorder the mappings according to the indices of the tile images, resulting in a *mapping sequence* *L* of the form: $T1 \rightarrow Bj1$, $T2 \rightarrow Bj2$, . . . , $Tn \rightarrow Bjn$.

Step 4. Create a mosaic image *F* by fitting the tile images into the corresponding target blocks according to *L*.

Stage 2. *Performing Color Conversions Between The Tile Images And The Target Blocks.*

Step 5. Create a *counting table TB* with 256 entries, each with an index corresponding to a residual value, and assign an initial value of zero to each entry (note that each residual value will be in the range of 0 to 255).

Step 6. For each mapping $Ti \rightarrow Bji$ in sequence *L*, represent the means μc and $\mu' c$ of *Ti* and *Bji*, respectively, by eight bits; and represent the standard deviation quotient *qc* appearing in (3) by seven bits, according to the scheme described in Section where $c = r, g,$ or b.

Step 7. For each pixel *pi* in each tile image *Ti* of mosaic image *F* with color value *ci* where $c = r, g,$ or b, transform *ci* into a new value *c'i* by (3); if *c'i* is not smaller than 255 or if it is not larger than 0, then change *c'i* to be 255 or 0, respectively; compute a residual value *Ri* for pixel *pi* by the way described in Section III(C); and increment by 1 the count in the entry in the counting table *TB* whose index is identical to *Ri*.

Stage 3. Rotating The Tile Images.

Step 8. Compute the RMSE values of each color transformed till image *Ti* in *F* with respect to its corresponding target block *Bji* after rotating *Ti* into each of the directions $\theta = 0^o$, 90^o, 180^o and 270^o;and rotate *Ti* into the *optimal* direction θ^o with the smallest RMSE value.

Stage 4. Embedding The Secret Image Recovery Information.

Step 9. Construct a Huffman table *HT* using the content of the counting table *TB* to encode all the residual values computed previously.

Step 10. For each tile image *Ti* in mosaic image *F*, construct a bit stream *Mi* for recovering *Ti* in the way as described in Section III(D), including the bit-segments which encode the data items of: 1) the index of the corresponding target block *Bji*; 2) the optimal rotation angle $\theta°$ of *Ti*; 3) the means of *Ti* and *Bji* and the related standard deviation quotients of all three color channels; and 4) the bit sequence for overflows/underflows with residuals in *Ti* encoded by the Huffman table *HT* constructed in Step 9.

Step 11. Concatenate the bit streams *Mi* of all *Ti* in *F* in a raster-scan order to form a total bit stream *Mt* ; use the secret key *K* to encrypt *Mt* into another bitstream M'_t; and embed M'_t into *F* by the reversible contrast mapping scheme proposed

Step 12. Construct a bit stream *I* including: 1) the number of conducted iterations *Ni* for embedding M'_t; 2) the number of pixel pairs *Npair* used in the last iteration; and 3) the Huffman table *HT* constructed for the residuals; and embed the bit stream *I* into mosaic
image *F* by the same scheme used in Step 11.

Algorithm 2 Secret image recovery

Input: a mosaic image *F* with *n* tile images $\{T_1, T_2, \ldots, T_n\}$ and the secret key *K*.

Output: the secret image *S*.

Steps:

Stage 1. Extracting The Secret Image Recovery Information.

Step 1. Extract from *F* the bit stream *I* by a reverse version of the scheme proposed and decode them to obtain the following data items: 1) the number of iterations *Ni* for embedding M'_t; 2) the total number of used pixel pairs *Npair* in the last iteration; and 3) the Huffman table *HT* for encoding the values of the residuals of the overflows or underflows.

Step 2. Extract the bit stream M'_t using the values of *Ni* and *Npair* by the same scheme used in the last step.

Step 3. Decrypt the bit stream M'_t into *Mt* by *K*.

Step 4. Decompose *Mt* into *n* bit streams *M*1 through *Mn* for the *n to-be-constructed* tile images *T*1 through *Tn* in *S*, respectively.

Step 5. Decode *Mi* for each tile image *Ti* to obtain the following data items: 1) the index *ji* of the block *Bji* in *F* corresponding to *Ti*; 2) the optimal rotation angle $\theta°$ of *Ti*; 3) the means of *Ti* and *Bji* and the related standard deviation quotients of all color channels; and 4) the overflow/underflow residual values in *Ti* decoded by the Huffman table *HT*.

Stage 2. Recovering The Secret Image.

Step 6. Recover one by one in a raster-scan order the tile images *Ti*, *i* = 1 through *n*, of the desired secret image *S* by the following steps: 1) rotate in the reverse direction the block indexed by *ji*, namely *Bji*, in *F* through the optimal angle $\theta°$ and fit the resulting block content into *Ti* to form an *initial* tile image *Ti*; 2) use the extracted means and related standard deviation quotients to recover the original pixel values in *Ti* according to (4); 3) use the extracted means, standard deviation quotients, and (5) to compute the two parameters *cS* and *cL*; 4) scan *Ti* to find out pixels with values 255 or 0 which indicate that overflows or underflows, respectively, have occurred there; 5) add respectively the values *cS* or *cL* to the corresponding residual values of the found pixels; and 6) take the results as the final pixel values, resulting in a *final* tile image *Ti*.

Step 7. Compose all the final tile images to form the desired secret image *S* as output.

V. EXPERIMENTAL RESULTS

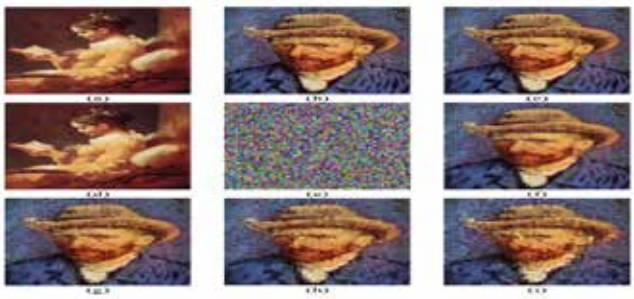

Fig. 3. Experimental Result of Mosaic Image Creation. (a) Secret image.(b) Target image. (c) Mosaic image created with tile image size 8×8. (d) Recovered secret image using a correct key with RMSE= 0.948 with respect to secret image (a). (e) Recovered secret image using a wrong key. (f)-(i) Mosaic images created with different tile image sizes: 16×16, 24×24, 32×32, and 40×40. with respect to the secret image.

A series of experiments have been conducted to test the proposed method using many secret and target images with sizes 1024×768 or 768×1024. To show that the created mosaic image looks like the preselected target image, the quality metric of root mean square error (RMSE) is utilized, which is defined as the square root of the mean square difference between the pixel values of the two images. An example of the experimental results is shown in Fig. 3; Fig. 3(c) shows the created mosaic image using Fig. 3(a) as the secret image and Fig. 3(b) as the target image. The tile image size is 8×8. The recovered secret image using a correct key is shown in Fig. 3(d) which looks nearly identical to the original secret image shown in Fig. 3(a) with RMSE= 0.948

VI. SECURITY CONSIDERATIONS

In order to increase the security of the proposed method, the embedded information for later recovery is encrypted with a secret key as seen in Algorithm 1. Only the receiver who has the key can decode the secret image. However, an eavesdropper who does not have the key may still try all possible permutations of the tile images in the mosaic image to get the secret image back. Fortunately, the number of all possible permutations here is $n!$, and so the probability for him/her to correctly guess the permutation is $p=1/n!$ which is very small in value. For example, for the typical case in which we divide a secret image of size 1024×768 into tile images with block size 8×8, the value n is (1024×768)/(8×8) = 12,288. So the probability to guess the permutation correctly without the key.

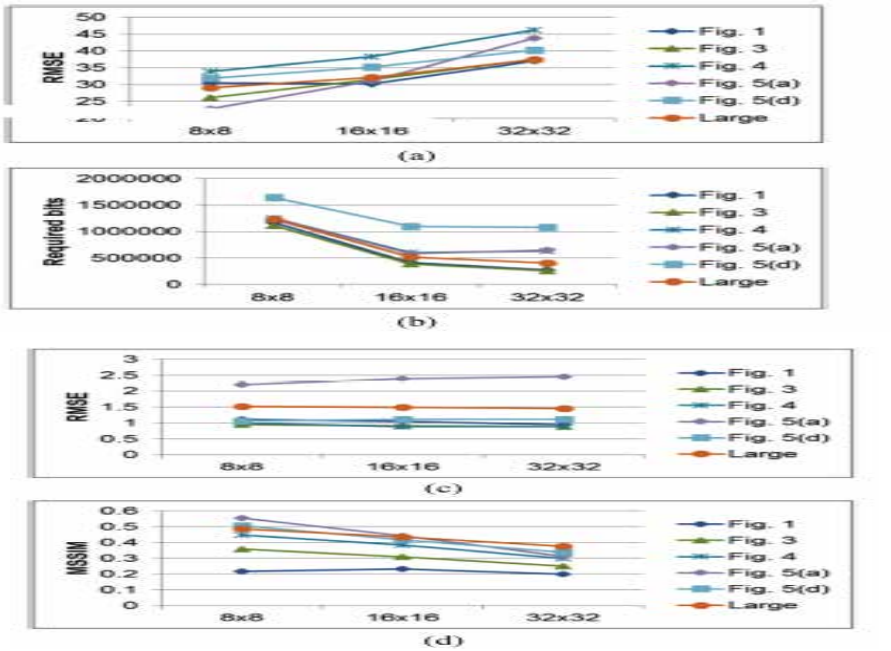

Fig4:. Plots of Trends of Various Parameters Versus Different Tile Image Sizes (8×8, 16×16, 32×32) With Input Secret Images Shown Previously And Coming From A Large Dataset. (a) RMSE values of created mosaic images with respect to target images. (b) Numbers of required bits embedded for recovering secret images. (c) RMSE values of recovered secret images with respect to original ones. (d) MSSIM values of created mosaic images with respect to target images.

is $1/n! = 1/(12{,}288!)$. So breaking the system by this way of guessing is computationally infeasible.

will observe the content of the mosaic image with a correct permutation, and try to figure useful information out of it. For example, an attacker might analyze the spatial continuity of the mosaic image in order to estimate a rough version of the secret image. To increase the security of the proposed method against this type of attack, one possible way to is to use the key to randomize important information of a secret image, such as the positions of the pixels in the secret image, before transforming the secret image into a mosaic image by the proposed method. Consequently, only authorized users with the key can know the correct secret image while an attacker cannot.

VII. CONCLUSION

A new secure image transmission method has been proposed, which not only can create meaningful mosaic images but also can transform a secret image into a mosaic one with the same data size for use as a camouflage of the secret image. By the use of proper pixel color transformations as well as a skillful scheme for handling overflows and underflows in the converted values of the pixels' colors, secret-fragmentvisible mosaic images with very high visual similarities to arbitrarily-selected target images can be created with no need of a target image database. Also, the original secret images can be recovered nearly losslessly from the created mosaic images. Good experimental results have shown the feasibility of the proposed method by using MAES. Future studies may be directed to applying the proposed method to images of color models other than the RGB.

REFERENCES

[1] J. Fridrich, "Symmetric ciphers based on two-dimensional chaotic maps," *Int. J. Bifurcat. Chaos*, vol. 8, no.6, pp. 1259–1284, 1998.

[2] G. Chen,Y. Mao, and C. K. Chui, "A symmetric image encryption scheme based on 3D chaotic cat maps,"*Chaos Solit. Fract.*, vol. 21, no. 3, pp. 749–761, 2004.

.[3] H. S. Kwok and W. K. S. Tang, "A fast image encryption system based on chaotic maps with finite precision representation," *Chaos Solit. Fract.*, vol. 32, no. 4, pp. 1518–1529, 2007.

[4] S. Behnia, A. Akhshani, H. Mahmodi, and A. Akhavan, "A novel algorithm for image encryption based on mixture of chaotic maps," *Chaos Solit. Fract.*, vol. 35, no. 2, pp. 408–419, 2008.

[5] D. Xiao, X. Liao, and P. Wei, "Analysis and improvement of a chaosbased image encryption algorithm," *Chaos Solit. Fract.*, vol. 40, no. 5, pp. 2191–2199, 2009.

[6] V. Patidar, N. K. Pareek, G. Purohit, and K. K. Sud, "A robust and secure chaotic standard map based pseudorandom permutationsubstitution scheme for image encryption," *Opt. Commun*., vol. 284, no. 19, pp. 4331–4339, 2011.

[7] C. K. Chan and L. M. Cheng, "Hiding data in images by simple LSB substitution," *Pattern Recognit.*., vol. 37, pp. 469–474, Mar. 2004.

[8] Z. Ni, Y. Q. Shi, N. Ansari, and W. Su, "Reversible data hiding," *IEEE Trans. Circuits Syst. Video Technol*., vol. 16, no. 3, pp. 354–362, Mar. 2006.

[9] J. Tian, "Reversible data embedding using a difference expansion," *IEEE Trans. Circuits Syst. VideoTechnol*., vol. 13, no. 8, pp. 890–896, Aug. 2003.

BIOGRAPHICAL NOTES

Mis. Y. Sasikala is presently pursuing M. Tech. final year in Electronics and Communication Engineering Department (Specialization in Digital Electronics Communication Systems) from A.I.T.S Rajampet, Andhra Pradesh, India.

Mr. K. Riyazuddin is working as a Assistant Professor in Electronics and Communication Engineering Department, A.I.T.S Rajampet, Andhra Pradesh, India.

CRITICAL SUCCESS FACTORS AND THEIR IMPACT ON KNOWLEDGE MANAGEMENT IN MEDIUM SIZED MANUFACTURING COMPANIES

S.D. Uma Mageswari[1], Dr. Chitra Sivasubramanian[2], Dr. Srikantha Dath[3]

[1]Research scholar, [2]Associate Professor, Department of Management studies, Pondicherry University, Puducherry (India)
[3]Professor, Department of Mechanical Engineering, RMK Engineering College, Thiruvallur District, Tamil Nadu, (India)

ABSTRACT

Globalization has turned competition in businesses into a war for survival and growth through competitiveness. Knowledge Management is a much felicitated strategy which provides competitiveness especially to manufacturing firms where agility is the need of the hour. Most of the manufacturing sector in India belongs to SME sector which suffers from resources constraints unique to them. This paper explores knowledge management adoption by the medium sized manufacturing firms, the road less travelled by the researchers. Survey method is adopted using a structured questionnaire. 103 medium sized firms in the southern part of India participated in the survey. A conceptual framework was developed with its theory rooted in the literature and is empirically validated Partial Least Squared – path modeling method. The results revealed that the influence of external factors are more predominant and emphasizes the needs for creating the conducive internal environment.

Keywords: External factors, Knowledge Management, Manufacturing, Medium enterprises, Path modeling.

I INTRODUCTION

Business world is experiencing a sea of change in their operating environment. Firms were operating in an environment where competition was less, independent and less linked and dependent on incremental and continuous improvement of productivity and Quality control [1]. But today's business environment is characterised by heightened competition and high level of uncertainty, shorter product life cycles, extensive profliferation of ICT and more deeply interconnected. To survive and grow in this more complex environment, brain power / knowledge / intellectual capital is the life line for the organisations. Harnessing and Managing knowledge and creating knowledge-philic work culture [1] is crucial for the firms' to be competitive and innovative. Managing knowledge is difficult because knowledge is intangible and difficult to measure and it cannot be bought in markets [2]. But it is unique in its feature that it increases through use [2] and it does not depreciate like normal economic productive factors do, and can generate increasing returns [3]. A survey on status of knowledge management in nine countries

conducted by Asian Productivity organization [1] reported that in India, KM is practiced by ICT companies extensively . India is one of the countries where KM is recognized by the Government as crucial for survival in the knowledge based economy and established National Knowledge Commission. But studies in India show that knowledge management is adopted by IT, ITES and few large manufacturing companies extensively.

This paper attempts to explore the status of knowledge management practices in medium sized manufacturing companies, to identify the factors to be considered for the success of KM and to ascertain the association between the success factors and the KM practices. The structure of the paper: It contains 5 sections. In section 2, previous research work is elicited followed the need for the study and its objectives. In section 3, research methodology is described followed by data analysis in Section 4. Results are discussed in Section 5.

II REVIEW OF LITERATURE

MSMED Act, 2006 defined medium sized firms in manufacturing is defined as those firms that has investment in plant and machinery between 5 crores to 10 crores in India.

Knowledge is available in abundance in organizations, in people, in processes, in documents and procedures. Firms should have adequate knowledge on customers, company's products and services, markets, competition. Processes and methods and regulatory environment [4]. Zins [5] quotes in an article that " ..... Knowledge is information that has been appropriate by the user. When information is adequately assimilated, it produces knowledge, modifies the individual's mental store of information and benefits his development and that of the society in which he lives....." Hence knowledge management is not information management, DBMS, Information systems or IT, HRM or IPRM [6].

The general idea of KM relates to unlocking and leveraging the knowledge of individuals so that this knowledge becomes available as an organizational knowledge [7]. KM is a multidimensional [8] process comprising of knowledge acquisition, knowledge creation, knowledge sharing, knowledge storing and knowledge application [9].

Knowledge Capture (KC): Knowledge is intangible and resides in the minds of the people in organisations. Retrieving the individuals' knowledge [10] and acquiring the required from external sources is termed knowledge capture [11].

Knowledge Creation (KCr): knowledge creation is the deliberate generation of knowledge though a concerted effort by an organization to acquire relevant knowledge through external and internal means [12, 10]. Nonaka and Takeuchi [13] argued that the success of Japanese firms is not because of their manufacturing prowess, but because of their skills and expertise at "Organisational knowledge creation". As knowledge is volatile and becomes obsolete very fast, ability to create new knowledge decides the success of the organisations.

Knowledge storage(KS) : The knowledge captured from internal and external sources have to be organised and stored for future reference. Use of technology facilitates knowledge storing. The challenge lies in exploring the tacit knowledge, codifying and storing it using technology would enable knowledge sharing within the organisation. Knowledge storage increases the organisational memory.

Knowledge transfer (KTr): Knowledge sharing is a process of exchanging knowledge and ideas through discussions to create new knowledge or ideas [10]. Sharing of knowledge is crucial in devising best practices. Favourable organisational culture and supportive leadership enhance the knowledge sharing culture. Motivation by the management to share knowledge by rewards and recognition will enhance knowledge sharing within organisations. Creation of multi disciplinary cross functional teams may also remedy the problem.

Knowledge Application (KAp):knowledge application is defined as the implementation, analysis, development, and protection of knowledge in a form where users can learn and generate new knowledge [10]. The ability of the individuals to apply the acquired knowledge for problem solving, decision making and generate new ideas enhances the efficiency of the organisation on the whole. Application of knowledge leads to creation of new knowledge. Knowledge that is not used, do not contribute to the organisations' value. Properly leveraged and utilised knowledge drive the organizations to become more innovative, competitive, and sustainable [14].

Organizations need to be cognizant of the factors that will influence the success of a KM initiative. CSFs are the factors that should be addressed and nurtured if they already existed in the organisations or be developed if they were not in place [15]. The critical success factors could turn potentially fatal if ignored and hinder the organisations' efforts to realise KM's full benefit. Hence the need for a systematic and deliberate study on these enablers becomes crucial for the success of KM initiatives. Many authors have investigated the CSFs for KM and its sub processes in different contexts. Myriad of KM enablers internal and external to the organisations are reported in the literature. For example,

- Inkpen [16] described one of the earliest sets of KM enablers comprising six factors; flexible learning objectives, leadership commitment, climate of trust, tolerance for redundancy, creative chaos and performance myopia.
- An exploratory study conducted by Davenport et al, [12] resulted in eight enablers and they are economic performance or industry value, a clear purpose and language, a standard and flexible knowledge structure, multiple channels for knowledge transfer, a knowledge-friendly culture, a technical and organizational infrastructure, change in motivational practices, and senior management support.
- Wong and Aspinwall [17] investigated the critical success factors (CSFs) for adopting knowledge management (KM) in small and medium-sized enterprises (SMEs) in UK. Two surveys were conducted for the purpose; one with a group of academics, consultants and practitioners in the KM field and the second from the companies. The study reported 11 enablers viz., management leadership and support; culture; strategy and purpose; resources; processes and activities; training and education; human resource management; information technology; motivational aids; organisational infrastructure; and measurement. In addition, benchmarking was also reported as a KM enabler in SMEs' context [18, 13; 19].
- Theriou, et al, [20] attempted to investigate the relationship between knowledge enabler factors on firm performance in the context of Greek medium and large firms. The CSFs /enablers used were leadership, culture, technology, KM strategy and people. The report concluded that leadership and culture are the two most important enablers deciding the KM effectiveness.

Of the many success factors of KM are reported in the literature, the set of enablers proposed by Wong and Aspinwaal [17] are considered for the study. Of the 11 enablers, Organisational culture, leadership and management support are the top most enablers from academicians' and industrialists' point of view. These factors are considered here for the study. In addition, two factors from external environment which are termed as potential influencers of firms' performance such as Use of Government facilities and competitors are also empirically analysed.

Literature studies revealed the emphasis on the need for Governments' support for managing knowledge for competitiveness and long-term sustainability [21]. A pilot study conducted in Malaysia [22] emphasised the need for government's role in providing training, R & D support and technical assistance. But not much of literature on the empirical analysis is available in literature.

Businesses often suffer from managerial myopia in identifying competitor threats [23]. The managers are so involved in their day-to-day activities and budgeting, they tend overlook the threats from the competitors. It is imperative for the managers to know what others are doing. Acquiring knowledge about the competitors is one of the crucial requirements of the firms [24, 4]. knowledge about competitors provides core capability, enhances dynamic capabilities of the firms [25] and competitive advantage.

Hence the factors "Use of government facilities" and "Competitor comparison" are identified and analysed for its impact on the firms' knowledge management practices.

2.1 Need for the study

Studies on knowledge management in India mainly focused on exploring the status of KM adoption by the firms from diversified sector or case study based. A holistic analysis of knowledge management practices and its success factors / enablers in medium sized manufacturing companies is practically unknown. Also, the impact of culture and technology on KM is analysed separately in few contexts, but the study involving combined effect of organizational culture, top management commitment and middle managers' support is scarce in the Indian scenario. Similarly, the study of impact of external influencers such as Government and competitors is first of its kind.

2.2 Objectives of the Study

- To study the extent of KM adoption by the medium sized manufacturing firms.
- To ascertain the impact of the identified KM enablers on each of KM processes through structural equation modeling.

To test the objectives, and based on the literature review, the following research model, given in Fig 1 is proposed.

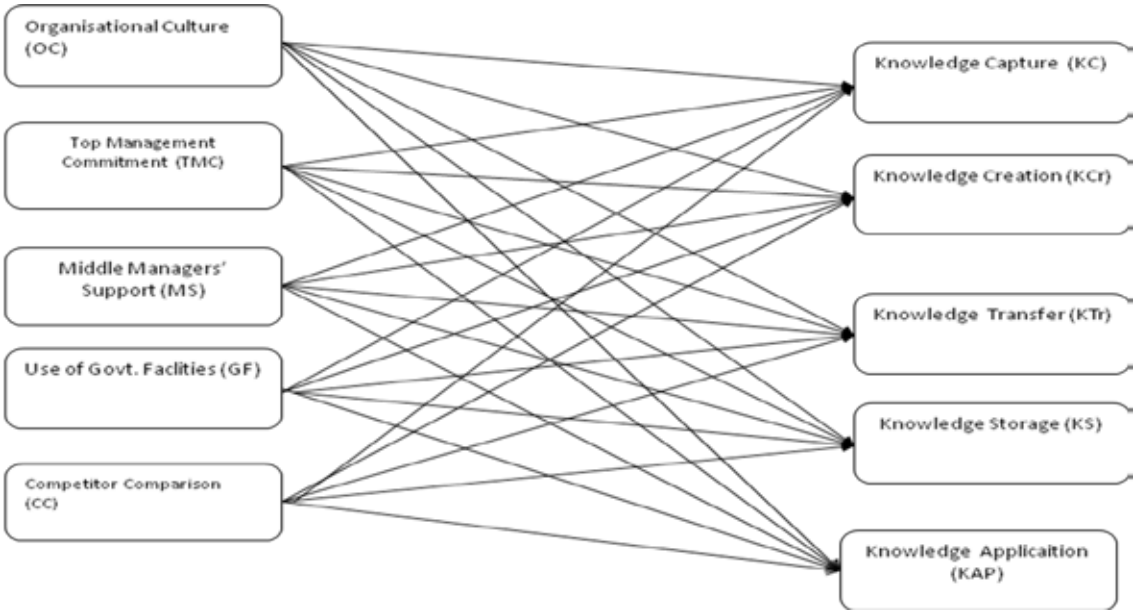

Figure 1 Research Model

III RESEARCH METHODOLOGY

3.1 Sampling

The sample in this investigation was drawn from medium sized manufacturing firms in India. 103 firms have taken part in the survey. The respondents are at the executive level in these firms. The respondents' years of service ranged from two to more than 15 years.

3.2 Data collection

Data concerning KM processes (Kc,KCr,KTr,KS and KAp), KM enablers (OC,TMC,MS, GF and CC) and the demographic details of the participating firms are collected through questionnaire. The instrument was adopted from literature with few modifications and additions. Wherever the items were not available, these were developed for the study and the questionnaire was validated by industry and academic experts. Responses were measured on a 5 point Likert-type scale, ranging from strongly agree (1) to strongly disagree (5). Questionnaire used for the study is given in Appendix 1.

3.3 Data Validation

The overall measurement model is evaluated first by testing for convergent validity and internal reliability. The extent to which the items identified for a construct measures the construct is convergent validity. Construct reliability (CR) and Average variance extracted (AVE) were used for testing convergent validity, which should be 0.5 or above. Internal reliability is tested using cronbach's alpha which should be above 0.6. As given in Table, our model showed that CR and AVE for all the constructs above 0.5 and internal reliability above 0.6.

Table 1 Measurement Properties of the Study Constructs

Measurement properties of KM processes						Measurement properties of KM Enablers					
Constructs	items	item loadings	AVE	CR	Cronbachs Alpha	Constructs	items	item loadings	AVE	CR	Cronbachs Alpha
KC	KC4	0.8317	0.518	0.7606	0.605	OC	OC2	0.7897	0.506	0.859	0.8031
	KC6	0.6256					OC3	0.7733			
	KC9	0.6862					OC4	0.7359			
KCr	KCR1	0.7661	0.5016	0.8006	0.669		OC5	0.6857			
	KCR2	0.7037					OC6	0.6677			
	KCR4	0.6686					OC7	0.5975			
	KCR5	0.6909				TMC	TM3	0.8106	0.51	0.8592	0.8009
KT	KT1	0.7994	0.5117	0.8378	0.7592		TM4	0.7137			
	KT3	0.5479					TM5	0.813			
	KT5	0.7316					TM6	0.7728			
	KT7	0.7203					TM8	0.5319			
	KT8	0.7519				LS	M1	0.7238	0.553	0.8602	0.7965
KS	KS1	0.742	0.5108	0.8791	0.8393		M2	0.8329			
	KS2	0.7511					M3	0.7602			
	KS3	0.6723					M4	0.6624			
	KS4	0.769					M5	0.7286			
	KS6	0.6809				GF	GF1	0.8147	0.513	0.8788	0.8372
	KS7	0.6252					GF2	0.7193			
	KS9	0.7504					GF3	0.7267			
KAp	KAP1	0.7554	0.5404	0.8237	0.7157		GF4	0.7129			
	KAP2	0.6381					GF5	0.7825			
	KAP3	0.8069					GF6	0.7152			
	KAP5	0.73					GF7	0.4998			
						CC	CC1	0.8226	0.6982	0.8223	0.6982
							CC2	0.8484			

IV DATA ANALYSIS

4.1 Descriptive statistics

Fig 2 given below shows the mean values of KM practices are between 3 and 4 depicting a moderate adoption of KM practices by the medium sized manufacturing companies.

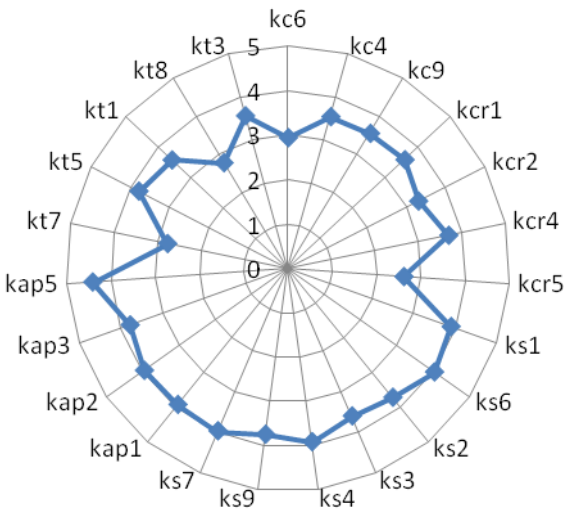

Figure 2 Mean values of KM practices in medium sized enterprises

4.2 Assessment of the research model

After the constructs are tested for their reliability and validity, the next step is to assess the results of structural model. A systematic five step approach to the assessment of structural model as proposed by Hair et al [26] is as given below:

- Step 1 : Assess structural model for collinearity issues
- Step 2 : Test for significance of path coefficients
- Step 3 : Assess the level of the R^2 values.
- Step 4 : Assess the effect size f^2
- Step 5 : Assess the predictive relevance (Q^2)

The abovementioned five step procedure is adopted to assess the structural model proposed.

4.2.1 Assessment of multicollinearity

The model is run using Smart PLS (Version2) software. From the report, latent variable scores (given in (Appendix 1) are then tested for multicollinearity using SPSS 16 software. The thumb rule used to indicate the collinearity is the values of variance inflation factor (VIF) should be below 5 and tolerance greater than 0.1. SPSS collinearity results using OC, BM, GF, TMC and LS as independent variables of KM processes are given in Table 2.

Table 2 Collinearity statistics of the study constructs

Independent Variables	Collinearity Statistics	
	Tolerance	VIF
CC	.881	1.136

GF	.905	1.106
MS	.331	3.020
TMC	.286	3.495
OC	.246	4.063
Dependent variables : KC, KCr, KS, KTr and KAp		

The results show that VIF values are less than 5 and tolerance values are well above the threshold value of 0.1 indicate the absence of multicollinearity.

4.2.2 Assessment of significance of the path coefficients

The significance of path coefficients is obtained using bootstrapping operation in SMARTpls (Hair, et al 2013). Bootstrapping in Smartpls is selected with number of cases equal to sample size and number of samples fixed at 2000. Path coefficients, given in original sample column, and significance of the path coefficients are obtained and are given in Table 3.

Table 3 Significance of Path coefficients

Structural paths	Original Sample	T Statistics	Significance
CC -> KAp	0.3106	3.0159	***
CC -> KC	0.3988	4.2868	***
CC -> KCr	0.4437	5.2048	***
CC -> KS	0.2039	2.2617	**
CC -> kTr	0.4046	3.8733	***
GF -> KAp	-0.124	1.0998	NS
GF -> KC	0.1182	1.182	NS
GF -> KCr	0.3336	4.2534	***
GF -> KS	-0.0211	0.2582	NS
GF -> kTR	0.3399	4.1022	***
MS -> KAp	0.2919	2.1362	**
MS -> KC	-0.0583	0.457	NS
MS -> KCr	0.1061	0.95	NS
MS -> KS	0.153	0.9287	NS
MS -> kTR	0.165	1.3583	NS
TMC -> KAp	0.3493	2.6102	**
TMC -> KC	0.0136	0.0791	NS
TMC -> KCr	0.0504	0.3229	NS
TMC -> KS	0.0426	0.2646	NS
TMC -> kTR	-0.0885	0.6176	NS
oc -> KAp	-0.0598	0.4443	NS

oc -> KC	0.3696	1.9192	*
oc -> KCr	0.1116	0.6755	NS
oc -> KS	0.4325	2.9604	**
oc -> kTR	0.17	1.38	NS
*p<0.1; **p<0.05; ***p<0.01			

The insignificant paths where T statistics <1.65 are given as "NS". It is observed that eleven (11) out of 25 paths are significant as given in Table 3 and Fig 3.

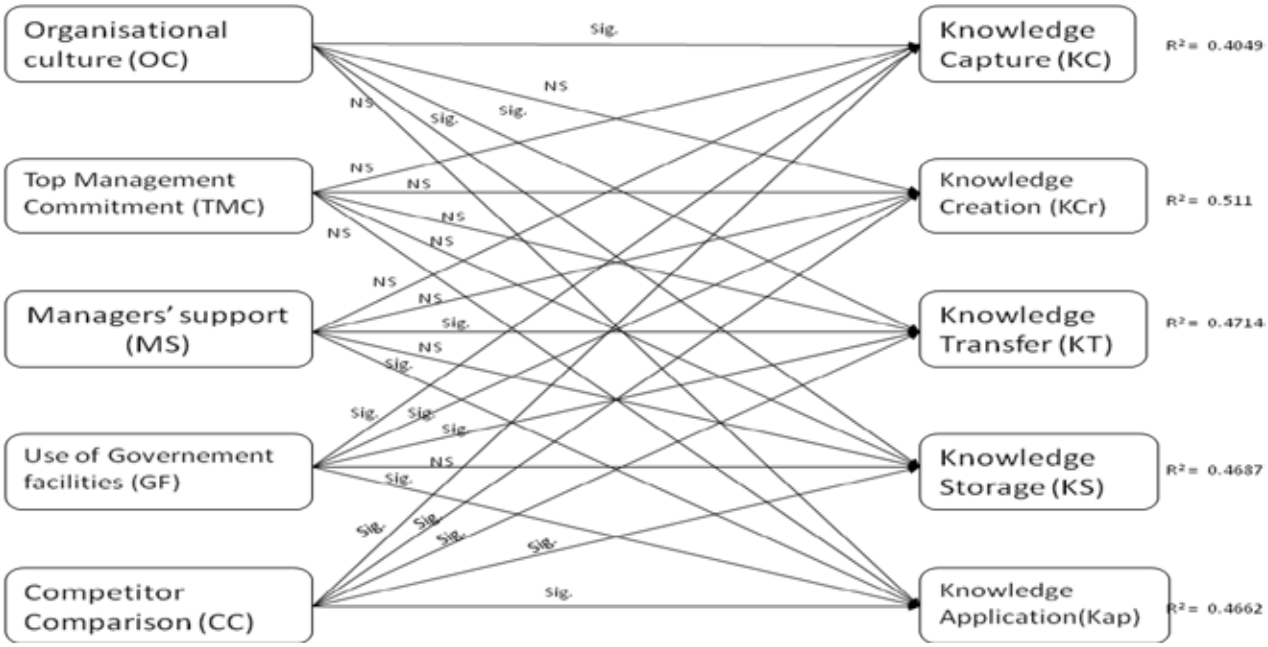

Figure 3 Significance of Path Coefficients (Research Model)

Next step is analysing the size of the path coefficients which indicates the relevance of the significant relationships. Larger path coefficient values denote greater impact of the exogeneous variable on the endogeneous variable. The results may be summarized as follows:

- The impact of competitor comparison on KM processes is the highest which ranges from 20% for KS to 44.3% for KCr. That is, a unit change of CC brings about 20% change in KS to 44.3% in KCr.
- "Use of Government Facilities (GF)" significantly influences KCr (33.3%) and KTr (33.3%) as shown by the path coefficients.
- Middle managers' support (MS) and Top management commitment (TMC) for KM is not encouraging. Only KAp is significantly influenced by MS to a magnitude of 29% and 34% respectively.
- The impact of organizational culture (OC) has a significant impact on KC (36.9%) and KS (43.2%) and not on KCr, KTr or KAp.

The size of the impact of the identified enablers are further assessed using R2 values and also the effect sizes are explored by f2 and q2 values in the forthcoming sessions.

4.2.3 Assessment of R^2

R^2 values exhibit the strength of relationship between independent variables and dependent variables. Values of 0.2 is considered high researches on consumer behaviour. n general, values 0.25,0.5 and 0.75 are considered to be weak, moderate and substantial for marketing studies(Cohen,) . For this study, R^2 values obtained are given in Table which shows a moderate influence of endogeneous variables on the KM processes.

Table 4 R^2 Values

Dependent variables / KM proceses	R^2
KC	0.4049
KCr	0.5110
KS	0.4714
kTR	0.4687
KAp	0.4662

4.2.4 Assessment of effect size f^2

f^2 values show the extent of impact of a particular independent variable on the dependent variables. f^2 values could be calculated using the estimated R2 using the following formula:

$$f^2 = \frac{R^2_{\text{included}} - R^2_{\text{excluded}}}{1 - R^2_{\text{included}}}$$

Where R^2included indicate the value of R2 by including the particular independent variable and R2excluded indicate the value of R2 by omitting the variable under study. Hence, f2 can be called as the measure of change in R2 when a particular independent variable is omitted from the model. The threshold values for assessing the f2 effect sizes are 0.02,0.15 and 0.35 for small, medium and large effects respectively.(Cohen,1988)

Table 5 Results of f^2 effect size assessment

KM processes (Endogeneous variables)	f^2				
	OC	MS	TMC	CC	GF
KC	.056	0	0	0.233	0.016

KCr	0.0075	0.0065	0	0.313	0.19
KS	0.08	0.013	0	0.066	0
KT	0.012	0.02	0.0069	0.248	0.173
KAp	0	0.0504	0.06	0.155	0.025

The above results show that f^2 effect sizes are substantial for BM on all the KM processes except that of KS where the f^2 effect size is small. Similarly, GF has a moderate f^2 effect size predictive value for KCr, KT and small effect size predictive values for KAp and KC. f^2 effect sizes are small for other critical success factors such as OC, LS and TMC.

4.2.5 Assessment of predictive relevance Q^2

While magnitude of R2 indicate predictive accuracy, Q2 values indicate predictive relevance of the model. Q2 values greater than zero explains the predictive relevance of the particular construct / variable. Like f2 effect size, Q2 values of 0.02, 0.15 and 0.35 are the indicators of small, medium and large predictive relevance of the constructs. Q2 values are measured by running the blindfolding operation in Smartpls for cross validated redundancy.

Table 6 Q^2 Values

Dependent variables / KM proceses	Q^2
KC	0.2187
KCr	0.2507
KS	0.2401
kT	0.2347
KAp	0.2477

The Q^2 values are well above zero which supports the predictive relevance of the critical success factors for the KM processes.

V RESULTS AND DISCUSSION

At the outset, a thorough literature analysis showed that the firms' internal and external environment are crucial for the success of KM. For this study, three factors pertaining to the internal environment (OC,MS and TMC) and the influence of two external factors (GF and CC) are considered.The data were validated and then subjected to explore the extent of adoption of KM practices by the respondent firms through descriptive statistical measure,mean. The mean values revealed a moderate adoption of KM practices by the respondent firms.

PLS path modeling analysis revealed that the influence of external environment is significant on the KM processes as given by the size of the path coefficients and R2 values.

"Competitor comparison (CC)" practices has a greater influence on KM processes such as KCr (0.443), KT (0.4076), KC (0.3959), KAp(0,309) and KS (0.2069). To be competitive in the market, CC provides critical information about the competitors. CC practices have enhanced the organisations' knowledge creation activities which further influences the other KM processes.

Similarly, Indian Government has taken enormous steps to nurture SMEs in India. Ministry of MSMEs through its departments and other members continuously thrive to enhance the performance of SMEs(Sivasubramanian et al, 2011). Whether the steps taken by the government is utilised by SMEs and their impact on knowledge management processes of the organisations is studied through the following items in the questionnaire.

It could be inferred that government facilities enhances knowledge creation activities (0.3854), knowledge transfer (0.3318) and to some extent on knowledge capture (0.1153). Medium companies are aware of the various measures taken by Indian government to enhance their knowledge related activities and is shown by the path coefficients. It should be noted that KS is not influenced by the government facilities.

As an indicator of companies' internal environment, we have chosen organisational culture, leadership and top management commitment for KM practices. While it is observed that the existing organisational culture does influence knowledge transfer and impact is not very significant. Knowledge application practices are definitely fostered by top management commitment(TMC) by way of rewards and recognition and it is indicated by a moderate path coefficient value of 0.34. Similarly leadership helps in knowledge transfer and knowledge Application.

VI CONCLUSION

The results of the analysis adds a new insight to the literature on the status of KM in Indian manufacturing firms with specific reference to medium sized firms. The study further corroborate that KM is adopted only informally and the extension of adoption is moderate. Hence the top management and middle managers have to support the effective KM adoption for better performance and also create a conducive organizational culture for the success of KM. The study also emphasizes the importance of creating awareness of the various Government's initiatives by the policy makers for successful KM adoption for competitiveness.

REFERENCES

[1] Talisayon, D. S. The status of knowledge management in Asia: results of an APO survey of nine member countries". In Proceedings from the Second International Conference on Technology and Innovation for Knowledge Management. Asian Productivity Organization, 2008.

[2] Wiig, K. M. (1995). Knowledge management methods: Practical approach to managing knowledge. (Arlington, Texas: Schema Press,1995)

[3] Eisenhardt, K. M., & Santos, F. M. Knowledge-based view: A new theory of strategy. Handbook of strategy and management, 2002, 139-164.

[4] Pillania, R. K. Organisational issues for knowledge management in SMEs. International Journal of Business and Systems Research, 1(3), 2007, 367-379.

[5] Zins,C. (2007). Journal of the American Society for Information Science and Technology, 58(4),2007, ,479–493.

[6] Pillania, R.K. IT strategy for knowledge management in Indian industry. Journal of Information and Knowledge Management (JIKM), 4(3), 2005, 32-43.

[7] Swan, J., & Scarbough, H. The Paradox of Knowledge Management. The Guest Editors, 11,2002

[8] Omerzel, D. G. The impact of knowledge management on SME growth and profitability: a structural equation modelling study, African Journal of Business Management, 4(16), 2010, 3417-3432

[9] Khalil, O., Claudio, A., & Seliem, A. Knowledge Management: The Case of the Acushnet Company. SAM Advanced Management Journal, 71(3), 2006, 34 -44.

[10] Lawson, S., Examining the relationship between organizational culture and knowledge management, Doctoral diss., Nova Southeastern University,2003..

[11] Holsapple, C. W., & Joshi, K. D. Organizational knowledge resources. Decision support systems, 31(1), 2001, 39-54.

[12] Davenport, T.H. and Prusak, L., (1998), "Working Knowledge – How Organisations Manage What They Know", Cambridge: Harvard Business School Press.

[13] Nonaka, I. and Takeuchi, H. The knowledge-creating company: how Japanese companies create the dynamics of innovation". New York, NY.

[14] Jafari, M., Fathian, M., Akhavan, P., & Hosnavi, R. Exploring KM features and learning in Iranian SMEs. Vine, 37(2), 2007, 207-218.

[15] Wong, K. Y. Critical success factors for implementing knowledge management in small and medium enterprises. Industrial Management & Data Systems, 105(3), 2005, 261-279.

[16] Inkpen, A. C. Creating Knowledge through Collaboration. California Management Review, 39, 1996, 123-140.

[17] Wong, K. Y., & Aspinwall, E. An empirical study of the important factors for Knowledge management adoption in the SME sector. Journal of knowledge management, 9(3), 2005, 64-82.

[18] Valmohammadi,(2010).Investigation and Assessment of Critical Success factors of KM implementation in Iranian SMEs. Journal of Applied Sciences, 10(19), 2010.

[19] Chong S. C. & Choi Y. S. (2005).Critical Factors in the Successful Implementation of Knowledge Management. Journal of Knowledge Management Practice, 6(1), 2005.

[20] Theriou, N., Maditinos, D., & Theriou, G. Knowledge Management Enabler Factors and Firm Performance: An empirical research of the Greek medium and large firms". In International Conference on Applied Business and Economics, Technological Educational Institute of Kavala, Kavala, Greece, 2010, 1-20.

[21] Lee, M. R., & Lan, Y. C. Toward a unified knowledge management model for SMEs, Expert Systems with Applications, 38(1),2011, 729-735.

[22] Ngah, R., & Ibrahim, A. R. The relationship of intellectual capital, innovation and organizational performance: a preliminary study in Malaysian SMEs. International Journal of Management Innovation Systems, 1(1), 2009, 1-13.

[23] Zajac, E. J., and M. H. Bazerman, (1991). Blind spots in industry and competitor analysis: Implications of interfirm (mis)perceptions for strategic decisions. Academy of Management Review, 16,1991, 37-56.

[24] KPMG.Knowledge Management Research Report, http://www.providersedge.com/docs/km_articles/kpmg_km_research_report_2000.pdf

[25] Sher, P. J., & Lee, V. C. (2004). Information technology as a facilitator for enhancing dynamic capabilities through knowledge management. Information & management, 41(8), 2004, 933-945.

[26] Hair Jr, J. F., Hult, G. T. M., Ringle, C., & Sarstedt, M. A primer on partial least squares structural equation modeling (PLS-SEM) (SAGE Publications, Incorporated.,2013).

APPENDIX 1
QUESTIONNAIRE

Constructs /Items	Item Descriptions
KNOWLEDGE CAPTURE (KC)	
KC4	We regularly attend courses, seminars or other training for skill development
KC6	We hire consultants when important skills/expertise or information about any activity are not available in our organisation
KC9	We attend presentations of innovations by our suppliers and customers
KNOWLEDGE CREATION (KCR)	
KCR1	We collaborate with Research institutes, Educational institutions for problem solving, projects, innovations
KCR2	We have a team to study and communicate the market scenario to the management for further action
KCR4	Brainstorming sessions among employees, managers and top management are frequently used for problem solving depending on the problems
KCR5	We do research to explore future possibilities of expansion in terms of capacity, markets etc.
KNOWLEDGE STORAGE (KS)	
KS1	We regularly update the working manuals and operating procedures
KS2	We frequently use our handbooks for updating information related to our area of operation

KS3	We have a dedicated and authorized person/ department for controlling, Updating and releasing the documents
KS4	We have a structured methodology to collect information from various regions, analyse and to prepare reports for future reference
KS6	We have up-to-date handbooks on processes, problem solving, rules or procedures throughout the organization
KS7	We regularly analyse our failures and successes and results are documented for future reference
KS6	We create working manuals and standard operating procedures for smooth day to day activities
KNOWLEDGE TRANSFER(KTR)	
KTR1	Problems related to processes are discussed openly in our organization
KTR3	We subscribe newsletters, bulletins and other material regularly for our employees
KTR5	Individual performance evaluations are given and discussed regularly
KTR7	We have a structured induction Program for new employees to get conversant with our system/Procedures of our organisation (like assigning a mentor)
KTR8	Business update meetings are held on a regular basis with suppliers, customers, stakeholders etc.
KNOWLEDGE APPLICATION (KAP)	
KAP1	New ideas on improving work methods and processes from employees are considered and implemented
KAP2	Customer feedback and complaints on products / services are considered seriously and corrections or improvements are made immediately
KAP3	We use existing skills/knowledge in creative ways to generate new ideas
KAP5	New projects are assigned based on skills and availability of qualified employees
LEADERSHIP	
ORGANISATIONAL CULTURE (OC)	
OC2	Our organization, established procedures for governing the daily activities
OC3	The speed of knowledge exchange among employees is good
OC4	We regularly spend time reviewing lessons learned
OC5	Open sharing of knowledge is encouraged
OC6	Our organization is result oriented and people are competitive and achievement oriented
OC7	Our organization is like an extended family
KAP3	Employees are rewarded for developing new ideas
TOP MANAGEMENT COMMITMENT (TMC)	
TM3	Our top management Encourages and rewards new ideas, innovation
TM4	Our top management Emphasizes security of job and stability in relationships.

TM5	Our top management Provides the necessary infrastructure and allocate funds
TM6	Management facilitates the reach of information to all the levels
TM8	the speed of knowledge exchange among employees is good
MIDDLE MANAGERS' SUPPORT (MS)	
M1	Managers openly shares knowledge with the employees
M2	Managers review and evaluate the organization's progress toward meeting its goals and objectives
M3	In our organization, leaders generate high levels of motivation and commitment in the workforce.
M4	Managers/supervisors/team leaders work well with employees of different backgrounds.
M5	Managers communicate the goals and priorities of the organization

USE OF GOVERNMENT FACILITIES (GF)	
GF1	The company subscribes newsletters by Government and other associations
GF2	The company regularly gets brochures on various schemes and programmes of the Government
GF3	Employees are deputed to attend programs conducted by Government of India and other industrial organisations
GF4	Employees are sponsored to attend the programs conducted by GoI and other industrial organisations
GF5	We utilize funds from the Government to attend tradefairs, conferences etc. in abroad and in India
GF6	We use Research & Development facilities offered by the Government of India (ex. Use Intelligence portal of GoI or NSIC business park)
GF7	We use directories, Yellow pages and other infomediary services provided by Government of India
COMPETITOR COMPARISON (CC)	
CC1	We regularly compare our performance with that of the strongest competitors in the field
CC2	Our competitors are a source of inspiration for developing new methods of production, processes etc.

A SURVEY ON LEACH BASED ENERGY AWARE PROTOCOLS FOR WIRELESS SENSOR NETWORK

Annu Ghotra[1], Jasmeet kaur[2], Nitika Soni[3]

[1,2]*Department of Electroincs Engineering, GNDU, RC Ladhewali Jalandhar, (India)*

[3]*Assistant Professor, Department of Electroincs Engineering,*

GNDU, RC Ladhewali Jalandhar, (India)

ABSTRACT

Wireless sensor network is a wireless network of sensor node and become one of the most interesting area of researches. Routing technique is one of the most challenging issue in the wireless sensor network. In Wireless sensor network routing among various routing techniques energy consumption is one of the most important criteria. LEACH protocol which is one of the most energy efficient clustering protocol. Leach is effective in prolonging the network life time by consuming a small percentage of the total dissipated energy in the system. The paper present survey of LEACH protocol along with mobile sink and various LEACH-Based hierarchal routing protocols like LEACH-C, I-LEACH , V-LEACH.

Keywords: Leach, Wsn, V-Leach, I-Leach, Leach-C

I.INTRODUCTION

Low Energy Adaptive Clustering Hierarchy (LEACH) protocol is widely used for the wireless networks which contain small battery powered devices, for example wireless sensor networks (WSN). When the battery power is drained in these devices/nodes then the network cannot be used and all the nodes spend most of the energy while transmitting the data. Therefore, to increase the lifespan of the network, each node has to do only minimal work for transmitting the data. LEACH protocol is widely used in WSN, because this protocol dissipates the energy in low level.

In LEACH protocol, all the nodes are grouped into the clusters, and in each cluster one of the nodes is assigned as a Cluster Head (CH). CH collects the data from the surrounding nodes and passes it to the base station. Usually, initial assignment of CH is random and the role of CH is rotated for every fixed duration so that each node will act as a CH at least once in its life span. LEACH algorithm has two phases. They are set up phase and steady state phase. Setup phase is used to choose a CH and steady state phase is used to maintain the CH during the transmission of data. A node n is selected as a CH in next round based on applying the following formula. If T(n) is 1 then the node n will be the CH in next round.

$$T(n)=\begin{cases}\dfrac{p}{1-p\times\left(r\times \bmod \dfrac{1}{p}\right)} & \text{if } n\in G \\ 0 & \text{otherwise}\end{cases} \qquad (1)$$

where p is the probability of node n being selected as a CH, r represents the current round number and G is the set of nodes that are not selected as a CH in the last 1/p rounds. Some of the unique features of the LEACH protocol [1] are (1)The coordination and control in the cluster is localized in the set up phase. (2)The role of the CH is rotated and randomized to distribute the energy requirements among the nodes of the network. (3) To reduce the total amount of data transmission, local compression techniques are used in the CH. 4. LEACH is suitable for homogeneous networks. The structure of the cluster of nodes in a wireless network is given in the following Fig.1. In the figure the non cluster nodes are represented in blue color, these nodes send the data to the corresponding cluster head and the cluster head forwards to the base station after performing aggregation or data fusion [2]. Cluster head allots the time intervals to the cluster member nodes so that non cluster nodes can transmit the data to the bases station in the assigned schedule. Time Division Multiple Access (TDMA) schedule is maintained by the CH.

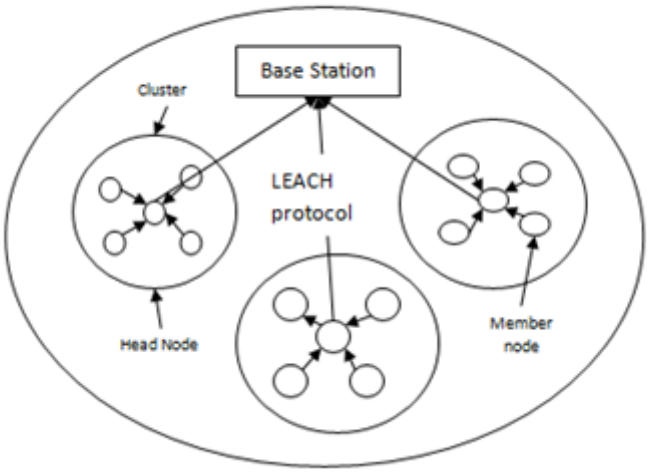

Fig1.General Sensor Network Architecture

Most of the wireless sensor networks use heterogeneous devices and the remaining power of these nodes may differ. Based on simple random rotation, if any node with low remaining energy is selected as a CH, its energy evaporates soon. Therefore, many number of LEACH routing with some enhancements were used by many researchers. Section 2 describes the literature surveyon various protocols and section 3 describes comparison of these algorithms.

II.LITERATURE SURVEY

Fuzhe zhao has proposed LEACH Routing Communication Protocol for a Wireless Sensor Network.Based on the LEACH, LEACH-C also organizes the sensor nodes into clusters with each cluster a cluster head and divides a round into set-up and steady-state phases. It differs from LEACH only in that it uses a high-energy base station to finish the choice of cluster heads. In the set-up phase of each round, every sensor node sends its information about energy to remote BS. Then the BS selects the cluster heads based on the energy information and broadcasts the IDs of cluster heads to other member nodes. This method can make the nodes with more energy and more chance to become the cluster head in the current round. But in this phase, every sensor node

needs to send its ID and energy information to remote BS to compete for the role of cluster heads, which causes energy consumption on the long distance transition [3].

Disadvantages.

(1) CHs' selection is random, which does not take into account the residual energy of every node or need the support of BS.

(2)The high frequency of reclustering wastes a certain amount of energy.

(3)It cannot cover a large area.

(4)CHs are not uniformly distributed, where CHs can be located at the edge of the cluster.

Beiranvand et al. have analyzed and proposed a new enhancement in LEACH named I-LEACH. An Improvement has been done by considering basically three factors; Residual Energy in nodes, Distance from base station and Number of neighboring nodes. A node has been considered as head node if it has optimum value for discussed three factors i.e. have more residual energy as compare to average energy of network, more neighbors than average neighbors for a node calculated in network and node having less distance from base station as comparison to node's average distance from BS in network. Reduction in energy consumption and prolongation in network life time has been observed. The proposed routing algorithm is compared to the previous proposed algorithms e.g., LEACH, DBS, and LEACH-C algorithms. Results of the simulations show that the proposed routing algorithm has been improved the WSN performance at least 65%, reduces the energy consumption of the WSN up to 62%, and improves the successfully delivered packet ratio by at least 56% as compared to the previous routing algorithms[4].

Ahlawat et al. proposed a new version of leach protocol called Improved VLEACH which aims to increase network life time. In this paper we first completely analysed the typical clustering Routing Protocol-LEACH and its deficiencies and proposed improved v-leach. The work to be done in improved v-leach protocol on selection of vice cluster head. The Vice Cluster head is that alternate head that will work only when the cluster head will die. The process of vice cluster head selection on the basis of three factors i.e. Minimum distance, maximum residual energy, and minimum energy. The proposed approach will improve the network life as never the cluster head will die. As a cluster head will die it will be replaced by it's vice Cluster head. After a number of simulations, it was found that the new version of improved v- LEACH outperforms the original version of leach protocol by increasing the network life time 49.37% [5].

S. Mottaghi et al. proposed an algorithm that combines the use of the LEACH clustering algorithm, MS and rendezvous points (RP). Simulation results showed that this method is more efficient than LEACH in terms of energy consumption, particularly in large regions. Wireless sensor networks are composed of a large number of disposable wireless sensors that collect information about their surrounding environment and transmit them to the end user. Because these sensors do not have rechargeable batteries, increasing their lifetime is important and various methods have been proposed to increase the lifetime of the sensor nodes in a network. Most of these methods are based on clustering or routing algorithms. The low energy adaptive clustering hierarchy (LEACH) algorithm is an efficient clustering algorithm where nodes within a cluster send their data to a local cluster head.

Some researchers recommend a mobile sink (MS) as a way to reduce energy consumption and a rendezvous node (RN) to act as a store point for the MS [6].

Disadvantages.

(1)The use of the inter cluster data aggregation has been neglected in the most of existing protocols.

(2)The use of ACO for efficient path selection has also been neglected by the most of researchers.

(3)However the rendezvous nodes based LEACH outperforms over the LEACH in terms of the network lifetime, but has very poor stability period i.e. the first node become dead too early.

III.COMPARISON

Several modification and enhancements are being done on LEACH to examine its existing performance. The following table shows the various enhancements made on LEACH algorithm.

Clustering routing protocol	Classification	Mobility	Scalablity	Hop count	Energy efficiency	Data aggregation	Self organisation	Use of location services
Leach	hierarchical	FixedBS	Limited	Single hop	High	Yes	Yes	No
Leach C	hierarichal	FixedBS	Good	Single hop	Very high	Yes	Yes	Yes
I Leach	hierarichal	FixedBS	Very good	Single hop	Very high	Yes	Yes	Yes
V Leach	hierarichal	FixedBS	Very good	Single hop	Very high	yes	Yes	Yes

REFERENCES

[1]. Wendi Rabiner Heinzelman, Anantha Chandrakasan and Hari Balakrishnan, “Energy-Efficient Communication Protocol for Wireless Micro sensor Networks”, *Proceedings of the 33rd Hawaii International Conference on System Sciences, 2000.*

[2]. Mortaza Fahimi Khaton Abad and Mohammad Ali Jabraeil Jamali, “Modify LEACH Algorithm for Wireless Sensor Network”, *International Journal of Computer Science Issues, Vol. 8, No. 5, pp. 219-224, 2011.*

[3] .Fuzhe Zhao, You Xu, and Ru Li, Department of Computer Science and Technology, *Central China Normal University, Wuhan 430079, China,Received 7 June 2012; Revised 7 November 2012; Accepted 19 November 2012.*

[4]. Beiranvand, Z., Patooghy, A. and Fazeli M., "I-LEACH: An Efficient Routing Algorithm to Improve Performance & to Reduce Energy Consumption in Wireless Sensor Networks", *5th IEEE International Conference on Information and Knowledge Technology, pp. 13-18, 2013.*

[5]. Ahlawat, A.and Malik, V. "An Extended Vice-Cluster Selection Approach To Improve V LEACH Protocol In WSN", *Third IEEE International Conference on Advanced Computing & Communication Technologies, pp.236-240, 2013.*

[6]. Mottaghi, Saeid, and Mohammad Reza Zahabi, "Optimizing LEACH clustering algorithm with mobile sink and rendezvous nodes", *AEU-International Journal of Electronics and Communications 69, no. 2 pp: 507-514, 2015.*

VISUAL QUALITY ACCOMPLISHMENT OF UNDERWATER IMAGES

Nisha Patel[1], Shailendra Dewangan[2]

[1,2] *Electronics and Telecommunication, CSIT, Durg, (India)*

ABSTRACT

Image enhancement is a process of improving the clarity of image by improving its characteristic. Object identification inside the water is a typical task as it suffers from low contrast, colour diminishing and low resolution due to poor visibility conditions. In order to improve the clarity of image a method has been proposed which restore then enhance the degraded image. Here we are estimating the dark prior channel then applying a soft matting which restore the degraded image followed by an HSV filter in order to enhance it. This approach reduces the scattering and colour diminishing effect, on comparing the PSNR and MSE parameters with others approach, it gives a much better result.

Keywords: ***Image Dehazing, The Dark Channel Prior, Underwater Dehazing, Soft Matting, HSV Filter.***

I INTRODUCTION

Image enhancement is the upgrading of digital image quality (wanted e.g. for visual inspection or for machine examination), without knowledge about the source of degradation. If the source of degradation is recognized, one calls the process image restoration. Among efforts to recover blurred underwater objects, many researchers resort to a physical-based solution as well as traditional image restoration theory. Both are iconical process, viz input and output is image. Underwater imaging is widely used in ocean discovery and other fields as it is crucial for scientific research and technology. Computer vision method are being used in a different areas e.g mine detection, inspection of underwater power and telecommunication cables, pipelines, nuclear reactor and columns of offshore platforms[1] and also for research in marine biology[2], mapping[3], archaeology[4] hence the quality of underwater images plays a pivotal role in scientific mission. Underwater images are basically characterized by their poor visibility because light is exponentially attenuated as it travels in the water. Haze is usually caused by the turbid environment(caused by organic particles like viruses, colloids, bacteria, phytoplankton's and inorganic like ground quartz sand, clay minerals or metal oxides).hence The irradiance received by the camera from the scene point is attenuated along the line of sight. Two types of scattering occurs first, forward scattering which usually leads to blur of the image quality. On the other hand, backscattering [18] generally restrict the contrast of the images, generating a characteristic veil that superimposes itself on the image and hides the scene. As water is 800times more denser than air (rarer medium). The main reason behind the colour degradation is the variation in the wavelength of colour as we go deeper into the water, colour drop off

one by one depending on the wavelength of the colour. Due to the reason of having shortest wavelength of blue colour it can travels a long distance results more dominant than other colour in water.

II LITERATURE REVIEW

The research on underwater image processing, many researchers have developed preprocessing techniques for underwater images using image enhancement methods. Bazeille et al. [10] and prabhakar C. J.[11] propose an algorithm to pre-process underwater images. Recently single image haze removal [25] has made a significant approach for dehazing using dark channel prior in order to recover the degraded image. John et al.[12] proposed a novel efficient approach by dehazing algorithm, which compensate the attenuation discrepancy along the propagation path, and to take the influence of the possible presence of an artificial light source into consideration. The main advantage of this paper is it can handle light scattering and color change distortions suffered by underwater images simultaneously but is unproductive in removing the image blurriness caused by light scattering. Fang et al. [13] Introduces a single image enhancement approach based on image fusion strategy.

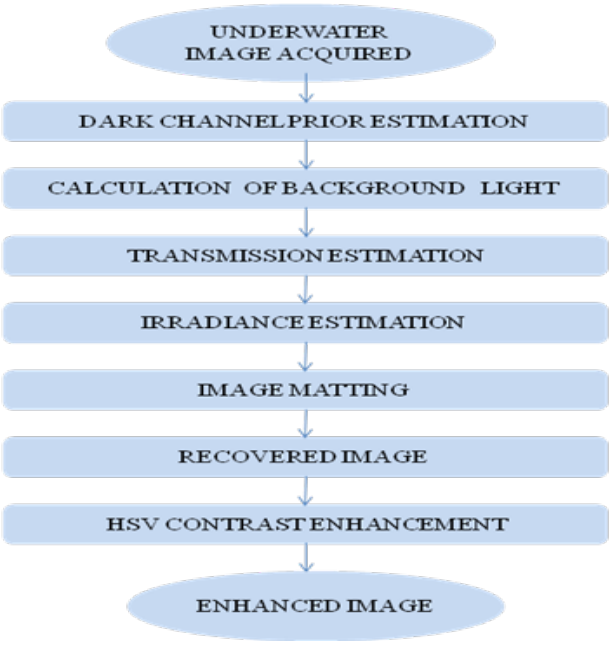

Fig.1 Block Diagram of the proposed method

They have shown that by choosing appropriate weight maps and inputs. Zhyang et al. [14] proposed a new restoration method called removing water-compensating attenuation–optimization. Guoliang et al.[15] proposed a dual-band underwater image denoising and enhancement algorithm in this the original image was decomposed into high-frequency part H and low frequency part L, and then H was filtered into F by mean shift algorithm which was improved by using the intermediate iteration results. Based on the haze imaging model a contrast enhancement method was proposed and was applied on L and F. Iqbal et. al.[16] introduces a slide stretching algorithm both on RGB and HSI colour models to enhance underwater images. The main advantage of applying two stretching models is that it helps to equalize the colour contrast in the images. It also addresses

the problem of lighting and the quality of the images which is stastically illustrated through the histograms. The main degradation in the image quality is due to forward scattering and backward scattering. Halleh[18] proposed a method to compensates the effect of optical back-scatter with no Information of the physical properties of the medium. Chao et. al.[19] proposed a dark channel prior method to restore the original clarity of the images underwater. Yoav[21] discussed about the image degradation due to backscatter. analysis in this paper used the single scattering approximation. Mohit et al.[24]presented a technique of polarized light striping based on combining polarization imaging and structured light striping.

Our approach is focusing on recovery of degraded image followed by enhancement. Proposed methodology is related to dark channel prior phenomenon. Where we combine the haze imaging model with a soft matting interpolation method, in order to get a hi-quality haze-free underwater images followed by HSV filter.

III. IMAGING MODEL

Underwater hazy image [5,6,7] can be described by the following equation:

$$I(x) = J(x)t(x) + B(1- t(x)) \qquad (1)$$

Where **I** is the obtained hazy image, **J** is the surface radiance, **B** is the backscattering. As **B** is assumed to be constant globally, it is independent from location x. t is the medium transmission which is not scattered and reaches the camera. The goal of proposed method is to recover J, B and t from I.

On the right hand side of equation(1) the first term J(x)t(x) is called *direct attenuation* and the second term B(1-t(x)) is called scattered light.

t is the medium Transmission, which is expressed as:

$$t(x) = e^{-\beta d(x)} \qquad (2)$$

Where β is the scattering coefficient of the medium. This equation (2) describes that the scene

Radiance is attenuated exponentially with the depth. If we can recover the transmission, we can also recuperate the depth up to an unknown scale.

3.1 Dark Prior Channel

The dark channel of an underwater image approximates the hydrosol darkness well; we can use the dark channel to recover the particle spherical light estimation.

The dark channel prior is based on the following observation on turbid free or haze-free images: In most of the patches, at least one among the three color channel (R,G,B) has some pixels whose intensity are very low and close to zero.

The low intensities in the dark channel are mainly due to two factors:

- Shadows, for example, shadow of underwater dark creatures, planktons, plant life or rocks in sea bed images.
- Colourful substance or surface, for example, colourful plant life and sands, and colourful rocks/minerals lacking color in any color waterway will result in low values in the dark channel.

Equivalently, the lowest intensity in such a patch is close to zero.

$$J^{dark}(x) = \min_{c\in[r,g,b]} \left(\min_{y\in\Omega(x)} \left(J^c(y) \right) \right), \qquad (3)$$

Where J^c is the colour channel of J and Ω(x) is called local patch centered at x.

To verify how good the dark channel prior is, we have captured some real underwater images and collected few images from bubble.com .The images are resized so that the maximum of width and height is 300x300 pixels and their dark channels are computed by taking a patch size 15x15.

Figure 2. Haze removal using a single image. (a)input underwater hazy image (b) image after haze removal using our method (c) our recovered depth map

Using the concept of a dark channel, our observation says that if J is the haze-free image, the intensity of J's dark channel is low and tends to be zero:

$\longrightarrow$ J^{dark} 0 (4)

3.2 Estimating the Transmission

Here, assume that the transmission in a local patch Ω(x) is constant. We denote the patch's transmission as $\tilde{t}(x)$. By taking the min operation in the local patch on the underwater haze image we have:

$$\min_{y\in\Omega(x)}\left(I^c(y)\right)\tilde{t}(x) = \min_{y\in\Omega(x)}\left(J^c(y)\right) + \left((1-\tilde{t}(x))B^c\right) \quad (5)$$

Observe that the min operation is performed on the three colour channels independently. Hence the equation will be equivalent to:

$$\min_{y\in\Omega(x)}\left(\frac{I^c(y)}{B^c}\right) = \tilde{t}(x)\min_{y\in\Omega(x)}\left(\frac{J^c(y)}{B^c}\right) + (1-\tilde{t}(x)) \quad (6)$$

By applying the min operator among three color channels on the above equation we get:

$$\min_c\left(\min_{y\in\Omega(x)}\left(\frac{I^c(y)}{B^c}\right)\right) = \tilde{t}(x)\min_c\left(\min_{y\in\Omega(x)}\left(\frac{J^c(y)}{B^c}\right)\right) + (1-\tilde{t}(x)) \quad (7)$$

According to the dark channel prior, J^{dark} of turbid free image radiance J should be tends to zero ie;

$$J^{dark}(x)=\min_c\left(\min_{y\in\Omega(x)}\left(J^c(y)\right)\right) = 0 \quad (8)$$

As B^c is always positive, which tends to:

$$\min_c\left(\min_{y\in\Omega(x)}\left(\frac{J^c(y)}{B^c}\right)\right) = 0 \quad (9)$$

Substituting the equation (9) into equation (7), the transmission $\tilde{t}$ can be estimated:

$$\tilde{t}(x) = 1 - min_c\left(_{y\in\Omega(x)}^{min}\left(\frac{I^c(y)}{B^c}\right)\right) \qquad (10)$$

If we take out the haze methodically, the image may appear unnatural and we may possibly lose the feeling of depth. So, we can optionally keep a very little amount of haze for the far objects by introducing a constant parameter ($0 < G\omega \leq 1$) into equation (10):

$$\tilde{t}(x) = 1 - G\omega\, min_c\left(_{y\in\Omega(x)}^{min}\left(\frac{I^c(y)}{B^c}\right)\right) \qquad (11)$$

The value of $G\omega$ is totally based on application, here we are assuming it 0.95. fig (2(a)) is the estimated transmission map for raw input image with patch size of 15x15. Nextly we need to refine the image by using soft matting method.

3.3 Soft Matting

We notice that the haze imaging equation (1) has a similar form as the image matting [9] equation:

$$I=\vec{F}\alpha + \beta(1-\alpha) \qquad (12)$$

Where $\vec{F}$ and $\vec{B}$ are foreground and background colors, respectively, and α is the foreground opacity. A transmission map in the haze imaging equation is exactly an alpha map. Therefore, we can apply a closed-form framework of matting [8] in order to refine the transmission. By denoting the refined transmission map by t(x).we can Rewrite t(x) and $\tilde{t}(x)$ in their vector forms as t and $\tilde{t}$, we minimize the following cost function:

$$E(t) = t^T Lt + \lambda(t-\tilde{t})^T(t-\tilde{t}) \qquad (13)$$

Here, the first term is a denoting the smoothness term and the second term is denoting a data term with a weight λ. The optimal t can be obtained by solving the following sparse linear system:

$$(L+\lambda U)t = \lambda\,\tilde{t} \qquad (14)$$

Where, U is an identity matrix of the same size as L. We set a small value on λ (10^{-4} in our experiments) so that t is softly constrained by $\tilde{t}$.

3.4 Restoring Radiance J(X)

By using the transmission map, we can get back the scene radiance according to Equation (1). But the direct attenuation term J(x) t(x) can be very close to zero when the transmission $t(x)\rightarrow 0$. The directly restored scene radiance J is prone to noise. Therefore, we confine the transmission t(x) to a lower bound to, which means that a small certain amount of haze are conserved in very dense haze regions. The final scene radiance J(x) is recovered back by:

$$J(x) = \frac{I(x)-B}{\max(t(x),t_0)} + B \qquad (15)$$

The typical value of t_0 is 0.1.Since the scene radiance is generally not as bright as the atmospheric light, the image after haze removal looks faint. So, we increase the exposure of J(x) for display.

Figure .3 estimating the background light. (a) Input underwater image (b) dark region (c) and (d): two patches that contain pixels brighter than the background.

This method, the clarity of the images is improved greatly and by using the HSV filter the colour can be enhanced. In the next [F] subsection we will discuss about HSV filter.

3.5 Estimating the Background Light

First we pick the brightest pixels in the dark channel according to the size of the image. These pixels are most opaque (dense) but lighted by the background light. Among these pixels, the input pixels which is having the highest intensity is selected as the background light,

$$B(RGB) = I(X) \quad (16)$$

Where

$$x = \max (J_{dark} (i , j)) \quad (17)$$

These pixels may not be the brightest pixel in the entire image. This simple method based on the dark channel prior is superior than the "brightest pixel" method.

3.6 Colour Enhancement Using HSV Filter

Finally the enhancement is done by HSV filter which convert an RGB colour map m to an HSV colour map. Both colour maps are in between 0 to 1. The column of the input matrix M represents intensities of red, green blue respectively. HSV is returned as an M-by-N-3 image array whose three planes contains the hue, saturations and value components for the image.

IV EXPEIMENTAL RESULT

4. 1.(a) (b) (c) (d) (e)

4.2.(a) (b) (c) (d) (e)

4.3. (a) (b) (c) (d) (e)

Fig4.1(a),2(a),3(a) are the real underwater images captured by the camera, (b) showing the dark channel,(c) transmission map(underestimated), (d) result obtained by the preprocessing enhancement techniques, (e) result obtained by our technique.

IMAGE	MSE(after image matting)	PSNR(after image mating)	MSE(after HSV)	PSNR(after applying HSV)
1.	0.034	65.213	0.0242	67.78
2.	0.014	63.108	0.0040	66.067
3.	0.0102	57.592	0.0100	59.9268

Table.1 MSE and PSNR values of fig.4

V CONCLUSION

On seeing the experimental results, it has been proved that it gives a better result than previous enhancement technique. The scattering problem and colour diminishing problem has been solved. The only drawback of this method is, it is time consuming. The dehazing technique by using the dark channel prior is more powerful for outdoor images, but it also gives the comparative better results than the any other techniques used for underwater images. Lastly after introducing the HSV filter we obtained the enhanced image.

REFERENCES

[1] G. L. Foresti,"visual inspection of sea bottom structures by an autonomous underwater vehicle," IEEE trans. Syst. Man cybern. Vol.31 pp691-705, oct. 2001

[2] L. B.Wolff, "Polarization vision: A new sensory approach to image understanding," Image Vis. Compute., vol. 15, no. 2, pp. 81–93, 1997.

[3] X. Xu and S. Negahdaripour, "Automatic optical station keeping and navigation of an ROV: Sea trial experiment," in Proc. Marine Technology Society (MTS)/IEEE OCEANS, vol. 1, Seattle, WA, pp. 71–76,1999.

[4] D. F. Coleman, J. B. Newman, and R. D. Ballard, "Design and implementation of advanced underwater imaging systems for deep sea marine archaeological surveys," in Proc. Marine Technology Society (MTS)/IEEE OCEANS, vol. 1, Providence, RI, pp. 661–665 , 2000.

[5] R.Tan,"Visibility in bad weather from a single image". CVPR, 2008.

[6] R. Fattel." Single image dehazing". In SIGGRAPH, page 1-9,2008.

[7] S.G Narasimhan and S. K. Nayar. "Chromatic framework for vision in bad weather". CVPR, 2000.

[8] A. Levin. D. Lischinski, and Y. Weiss. A Closed form solution to natural image matting. CVPR, 2000.

[9] Kaiming He, Jian Sun, and Xiaoou Tang,"single image haze removal using dark channel prior", IEEE transactions on pattern analysis and machine intelligence, vol. 33, no. 12, dec 2011.

[10] Stephane bazeille, isabelle quidu, luc jaulin, jean-phillipe Malkasse "Automatic Underwater Image Pre-Processing", CMM(2006)

[11] Prabhakar c.j.,Praveen kumar p.u. "An Image Based Technique For Enhancement Of Underwater Images", International Journal of Machine Intelligence ISSN: 0975–2927 & E-ISSN: 0975–9166, Volume 3, Issue 4, (2011)

[12] John Y. Chiang and Ying-Ching Chen(2012) "Underwater Image Enhancement by Wavelength Compensation and Dehazing" IEEE transactions on image processing, vol. 21, no. 4, april 2012

[13] Shuai Fang, Rong Deng, Yang Cao, Chunlong Fang, "Effective Single Underwater Image Enhancement", journal of computers, vol. 8, no. 4, april 2013

[14] B. Zhang, W.N. Huang Z.J. Fang X.F. Lv, Z.X. Xie," Contrast Enhancement and Optimization for Underwater Images", ICCSEE 2013

[15] Guoliang Yang, Fuyuan Peng, Kun Zhao, "A Dual-band Underwater Image Denoising and Enhancement Algorithm", 2nd International Conference on Computer Application and System Modeling (2012)

[16] Kashif iqbal, Rosalina abdul salam, azam osman and Abdullah zawawi talib(2007), " Underwater Image Enhancement Using an Integrated Colour Model" IAENG International Journal of Computer Science, 34:2, IJCS_34_2_12

[17] Dr.G.Padmavathi, Dr.P.Subashini, Mr.M.Muthu Kumar and Suresh Kumar Thakur." Comparison of Filters used for Underwater Image Pre-Processing" IJCSNS vol.10 No.1, January 2010

[18] Halleh Mortazavi, John P. Oakley and Braham Barkat," Mitigating the Effect of Optical Back-scatter in Multispectral Underwater Imaging"(2012)

[19] Liu Chao, Meng Wang, "Removal of Water Scattering", 2nd International Conference on Computer Engineering and Technology,volume2, (2010)

[20] Yan Wang and Bo Wu," Fast Clear Single Underwater Image "(2010)

[21] Tali Treibitz, and Yoav Y. Schechner," Active Polarization Descattering" IEEE transactions on pattern analysis and machine intelligence, vol. 31, no. 3, march 2009

[22] Yoav Y. Schechner and Nir Karpel, "Recovery of Underwater Visibility and Structure by" IEEE journal of oceanic engineering, vol. 30, no. 3, july 2005

[23] Yan Chen and Jin Hua (2012)," Image Restoration Algorithm Research on Local Motion-blur" I.J. Information Engineering and Electronic Business, 2011, 3, 23-29

[24] Mohit Gupta, Srinivasa G. Narasimhan AND Yoav Y. Schechner," On Controlling Light Transport in Poor Visibility Environments".

[25] Dataset: from "An image based techniques for enhancement of underwater images " by Dr.Prabhakar C.J, Dept. of computer science.

PERFORMANCE EVALUTION OF LIQUID FLAT PLATE COLLECTOR BY COMPARING THE NORMAL WATER WITH NaCl SOLUTION AS A WORKING FLUID

Taliv Hussain[1], Md.Sabbir Ali [2], Kapil Dhankher[3]

[1,2,3]Department of Mechanical Engineering,

Lovely Professional University Phagwara, Punjab (India)

ABSTRACT

With over exploitation of fossil fuels, each passing day we are inching closer to witness the extinction of natural resources. This can cause imbalance in nature. Many scientists believe it is a distant threat of which humans are not aware off. Scientists are rigorously working on to reduce the threat. One such is alternative of fossil fuels, which can reduce its exploitation to a great extent. Non conventional energy proved handful in this situation of energy crisis. Sources like, solar, wind, hydal are abundant in nature and can be harnessed to any extent.In this experiment, water and salt solution is used as liquid to be heated up within the copper pipes. Two experiments are conducted simultaneously; in first instance water is taken as the liquid to be flown inside the copper pipe. When sunrays falls on the aluminium sheet beneath which copper pipe is brazed, water gets heated up, the inlet and outlet temperature are observed. In second instance, water is mixed with common salt (NaCl) and salt solution is prepared, this solution is made to run through and the copper pipes and further it gets heated up. Inlet and outlet temperature of the salt solution at extreme end of the pipe is observed via hydrometer.On using Nacl solution there is an increase in 5-6% collector efficiency as compare to normal water.

Keywords: Liquid Flat Plate Collector, Nacl Solution, Water

I .INTRODUCTION

With the natural resources hitting new lows with each passing days, it has dented the economy of many countries which relied heavily on them. Scientists are working hard on finding alternatives for these resources. Non conventional energy resource turns out be boon in this acute energy crisis situation. Non conventional energy is far much better than the fossil fuels and other resources. In terms of availability, costs, affect on environment and many more factors under which non conventional energy is preferable over fossil fuels. The only factor which underlines the advantages is it's sparsely distribution across the earth. With the advancement of technical era, more and more technology is put into work to harness non conventional energy. Major products being solar cell and wind mill are the gift of technology. Our area of concern is solar liquid collector, which utilizes solar energy to heat up water.

K. Chung et al: Evaluated the pressure variation on the collector and the wind uplift force. Two suggestions are composed to reduce the wind uplift; these are lifting the model and guide plate. Wind speed used for the evaluation of wind uplift is in the range of 20-50 m/sec. There is significant effect on wind uplift using guide

plate normal to the wind. The effect of lifting the model is not much effective to reduce the wind lift.**Ahmet Koca et al:** Experiment was performed to evaluate the exergy and energy performance of the integrated flat plate solar collector with phase changing material for thermal storage. Mobilterm 605 is used as a working fluid with thermal conductivity .145W/mK. PCM material used is CaCl2.6H2O. Energy and exergy efficiencies are 45% and 2.2%.**Katharina Resch et al:** a review was done on the Thermotropic layers used for the overheating protection. Their transmittance is the function of the temperature of the collector. At greater temperatures transmittance declines reduce the collector temperature. Thermotropic hydrogels, thermotropic polymer blends and thermotropic systems with fixed domain are mainly applied for overheating protection.

II.EXPERIMENTAL SETUP

The setup used in the experiment consists of a wooden frame, a thin glass sheet, aluminium sheet, copper pipe and insulating material. The dimension of wooden frame is 900mm x 1245mm. Wooden frame is being insulated using glass wool having 5 cm thickness, copper pipe of 10 mm diameter is placed inside the frame, which is brazed over aluminium sheet of 3 mm thickness. Glass sheet is placed above the aluminium sheet which is directly facing the sun. In this way when sun rays falls over the glass sheet, it concentrate the rays on the aluminium sheet resulting in the heating of the metal sheet. This heated metallic sheet heats up the copper pipe beneath it by conduction. As a result, liquid flowing inside the pipe gets heated up.

Figure 1. Solar Collector for Water Heating

2.1 Important Dimensions

inner diameter of copper tube	10mm
thickness of tube	2 mm
spacing between tubes	100 mm

2.2 Equipments Used

1. Solar power meter
2. Temperature Sensors

3. Rotameter

1. Solar power meter: Solar power meter is used to measure the intensity of solar radiations.
2. Temperature Sensor: The Dial gauge type temperature sensor is used to measure the temperature of the inlet and outlet water from the liquid flat plate collector.
3. Rotameter: It is a device to measure the flow rate of water which is circulated in the collector. It gives the amount of water flowing through the tubes of collector.

III.CALCULATION AND RESULT

3.1 Formulae Used

Collector efficiency is defined as the ratio of the heat transferred to the flowing fluid to the heat received from the incident radiation (I) falling on the surface of the collector.

Collector efficiency= $\eta = \left(\frac{m * C_p * \Delta T}{I * A}\right)$

M_f= mass flow rate of liquid

C_p= specific heat capacity of liquid

ΔT= change in outlet and inlet temperature of the liquid

I=Solar intensity

A= Area of collector

Table1. Data Obtained in Experiment

FOR NORMAL WATER AS A WORKING FLUID:

Time	Outlet Temperature of water T_2 (°C)	Inlet Temperature of water T_1 (°C)	Water Flow Rate M_f (kg/s)	Solar Intensity I (W/m^2)	Temperature difference ΔT (T_2-T_1) (°C)	Efficiency η (%)
10:30 AM	32	26	0.007	613	6	25.5
11:30 AM	36	26	0.007	654	10	39.9
12:30 PM	39	26	0.007	727	13	46.7
1:30 PM	42	26	0.007	800	16	52.2
2:30 PM	40	26	0.007	740	14	49.4
3:30 PM	33	26	0.007	625	7	29.2
4:30 PM	31	26	0.007	602	5	21.6

Table 2.Data Obtained in Experiment

FOR SALT SOLUTION AS A WORKING FLUID:

Time	Outlet Temperature of water T_2 (°C)	Inlet Temperature of water T_1 (°C)	Water Flow Rate M_f (kg/s)	Solar Intensity I (W/m^2)	Temperature difference ΔT (T_2-T_I) (°C)	Efficiency η (%)
10:30 AM	33	26	0.007	613	7	29.7
11:30 AM	37	26	0.007	654	11	43.6
12:30 PM	40	26	0.007	727	14	49.8
1:30 PM	44	26	0.007	800	18	58.4
2:30 PM	41	26	0.007	740	15	52.8
3:30 PM	34	26	0.007	625	8	33.1
4:30 PM	32	26	0.007	602	6	25.9

3.2 Graph Analysis

Comparison of efficiency of liquid used within collector (normal water and salt solution)

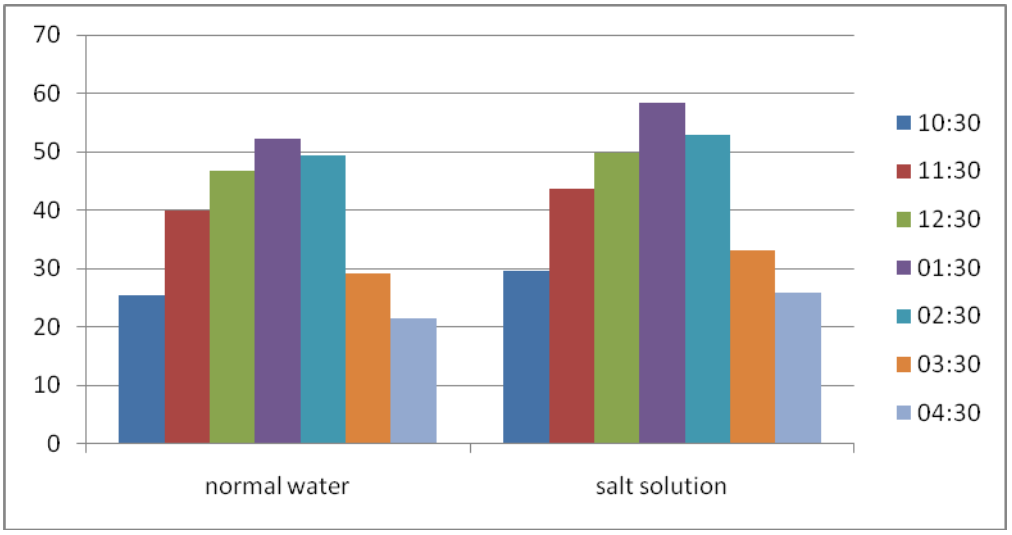

Table 3.Comparison Between Two Working Fluids

Type of Working fluid	Maximum efficiency η(%)	Max Temperature difference ΔT(°C)	Mass flow rate m_f(kg/sec)
Normal Water	52.2%	16	0.007
Nacl Solution	58.4%	18	0.007

IV.CONCLUSION

At last we came to conclusion after conducting experiment and doing research analysis that liquid solar collector using salt solution as liquid will be more efficient than the one using normal water as is its liquid. There is difference of 5-6% in terms of collector efficiency of normal water and solar collector using salt solution.

REFERENCES

[1] P.G. Loutzenhiser, H. Manz, C. Felsmann, P.A. Strachan, T. Frank and G.M. Maxwell, Empirical validation of models to compute solar irradiance on inclined surfaces for building energy simulation, Solar Energy 81 (2007) 254–267

[2] K. Chung, K. Chang and Y. Liu, Reduction of wind uplift of a solar collector model, Journal of wind engineering and Industrial Aerodynamics, 96 (2008) 1294-1306

[3] Katharina Resch Thermotropic layers for flat-plate collector – A review of various concepts for overheating protection with Polymeric materials, Solar energy materials & solar cells, 93 (2009)119-128

[4] Ahmet Koca Forecasting of thermal energy storage performance of Phase Change Material in a solar collector using soft computing techniques, Expert Systems with Applications, 37 (2010)2724–2732

[5] L.M. Ayompe, A. Duffy, S.J. McCormack , M. Conlon, Validated TRNSYS model for forced circulation solar water heating systems with flat plate and heat pipe evacuated tube collectors, Applied Thermal Engineering, 31 (2011) 1536-1542

BIOGRAPHICAL NOTES

Taliv Hussain as an Assistant Professor in Mechanical Engineering Department from Lovely Professional University, Phagwara, Punjab, India.

Md.Sabbir Ali as an student of Mechanical Engineering Department from Lovely Professional University, Phagwara, Punjab, India.

Kapil Dhankher an student of Mechanical Engineering Department from Lovely Professional University, Phagwara, Punjab, India.

TO EVALUTE THE PERFORMANCE OF LIQUID FLAT PLATE COLLECTOR BY COMPARING TWO DIFFERENT INSULATION MATERIALS AS GLASS WOOL AND FOAM

Taliv Hussain[1], Saddamul Haque[2], Rocky Singh Labana [3]

[1,2,3] *Department of Mechanical Engineering, Lovely Professional University Phagwara, Punjab (India) -144402*

ABSTRACT

Energy consumption is increasing very rapidly as the world is developing. Conventional sources are not able to fulfil the today's energy needs. Renewable energy sources eliminate the weaknesses of conventional sources. But because of less knowledge about these sources and high initial cost of the conversion systems we limit the use of these resources. Solar energy is one of the such renewable source which is in abundant in nature but it cannot be effectively utilized because of its intermittent nature. There is a need to trap this energy in some form to make it a reliable energy source.

In this present work, various studies and investigations are being done to develop the system and device that can effectively utilize the renewable energy resources for the purpose of industrial and domestic use. One such device is water flat plate collector which is used for heating water by using solar energy and hence investigations are being done to check out the performance characteristics of efficiently heating water using different selective insulating materials like glasswool and foam. It has been seen that on using glass wool as insulating material maximum collector efficiency is 44.4% and while using foam as insulating material maximum collector efficiency is 48.6%.Thus by using effective insulation and by varying thickness of insulation material we can increase the solar collector efficiency.

Keywords: Solar Collector Efficiency, Glass Wool, Foam

I. INTRODUCTION

Depletion of conventional energy resources and its adverse impact on environment have created renewed interest for the use of renewable energy resources. Hence developments of devices and instruments that can free us from use of conventional energy resources are of crucial importance. As a result, considerable research and development activities have taken place to identify reliable and economically feasible alternative clean energy sources. The solar energy is such a renewable energy resource, the direct incident energy in the form of sunlight can be converted to thermal energy and transferred to heating devices that are capable of trapping it for long hours. The purpose of solar water heater is to convert the solar radiation into heat to satisfy energy needs but

with some limitations it is not being used on grid scale because of its poor efficiency and higher initial cost. So there is a requirement of advancement in the solar water heater using flat plate collector to overcome its limitations so that it can be used as a replacement of conventional heaters and power generation devices. Solar collector absorbs the incoming solar radiation, converting it into thermal energy at the absorbing surface, and transferring the energy to a fluid flowing through the collector.

Clarence Kemp et al. patented the old design of metal tanks exposed to the sun by adding a metal panel to the tank, in order to increase the efficiency of the solar tank. In the beginning of the 20th century, inventors designed improved systems, but still the heating and the storage unit were one, and both were exposed to the weather and the cold nights. **William Bailey et al.** began selling the Day and Night solar water heater, which provided an insulated indoor water storage tank, supplied by a separate solar collector located outside the house and facing south. The collector consisted of a coiled pipe inside a glass covered box which had to be mounted below the storage tank. This allowed the hot water to circulate from the collector to the storage tank by natural convection. **Otanicar et al.** proposed a direct absorption solar collector operated on nanofluids. They demonstrate efficiency improvement up to 5% by utilizing nanofluids as the absorption mechanism. **E. Natarajan and R. Sathish et al.** suggest the use of nanomaterials in the solar devices to increase the heat transfer and that can be useful in energy saving and compact designs**. Groenhout et al.** suggested a novel design of a double-sided absorber with low emissivity selective surface coupled with high reflectance stationary concentrators to reduce the radiative and conductive losses through the back of the collector. This particular design reduce the net heat loss to be 30– 70% lower than conventional systems.

II. EXPERIMENTAL SETUP

The set up comprises of the wooden frame of dimension 900mm* 1245mm. Two ports one as inlet and other at other end as outlet are made and the water is allowed to pass through the copper tubes that are installed below the absorber sheet and the glass cover. The aluminium sheet of 3 mm thickness is used as absorber sheet. The first experiment is carried out with glass wool as insulating material and other with the foam as insulating material. The thickness of insulating materials is same i.e 5 cm.

The dimensions of tubes are:

Inner Diameter of Tube	10 mm
Thickness of Tube	2 mm
Spacing between Tubes	100 mm

the function of tubes and channels is to circulate the water. The water flowing through these tubes takes away the heat from the absorber plate.

Figure 1. Liquid flat plate collector

Measuring devices and instruments

The different parameters are measured in this study. The instruments used are as follows:

1. Solar power meter
2. Temperature Sensor
3. Liquid mass flow rate Measurement

1. Solar power meter: Solar power meter is used to measure intensity of radiation falling on collector Surface in watt/m^2

2. Temperature Sensor: The Dial gauge type temperature sensor is used to measure the temperature of the inlet and outlet water from the Water flat plate collector. The range of the dial gauge type temperature sensor is from 0-250°C.

3. Liquid mass flow rate Measurement: The liquid flow rate is measured by conventional method in which we have recorded the time required to fill the beaker of known volume. By the help of this data, we have calculated discharge(volume/time) at the outlet of the water flat plate collector.

III.CALCULATION AND RESULT

Formulae used and nomenclature:

Collector efficiency is defined as the ratio of the heat transferred to the flowing fluid to the heat received from the incident radiation (I) falling on the surface of the collector.

$$\eta = \left(\frac{m * C_p * \Delta T}{I * A}\right)$$

where m_f = mass flow rate in kg/sec

C_p = specific heat at constant pressure in J/kg.k

$\Delta T = T_2 - T_1$ T_2 is the exit temperature

T_1 is the inlet temperature

I = Intensity of radiation falling on Collector Surface in watt/m^2

A = Area on which the radiation is falling in m^2

Table 1. Data obtained in experiment

WHEN GLASS WOOL IS USED AS INSULATION MATERIAL

THICKNESS OF GLASS WOOL=5 CM

Time	Outlet Temperature of water T_2 (°C)	Inlet Temperature of water T_1 (°C)	Water Flow Rate M_f (kg/s)	Solar Intensity I (W/m^2)	Temperature difference ΔT (T_2-T_I) (°C)	Efficiency η (%)
10:30 AM	31	24	0.005	615	7	21.2
11:30 AM	35	24	0.005	658	11	31.1
12:30 PM	40	24	0.005	733	16	40.7
1:30 PM	43	24	0.005	805	19	44.4
2:30 PM	41	24	0.005	742	17	42.7
3:30 PM	33	24	0.005	630	9	26.6
4:30 PM	30	24	0.005	605	6	18.5

Table 2. Data obtained in experiment

WHEN FOAM IS USED AS INSULATION MATERIAL

THICKNESS OF FOAM=5 CM

Time	Outlet Temperature of water T_2 (°C)	Inlet Temperature of water T_1 (°C)	Water Flow Rate M_f (kg/s)	Solar Intensity I (W/m^2)	Temperature difference ΔT (T_2-T_I) (°C)	Efficiency η (%)
10:30 AM	32	24	0.005	615	8	24.2
11:30 AM	37	24	0.005	658	13	36.8
12:30 PM	41	24	0.005	733	17	43.2
1:30 PM	45	24	0.005	805	21	48.6

2:30 PM	42	24	0.005	742	18	45.2
3:30 PM	35	24	0.005	630	11	32.5
4:30 PM	32	24	0.005	605	8	24.6

IV. GRAPH ANALYSIS

Comparison of efficiency of insulating material (glass wool and foam)

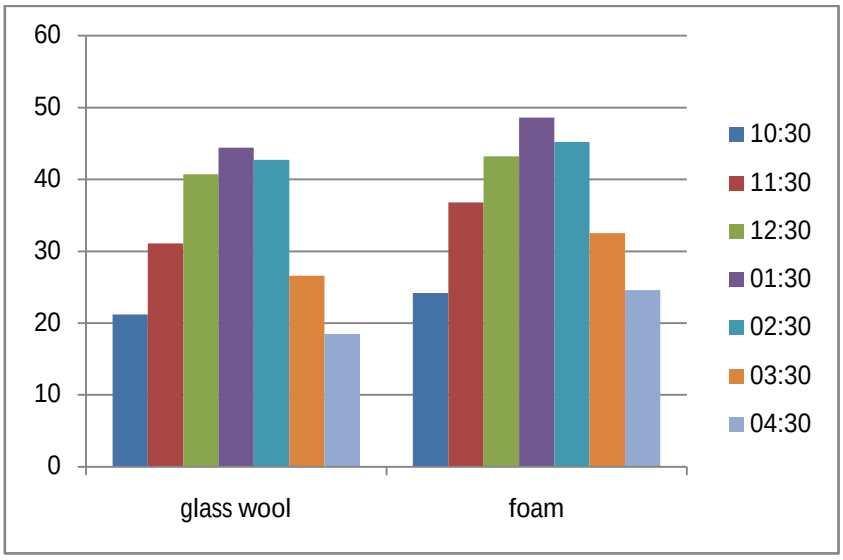

Table 3. Comparison between two different insulation materials

Type of Insulating material	Maximum efficiency **(η)**	Max Temperature difference **ΔT (°C)**	Thickness of material **(cm)**
Glass wool	44.4	19	5
Foam	48.6	21	5

V. CONCLUSION

Based on the review of the literature on solar collector, it has been found that solar collector was widely investigated both analytically and experimentally. A number of studies have been carried out in order to investigate the effect of various parameters on the performance of solar collector. Several promising advancement are taking place in the field of solar water heating system using flat plate collector. It is quite evident that by improvement in solar collector it can be used when conditions are not favourable. Optimization of operating parameters like orientation, fluid flow rate can also increase the efficiency. Thus we can conclude that by using different effective insulation materials and by varying the thickness of insulation materials we can increase the efficiency of Liquid flat plate collector.

REFERENCES

[1] N. K. Groenhout, M. Behnia, G.L. Morrison, (2002). "Experimental measurement of heat loss in an advanced solar collector", Experimental Thermal and Fluid Science, 26, 131–137

[2] Chow TT. Performance analysis of photovoltaic-thermal collector by explicit dynamic model. Solar Energy (2003); 75:143–52.

[3] E. Natarajan, R. Sathish, (2009). "Role of nanofluids in solar water heater".

[4] T. P. Otanicar, P. E. Phelan, R. S. Prasher, G. Rosengarten, and R. A. Taylor, (2010). "Nanofluid-based direct absorption solar collector" journal of renewable and sustainable energy, 2, 033102.

[5]. Madhukeshwara. N, E. S. Prakash, An investigation on the performance characteristics of solar flat plate collector with different selective surface coatings, International Journal of Energy and Environment, 3, Issue 1 (2012) 99-108

Biographical Notes

Taliv Hussain as an Assistant Professor in Mechanical Engineering Department from Lovely Professional University, Phagwara, Punjab, India.

Saddamul Haque as an student of Mechanical Engineering Department from Lovely Professional University, Phagwara, Punjab, India.

Singh Labana an student of Mechanical Engineering Department from Lovely Professional University, Phagwara, Punjab, India.